Assessment of speed variability on the horizontal curves using vehicle trajectories for geometric design consistency and safety evaluation of a two-lane rural highway passing through mountainous terrain

A thesis submitted in partial fulfilment of the requirements

for the award of the degree of

Doctor of Philosophy

in

Civil Engineering

by

Anna Venkata Anjeneya Bharat Kumar

(Roll No. 156104007)

Under the supervison of

Prof. Mallikarjuna C.

Prof. Venkatesh T.

DEPARTMENT OF CIVIL ENGINEERING,

INDIAN INSTITUTE OF TECHNOLOGY GUWAHATI,

GUWAHATI, ASSAM-781039, INDIA

March, 2023

Department of Civil Engineering
Indian Institute of Technology Guwahati,
Guwahati, Assam-781039, India

Certificate

This is to certify that the work contained in this thesis entitled **'Assessment of speed variability on the horizontal curves using vehicle trajectories for geometric design consistency and safety evaluation of a two-lane rural highway passing through mountainous terrain',** submitted by **Anna Venkata Anjeneya Bharat Kumar (Roll No. 156104007)** to the Indian Institute of Technology Guwahati, for the award of Doctor of Philosophy in Civil Engineering. The study and results in the thesis are original work carried out by the student himself under my supervision and has not been submitted elsewhere for the degree.

Prof. Mallikarjuna C.
Professor
Department of Civil Engineering
Indian Institute of Technology Guwahati,
Guwahati, Assam-781039, India
Date: 9/3/2023

Prof. Venkatesh T.
Professor
Department of Computer Science and Engineering
Indian Institute of Technology Guwahati,
Guwahati, Assam-781039, India
Date:

Declaration

I, **Anna Venkata Anjeneya Bharat Kumar** (Roll No. 156104007), declare this thesis titled **'Assessment of speed variability on the horizontal curves using vehicle trajectories for geometric design consistency and safety evaluation of a two-lane rural highway passing through mountainous terrain',** and the work presented in it has been carried out by me under the supervision of **Prof. Mallikarjuna C.**, Department of Civil Engineering and **Prof. Venkatesh T.**, Department of Computer Science and Engineering, Indian Institute of Technology Guwahati. The work has not been submitted anywhere for the award of any degree.

Anna Venkata Anjeneye Bharat Kumar
Roll No. 156104007
Department of Civil Engineering,
Indian Institute of Technology Guwahati,
Guwahati, Assam-781039, India.
Date: 09/03/2023

Acknowledgement

This thesis work would not have been possible without the support of a number of people who have contributed in some way or the other to the successful completion. First and foremost, I would like to express my gratitude and heartful thanks to my supervisor Prof. Mallikarjuna C., Department of Civil Engineering, and co-supervisor, Prof. Venkatesh T., Department of Computer Science and Engineering, Indian Institute of Technology Guwahati, Guwahati, Assam, India, for their constant supervision, encouragement, and generous support during my research work. Their suggestions, continuous motivation, and patience helped me to overcome the difficult stages during the journey and improve my technical skills for the successful completion of the project.

I am sincerely grateful to the chairman of my doctoral committee, Prof. T.L. Ryntathiang, and the committee members, Dr. Anjan Kumar S. and Prof. Rohit Sinha, for their guidance and suggestions in improving the quality of my research work. I would like to extend my gratitude to the Head, Department of Civil Engineering, IIT Guwahati, for his direct and indirect support and encouragement in carrying out the research work. I would also thank the non-teaching staff for their assistance and support in various ways.

I thank my research group members Dr. Suvin P.V., Dr. Regulus D. K. Shallam, Pranab Kar, and Koustab Borah, for their consistent support and encouragement in my hard times. I would like to thank other research group members in transportation engineering Dr. Sanhitha Das, Dr. Bhaskar, Dr. Nishanth, Dr. Santhanu, Nama Suresh, Ibaiahun Nongbet Sohlang, Dr. Arunabha and Saswathi. I would also thank my friends from other research groups in campus for their support during the journey.

I would like to thank my better half, Mrs. A.V.V. Amani, for her support over the last two years, without which I could have not completed the research work at the earliest. Finally, my utmost gratitude must go to my father, Shri. A.Narasimha Rao and mother, Smt. A.V.R. Subhashini for their unconditional love and support during my hard times since childhood and especially during the journey in IIT Guwahati.

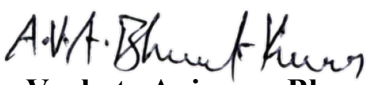

Anna Venkata Anjeneya Bharat Kumar
Date: 09/03/2023

This thesis is dedicated to

my parents and my wife

Abstract

Horizontal curves play a crucial role in providing a smooth and safe transition from one tangent to the successive tangent. But, the crash data corresponding to Indian highways shows that the crashes on curves went up by 46.05% on average between 2016 to 2021. This is a significant change to the 1.9% increase corresponding to the straight sections during the same period. Further, the crash statistics corresponding to the northeastern states of India, located in the mountainous region, showed an increase in the crashes by an average of 5.2% in rural areas from the year 2016 to 2021. Thus, horizontal curves of the two-lane undivided national highways, specifically that are passing through mountainous terrain, are the key hotspots for road crashes. In this scenario, evaluating the consistency of horizontal curves is important to improve safety.

Geometric design consistency has a close relationship with the safety of geometric elements. Operating speed-based consistency measures developed by Lamm are widely used for evaluating the geometric design consistency. However, the majority of the existing studies have evaluated the horizontal curves based on the speed data collected at the center of the curve. The main reason for this is, collecting the data at the curve center is relatively easier. Further, these studies primarily assume that the vehicle speed on the curve remains constant and the complete acceleration and deceleration take place on the tangents.

In this context, several researchers have investigated the constant speed assumption using continuous speed profiles collected from instrumented vehicles and driving simulators. The majority of the researchers found that speed is not constant on the curve and emphasized the importance of minimum speed on the curve in operating speed reduction modeling. But, no study has assessed the impact of speed collected at the center of the curve and minimum speed on the curve for operating speed consistency and safety evaluation. Moreover, a majority of speed reduction models were developed for rural highways in plain terrain, and these models are not applicable to the highways passing through mountainous terrain.

Besides, the continuous speed profiles collected from the instrumented vehicles and the driving simulators have significant issues. The existing videography-based image-processing techniques for vehicle trajectory collection are suitable only for plain terrain. Thus, the objective of this study is to assess the role of minimum and maximum speed on the curve in evaluating the design and operating speed consistency and safety aspects of two-lane undivided

rural highways passing through mountainous terrain. To achieve the objective, four tasks were performed in this research.

In task-1, a multiple-homography-based coordinate transformation technique was proposed for collecting the trajectory data from a non-planar horizontal curve using a videography-based image-processing technique. The proposed approach was based on the Direct Linear Transformation (DLT) method, where a non-planar road section was divided into a sequence of planar regions, and a separate homography matrix was estimated for each planar region. The proposition was verified using the trajectory data obtained using V-box equipment. The speed profiles estimated using the proposed approach and the data from the instrumented vehicle were compared. The comparative analysis shows that the speed profiles estimated using the multiple-homography approach were more accurate (RMSE of 0.44 km/h) compared to that of a single homography approach (RMSE varied between 1.5 and 3.7 km/h). The findings highlight the necessity of using the multiple-homography approach to collect more realistic trajectory data from non-planar geometric elements. Further, video footage of the traffic stream was collected from fourteen horizontal curves of a two-lane undivided rural highway located in Meghalaya, India. The extracted trajectories were smoothed for noise removal. For analysing the driver behavior on the horizontal curves, several speed and acceleration variables were extracted corresponding to the free-flowing vehicles.

In task-2, the driver behavior on the horizontal curves was analysed through longitudinal acceleration and speed profiles of individual vehicles. From the acceleration profiles, it was observed that 98% of the drivers entered the curve, either accelerating or decelerating and then decelerating or accelerating before leaving the curve. The acceleration and deceleration lengths measured from the point of curvature showed that, car and loaded trucks decelerated up to 70% and 40% of the curve length and accelerated up to 50% and 30% of the curve length, respectively. From the speed profiles, the speed variability on the curve was assessed through operating speed profiles, comparison of minimum and maximum speeds and their locations. The analysis found that speed is not constant on the curve and, the minimum and maximum speeds occurs all along the curve, for both car and loaded trucks. Speed variability, measured as maximum speed difference on the curve, was modeled for both the vehicles and important determinants were found. Given the speed variability on the curve, consistency evaluation based on the operating speed corresponding to the curve center could lead to erroneous results.

For a realistic evaluation of operating and design speed consistency, it is necessary to estimate the 85th percentile of maximum speed (V_{Max}^{85}) and 85th percentile of minimum speed (V_{Min}^{85}). But, identifying the point at which the minimum and maximum speeds occur on the curve for all the vehicles is not possible without having continuous speed profile data. At the same time, collecting naturalistic vehicle trajectories through videography approach on the horizontal curves in mountainous terrain is not possible in all the scenarios as it depends on the availability of clear vantage points. Thus, in task-3, the correction factors for the operating speed corresponding to the center of the curve, were modeled for estimating the maximum and minimum 85th percentile speeds. The estimated correction factors were used to adjust the operating speeds corresponding to curve center and obtain V_{Max}^{85} and V_{Min}^{85} on the curve.

In task-4, the role of V_{Max}^{85} and V_{Min}^{85}, as compared to the 85th percentile of speed at the center of the curve (V_{CC}^{85}), in the Lamm's safety criteria based geometric design consistency was assessed, for both car and loaded trucks. The comparison of individual curve classification corresponding to V_{CC}^{85} and, V_{Max}^{85} and V_{Min}^{85} reveals significant changes across the criteria. The effect of change in classification due to V_{Max}^{85} and V_{Min}^{85} in the consistency evaluation was assessed through level of agreement. The level of agreement between safety criteria and the crashes corresponding to trucks showed that, considering V_{Max}^{85} and V_{Min}^{85} in geometric design consistency improves the identification of poorer sections compared to that of V_{CC}^{85}. Further, the crash frequency models corresponding to the three safety criteria revealed that, application of V_{Max}^{85} and V_{Min}^{85} has a significant impact on consistency evaluation. Thus, the findings of the research strongly recommend to consider the speed variability (V_{Max}^{85} and V_{Min}^{85}) on the horizontal curves while assessing the geometric design consistency of undivided highways passing through mountainous terrain.

The contributions of the thesis have potential applications in improving the safety of rural highways. The proposed multiple homography approach enables researchers and practitioners to collect naturalistic vehicle trajectories from the horizontal curves located in a non-planar region. This study emphasized the role and importance of speed variables (V_{Min} and V_{Max}) for the safety and consistency evaluation of the geometric elements (horizontal curves) in mountainous terrain.

Table of Contents

List of Figures

List of Tables

List of Symbols

CCR_S	= Curvature Change Rate (Lamm) in degrees/km;
CCR	= Curvature Change Rate (others) in degrees/km;
D	= Travel Direction (it is a binary variable with left turning = 1 and right turning = 0);
DC	= Degree of curvature in degrees;
e	= Super elevation in percentage;
f_{RA}	= Side friction assumed
f_{RD}	= Side friction demand
f_{RD}^{CC}	= Side friction demand corresponding to V_{CC}^{85};
f_{RD}^{Max}	= Side friction demand corresponding to V_{Max}^{85};
G	= Gradient in percentage (it is a binary variable with upgrade = 1 and downgrade = 0);
L_T	= Tangent length in m;
L_{AT}	= Length of approach tangent in m;
L_C	= Length of the curve in m;
L_{PC}	= Length of the previous curve in m;
L_{ET}	= Length of exit tangent in m;
L_W	= Lane width in m;
LD	= Lateral Distance between center of the vehicle to nearest outer edge in m;
LD_{PC}	= Lateral Distance at PC in m;
LD_{CC}	= Lateral Distance at CC in m;
LD_{PT}	= Lateral Distance at PT in m;
$Max\Delta_{85}V$	= 85th percentile of maximum speed difference on the curve in km/h;
ND	= Naturalistic Driving;
PC	= Point of curvature;
PT	= Point of transition;
Q_1	= 25th percentile speed in km/h;
Q_3	= 75th percentile speed in km/h;
R	= Radius in m;

R_{PC} = Previous curve radius in m;

T_L = Transition length in m;

V^{85} = Operating speed in km/h;

V^D = Design speed in km/h;

V_{PC} = Speed at PC in km/h;

V_{CC} = Speed at CC in km/h;

V_{PT} = Speed at PT in km/h;

V_{avg} = average speed on the curve in km/h;

V_{Max} = Maximum speed on the curve in km/h;

V_{Min} = Minimum speed on the curve in km/h;

V_{CC}^{85} = 85th percentile of speed at center of the curve in km/h;

V_{Max}^{85} = 85th percentile of maximum speed in km/h;

V_{Min}^{85} = 85th percentile of minimum speed in km/h;

V_i^{85} = Operating speed at the approach tangent in km/h;

V_{i+1}^{85} = Operating speed on the curve in km/h;

$\Delta_{85}V$ = 85th percentile speed differential;

ΔV_{85} = Difference between 85th percentile operating speed;

ΔV_{MaxCC} = Speed difference between V_{Max} on the curve and V_{CC} in km/h;

ΔV_{MinCC} = Speed difference between V_{Min} on the curve and V_{CC} in km/h;

ΔV_{MaxCC}^{85} = 85th percentile of the speed difference between V_{Max} on the curve and V_{CC} in km/h;

ΔV_{MinCC}^{85} = 85th percentile of the speed difference between V_{Min} on the curve and V_{CC} in km/h;

Δ = Deflection angle in degrees;

μ = Mean;

σ^2 = Variance;

List of Abbreviations

AT	= Approach tangent;
CC	= Center of the curve;
DLT	= Direct linear transform;
ET	= Exit tangent;
GPS	= Global positioning system;
IP	= Image processing;
IQR	= Inter quantile range;
MAD	= Mean absolute difference;
MH	= Multiple homography;
MSR	= Maximum speed reduction;
ND	= Naturalistic driving;
NH	= National highway;
NHAI	= National highway authority of India;
OLS	= Ordinary least square;
PC	= Point of curvature;
PT	= Point of transition;
RMSE	= Root mean square error;
RELP	= Recursively ensembled low-pass;
RWLS	= Robust weighted least square;
SH	= Single homography;
SC	= Safety criterion;
WLS	= Weighted least square

1 Introduction

1.1 Background

Road infrastructure plays a pivotal role in the growth of a country's economy. Safety is given utmost importance while developing the road infrastructure. In spite of this, close to 1.35 million fatalities are attributed to road crashes. The majority of road crashes occur in low and middle-income countries. Road crashes also have huge economic consequences. According to a world health organization (WHO 2022) report, road crashes cost most countries about 3% of their Gross Domestic Product (GDP). India has the second largest road network in the world and ranks first in the number of road-related fatalities (BRS 2018; MORTH 2019). In India, national highways account for two percent of the total road network and carry 40 percent of the country's traffic (MORTH 2020). Among the national highways, 48.76% of the road length is covered by two-lane undivided highways, followed by 29.13% of single or intermediate-lane roads, and the remaining percentage of the road length is covered by four-lane and six-lane highways (BRS 2018).

National highways contributed to 30.63% of crashes and 35.6% of crash fatalities on average from 2016 to 2021(MORTH 2016-2021). A majority of existing highways are two-lane undivided roads. Approximately 30% of road accident fatalities occur on two-lane undivided roads (Chatterjee and Mishra 2019). Although horizontal curves play a crucial role in providing a smooth and safe transition from one tangent to the successive tangent, they are found to be the key hotspots for road crashes. The crash data in India shows that the crashes on curve went up by 46.05% on average between 2016 to 2021 (MORTH 2016-2021). This is a significant change to the 1.9% increase corresponding to the straight sections during the same period. Joshi et al. (2015), based on a study conducted in Uttarakhand, observed that majority of crashes had taken place in districts with mountainous terrain. The crash statistics corresponding to the northeastern states of India located in the mountainous region showed an increase in the number of crashes by an average of 5.2% in rural areas from the year 2016 to 2021 (MORTH 2016-2021). Thus, it is evident from the accident statistics that horizontal curves of two-lane undivided national highways, specifically passing through mountainous terrain, are the key hotspots for road crash occurrences.

Factors contributing to road crashes are broadly categorized into driver error, vehicle condition, and road condition/environment (MORTH 2019; Malaghan et al. 2020). Corresponding to various driver errors, on average, over speeding alone accounted for 68% of total crashes from the year 2016 to 2021 (MORTH 2016- 2021). Among various weather conditions, on average about 72.8 % of the total crashes happened in sunny/clear weather conditions. Corresponding to the crashes based on neighbourhood, on average, 46% of total crashes took place in the open area. Among urban and rural areas, on average, 60.5% of the total crashes have occurred in the rural area. Further, driver and road infrastructure interaction alone accounted for 27 percent of road crashes (Ahmed 2013; Malaghan et al. 2021). The driver-road infrastructure-related crashes indicate that drivers' misperceptions of the alignment leads to crashes (Ahmed 2013; Shallam et al. 2019; Malaghan and Pawar 2022). Driver's perception mainly relies on two factors; one is the visual information attained while traversing the geometric elements, and the other is the travel experience on that alignment (Alexander 1986; Shallam et al. 2019; Malaghan et al. 2020). Geometric designs corresponding to plain and mountainous terrain differ in terms of alignment and traffic characteristics. The design of two-lane undivided rural highway alignment in mountainous terrain is constrained by land availability that leads to complex geometric elements. Thus, the driver's perception of the highway alignment passing through plain and mountainous terrain would be different. Analysis of the vehicle response patterns (individual speed and operating speed) that reflect the driver's perception of the alignment is one of the most common approaches used to understand driver-road interaction.

Geometric design consistency is a technique widely used across the world to assess the safety of a highway alignment. Alexander (1986) defined geometric design consistency as the conformance of the highway's geometric and operational features with the driver's expectancy. Al-Masaeid et al. (1995) defined geometric design consistency as the degree to which highway systems are designed to avoid critical driving manoeuvres and ensure safe traffic operations. A consistent geometric alignment ensures that successive geometric elements act in a coordinated way so that they produce harmonized driving performance without surprising events (Gibreel et al. 1999). A geometric alignment is inconsistent when a driver makes abrupt speed adjustments due to the events that surprise while traversing a geometric element. The higher speed variability within the geometric element or between the successive geometric elements has a great propensity for crash occurrences. Therefore, assessing geometric design consistency is essential to ensure the safety of existing and newly proposed alignments. Consistency

measures are helpful in identifying the locations on the highway alignment that are prone to crashes.

Consistency measures are classified based on various parameters such as operating speed, driver workload, alignment indices, side friction, and driving dynamics for assessing geometric design consistency. Among various measures, Lamm's criteria developed based on operating speed, is widely accepted across the world and used for consistency evaluation (Anderson et al. 1999; Hassan et al. 2000; Castro et al. 2008; Žilionienė and Vorobjovas 2011; Wang et al. 2013; Goyani et al. 2022; Chaudhari et al. 2022). Operating speed is widely considered as a response pattern of the vehicles that reflects the driver's perception of a geometric element. Operating speed is defined as the 85th percentile speed value at which drivers are observed at a location to operate their vehicles under free-flow conditions (AASTHO 2011).

1.2 Need for the study

Evaluating a highway alignment for geometric design consistency is necessary to improve the safety of existing as well as new highway alignments. Operating speed-based criteria are widely used across the world for this purpose. To assess the design and operating speed consistency, a majority of existing studies estimated operating speed (V_{85}) using spot speed data collected at the centre of the curve (Leisch and Leisch 1977; Lamm and Choueiri 1987; Krammes et al., 1995; Gibreel et al., 1999; García et al. 2013; Shallam el at 2022). The main reason for this is, collecting the data at the curve centre is relatively easier (Krammes et al. 1995; Passetti and Fambro 1999). Further, these studies primarily assume that the vehicle speed on the curve remains constant, and the complete acceleration and deceleration take place on the tangents. But, for evaluating the design and operating speed consistency, it is necessary to collect the minimum and maximum operating speed on the curve.

In this context, several studies from different countries have collected vehicle trajectories that provide continuous speed profiles along a particular geometric element using either instrumented vehicles or driving simulators (Pérez-Zuriaga et al. 2013; Calvi and Bella 2014; Montella et al. 2014a; Montella et al. 2014b; Choudhari and Maji 2019; Malaghan et al. 2020). Most of these studies have developed speed reduction models for operating speed consistency evaluation. A few studies have assessed the constant speed assumption on the horizontal curves and found that the speed is not constant on the curve, and the minimum speed does not occur at the centre of the curve. Although many researchers have developed speed

reduction models corresponding to the minimum speed on the curve, no study has assessed its impact on the operating speed consistency and safety. Moreover, a majority of speed reduction models are meant for rural highways in plain terrain, and these models are not applicable to the highways passing through mountainous terrain. Further, no study has attempted to study the design speed consistency corresponding to maximum speed on the curve.

Besides, the continuous speed profiles collected from the GPS instrumented vehicles and the driving simulators have significant issues. The speed data corresponding to GPS instrumented vehicles are limited to a specific category of vehicles, and the actual driving behaviour captured in this process could be biased (Farah et al. 2017; Xu et al. 2018; Malaghan et al. 2021). On the other hand, driving simulator studies are specific to controlled conditions (Montella et al. 2014a; Calvi and Bella 2014; Choudari and Maji 2019). Thus, neither the GPS instrumented vehicles nor the driving simulators could collect the data necessary for a realistic estimation of geometric design consistency. These gaps motivated this study to develop a multiple homography approach for collecting videography-based naturalistic continuous speed profiles on the two-lane undivided rural highway passing through mountainous terrain. Further, the role of minimum and maximum speed on the curve in operating speed and design speed consistency is assessed.

1.3 Objectives

The objective of this study is to assess the role of minimum and maximum speed on the curve in evaluating the design and operating speed consistency and safety aspects of two-lane undivided rural highways passing through mountainous terrain. The following tasks were performed to achieve this objective.

1. To understand and address the issues in collecting the naturalistic trajectory data from the curves located in mountainous terrain. The review of existing videography-based naturalistic trajectory data collection approaches found that they are not suitable for collecting trajectory data on horizontal curves located in mountainous regions. In this task, a multiple homography approach was proposed that enables the researches to collect vehicle trajectories on the horizontal curves accurately. The proposed approach was evaluated using the existing single homography approach.
2. To understand and model the speed variability on the horizontal curves. In this task, operating speed profile models, statistical test for speed variables (V_{Max}, V_{Min}, V_{CC}) and their locations, and the analysis of acceleration and deceleration length were performed

to understand the speed variability on the curve. Considering the speed variation on the curve, MaxΔ_{85}V was modeled, and important determinants were found.

3. To develop operating speed correction models for 85th percentile minimum and maximum speed on the curve. In this task, with reference to the speed at center of the curve, two operating speed correction models were developed. One model is for estimating the correction factor for minimum speed, and another is for maximum speed on the curve.
4. To assess the role of minimum and maximum operating speeds in design consistency and safety evaluation. In this task, the role of V_{Min}^{85} and V_{Max}^{85} in the safety and consistency evaluation of horizontal curves were assessed through the endangerment level proposed by Lamm and crash frequency modeling.

1.4 Scope of the study

The scope of the study is limited to horizontal curves constituting the two-lane undivided rural highways passing through mountainous terrain. The data used and the results presented in this study are limited to daylight and dry weather conditions.

1.5 Organisation of the report

The thesis is organized into seven chapters. The first chapter presents an "Introduction" followed by the need and objectives of the study. The second chapter presents the literature review corresponding to trajectory data collection on the horizontal curves, geometric design consistency approaches and operating speed models for geometric design consistency and safety. The third chapter, "Data collection," proposes a multiple homography approach for collecting naturalistic vehicle trajectories from the horizontal curves located on mountainous terrain. Further, the chapter provides a description of field data collection and the extraction of microscopic data. The fourth chapter deals with the analysis and modelling of speed variability on the horizontal curves. The operating speed correction models for correcting the estimated operating speed corresponding to the centre of the curve are presented in the fifth chapter. The sixth chapter presents the assessment of geometric design consistency and safety, and the last chapter presents the conclusion and future scope of the present study.

भारतीय प्रौद्योगिकी संस्थान गुवाहाटी
Indian Institute of Technology Guwahati

2 Literature Review

2.1 Introduction

Geometric design consistency assessment is useful in analyzing the safety aspects of two-lane undivided rural highways. Analyzing the safety is specifically important for the two-lane undivided rural highways passing through mountainous terrain, where the design of complex geometric elements is constrained by the terrain. Speed data observed from the field, as well as the consistency measure, play a crucial role in assessing the geometric design consistency. This chapter presents a review of various methodologies used in consistency evaluation. Further, a review of various data collection approaches and their implications in the consistency and safety evaluation are reviewed.

2.2 Geometric design consistency

Geometric design consistency is defined as the conformance of the highway's geometric and operational features with the driver's expectancy (Alexander 1986). Al-Masaeid et al. (1995) defined consistency as the degree to which highway systems are designed and constructed to avoid critical driving maneuvers which can lead to unnecessary accident risk. A consistent geometric alignment ensures that the successive geometric elements act in a coordinated way so and produces harmonized driving performance without surprising events (Gibreel et al. 1999). A geometric alignment is inconsistent when a driver makes abrupt speed adjustments due to the events that surprise while traversing a geometric element. Thus, the aim of geometric design consistency is to identify the faulty geometric elements in a highway alignment that do not conform to the drivers' expectations.

Various consistency measures were developed to evaluate a particular geometric element/entire highway alignment. The consistency measures are broadly classified based on the parameters such as alignment indices, driver workload, vehicle stability, and operating speed (Anderson et al. 1999; Gibreel et al. 1999; Hassan et al. 2001). Table 2.1 presents the available consistency measures for evaluating geometric elements/alignment.

Table 2. 1 Various consistency measures proposed for evaluating geometric elements/alignment

Details of the studies	Approach	Consistency measures
Fitzpatrick et al. (2000a)	Alignment indices	Average radius (AR)
		Ratio of maximum radius to minimum radius (RR)
		Ratio of individual curve radius to average radius (CRR)
		Average rate of vertical curvature (AVC)
Wooldridge et al. (1999 & 2000)	Driver workload	Percentage of time a driver observes the roadway
Messer (1980); Taylor and Thompson (1977)		Critical rating
Heger (1995); Furedy et al. (1992); Cafiso et al. (2004)		Psychophysiological parameter analysis
Mc Lean 1974; Morrall and Talarico 1994; Lamm et al. (1995)	Vehicle stability	Difference between supplied and demanded side friction
Vehicle speed consideration		
Leisch (1977); Lamm et al. (1988 & 1995); Fitzpatrick et al. (1997)	Operating speed-based indices	Design speed consistency
		Operating speed consistency (ΔV_{85})
Hirsh (1987)	Individual speed profiles	85th percentile speed differential ($\Delta_{85}V$)
McFadden and Elefteriadou (2000)		85th percentile maximum speed reduction (85MSR)
Polus and Matter-Habib (2004); Garach et al. 2014; Camacho-Torregrosa et al. (2013); Gracía et al. (2013)	Operating speed profiles based-indices	Normalized relative area (Ra)
		Standard deviation of operating speeds (σ)
		Average operating speed ($\bar{\upsilon}_{85}^2$)
		Average speed reduction ($\overline{\Delta v_{85}}$).
		Inertial consistency index (ICI)

2.3 Consistency evaluation using the Alignment Indices

Alignment indices are the quantitative measures that evaluate the general character of all the horizontal or vertical curves in a particular highway alignment. Fitzpatrick et al. (2000a) have proposed several alignment indices for measuring the design consistency of a highway alignment. The alignment indices include the average radius, the ratio of maximum radius to the minimum radius, the ratio of individual curve radius to the average radius, and the average rate of vertical curvature (Lamm et al. 1986; Anderson et al. 1999; Fitzpatrick et al. 2000a; Hassan et al. 2001). The average radius expresses the sharpness of the horizontal curves in a highway alignment. The ratio of maximum radius to minimum radius determines the range of

the radii corresponding to a highway alignment. The basic assumption behind this alignment index is that the ratio can represent the consistency of the design in terms of the use of similar horizontal radii along the alignment.

The first two alignment indices deal with the consistency evaluation of an entire highway alignment by combining all the horizontal curves, whereas the alignment index evaluates individual horizontal curves. On the other hand, the average rate of vertical curvature deals with the consistency corresponding to all the vertical curves in a highway alignment. It indicates the amount of change in the vertical alignment of a roadway. The basic assumption behind this alignment index is, there exists a significant relation between the amount of hilliness, the adopted speeds, and safety (Anderson et al. 1999). Thus, the four alignment indices together evaluate the entire highway alignment based on the horizontal and vertical curves. Nevertheless, there are concerns associated with the alignment indices. First, if the maximum radius of a single horizontal curve in a highway alignment is different from the radii of other horizontal curves, the curve with the maximum radius may be shown to be inconsistent. Second, the alignment indices do not recognize the effect of other geometric variables such as curve length and solely depend on the radii of the horizontal curves. Third, they do not consider the impact of the approach and departing tangents, and transition curves. Fourth, they do not consider the role of vehicle interaction with road infrastructure. Fifth, the alignment indices are considerably affected by a sharp flat curve. Moreover, these measures lack qualitative criteria such as good, fair and poor (Anderson et al. 1999; Hassan et al. 2001).

2.4 Consistency evaluation based on the Driver Workload

The abrupt changes in the features of geometric elements in an alignment might lead to increased driver workload for traversing the alignment safely. Increased driver workload is a proxy for design inconsistency, and it might result in more crashes. A few studies have measured the driver workload through critical rating factors and identified hazardous locations (Taylor and Thompson 1977; Messer 1980). Few others have performed psychophysiological parameter analysis through Electrocardiogram (ECG), video recording of driver activity and other sensors while driving to evaluate the driver workload (Furedy et al. 1992; Heger 1995; Cafiso et al. 2004). Despite the importance of driver workload in evaluating design consistency, analytical methods are not readily available to quantify the driver workload. However, Wooldridge et al. (1999 & 2000) have measured the visual demand as a percentage of time a driver observes the roadway. Then, analytical models that relate the visual demand to the curve

radius were developed (Hassan et al. 2001). The model results portrayed that design consistency based on predicted visual demand will always be biased against the designs with lower design speed. Further, driver workload is much less used than any other consistency measure because of its high degree of measurement difficulty (Camacho-Torregrosa et al. 2013). Thus, Hassan et al. (2001) suggested that a criterion based on design speed would be more appropriate for evaluating geometric design consistency.

2.5 Consistency evaluation based on the Vehicle Stability

Vehicle stability is another measure that is explicitly focused on the geometric design consistency of horizontal curves. This criterion assumes that, vehicles traversing the horizontal curves will experience centrifugal forces, and the excessive centrifugal forces could result in a vehicle rollover and head-on collisions (Mc Lean 1974; Morrall and Talarico 1994; Lamm et al. 1999; Hassan et al. 2001). The centripetal force applied to traverse the horizontal curve is sustained by the side friction between the vehicle's tires and pavement, and by a component of gravity, if the road is superelevated. A few studies have developed models for side friction demand as a function of speed, degree of curve and distance (McLean 1974; Lamm et al. 1991; Morrall and Talarico 1994). Lamm et al. (1995) recommended vehicle stability as a safety criterion to evaluate the design consistency of horizontal curves based on supplied and demanded side friction. Based on the difference between the supplied (f_{RA}) and demanded (f_{RD}) side friction, they qualitatively defined a particular geometric element as good, fair or poor. Table 2.2 presents Lamm's safety criterion for evaluating the geometric elements. Nevertheless, the differences between supply and demand frictions are generally biased towards the horizontal curves with higher design speeds. Moreover, the side friction is not as easy to recognize and measure as operating speed (Hassan et al. 2001; Donnell et al. 2016).

Table 2. 2 Vehicle stability - safety criterion-III (Lamm et al. 1995)

Frictional difference	Design quality	Recommendations
$+0.01 \leq f_{RA} - f_{RD}$	Good	Consistency; No corrections are required
$-0.04 \leq f_{RA} - f_{RD} \leq +0.01$	Fair	Minor inconsistency; Traffic warning devices required
$f_{RA} - f_{RD} \leq -0.04$	Poor	Strong inconsistency; Redesign recommended

Using Lamm's safety criterion-III, a few studies have evaluated the vehicle stability on horizontal curves located in plain, rolling and mountainous terrains (Hassan et al. 2001; Richl

and Sayed 2005; Žilionienė and Vorobjovas 2011; Wang et al. 2013). All these studies have considered speed at the center of the curve to estimate the demanded side friction.

2.6 Consistency evaluation using the operating speed

Vehicle speed is one of the characteristics that reflect the driver's expectation of the road geometry (Lamm and Choueiri 1987; Andjus and Maletin 1998; AASHTO 2011; Jacob and Anjaneyulu 2013; Shallam et al. 2019). Further, crash statistics reveal that the vehicle speed is a major contributing factor to crashes. Considering the importance of vehicle speed in geometric design and safety, several consistency measures were developed using the individual vehicle speed. Operating speed estimated using the spot speeds, and the operating speed profiles were used in assessing the consistency.

The Manual on Uniform Traffic Control Devices (MUTCD) defined operating speed (V^{85}) as “a speed at which a typical vehicle or the overall traffic operates”. Likewise, the American Association of State Highway and Transportation Officials (AASHTO, Green Book 1994) defined the operating speed as “the highest overall speed at which a driver can travel on a given highway under favorable weather conditions and prevailing traffic conditions”. Later in 2001, the AASHTO refined the definition as “the speed at which drivers are observed operating their vehicles during free-flow conditions”, and the same definition is being used till date (AASHTO Green Book 2001, 2004, 2011, 2018). Researchers and practitioners often used the 85th percentile of the free-flow distribution of speeds collected at a particular location as operating speed (AASHTO 2004). The 85th percentile speed is the speed at or below which 85% of the drivers operate without any restrictions under favorable conditions. The assumption underlying the 85th percentile speed is that most drivers operate their vehicles at speeds they perceive to be safe. Two widely used consistency measures called “design speed consistency” and "operating speed consistency" were developed using the operating speed.

Operating speed prediction models play a crucial role in estimating the operating speeds that later to be used for consistency evaluation (Misaghi and Hassan 2005). Several operating speed models were developed, and they can be classified based on vehicle type and type of terrain. Considering vehicle type, several models were developed for cars (Lamm and Choueiri 1987; Lamm et al. 1995; Krammes et al. 1995; Andjus and Maletin 1998; Fitzpatrick et al. 2000a; Misaghi and Hassan 2005; Castro et al. 2011; Jacob and Anjaneyulu 2013; Nalo et al. 2020; Shallam et al. 2021; Goyani et al. 2022), and for trucks (Lamm and Choueiri 1987; Morrall and Talarico 1994; Al-Masaeid et al. 1995; Donnell et al. 2001; Misaghi and Hassan

2005; Shallam et al. 2021). Considering the terrain type, several models were developed for the highways located in plain terrain (Krammes et al. 1995; Guzman 1996; Andjus and Maletin 1998; Lamm et al. 2001; Fitzpatrick et al. 2000a; Jacob and Anjaneyulu 2013; Nalo et al. 2020), rolling terrain (Dhahir and Hassan 2019a), and mountainous terrain (Fitzpatrick et al. 2000a; Lamm et al. 2001; Dhahir and Hassan 2019a; Shallam et al. 2021; Goyani et al. 2022). The explanatory variables in these models vary from study to study. It was also observed that the operating speed corresponding to the vehicle type varies depending on the location and terrain conditions (Leisch and Leisch 1977; Jacob and Anjaneyulu 2013; Nalo et al. 2020; Shallam et al. 2021; Goyani et al. 2022).

2.6.1 Design speed consistency

Design speed consistency evaluates individual geometric elements based on the difference between design and operating speeds (Lamm et al. 1995). The basic hypothesis behind this consistency measure is the supply and demand concept, i.e., how far the driver's expectations are met with the geometric design through operating and design speed (Lamm et al. 1988). The design speed (V^D) is defined as the selected speed to determine various geometric design features of the roadway (AASHTO 2011). In the highway design guidelines, the design speed is selected based on the road class, topography, and land use such that the design speed would be consistent with the anticipated operating speed (AASHTO 2018). In the design of horizontal curves, the speed is assumed to be constant along the curve (Krammes et al. 1995; AASHTO 2018).

Leisch (1977) was the first to study the difference between the operating and design speeds on a horizontal curve and concluded that for a safe vehicle operation the speed difference should not exceed 15 km/h. Later, Lamm et al. (1988 & 1995) defined speed difference ranges corresponding to various safety levels based on operating and design speeds collected from several highways located in different countries. Based on the speed difference range, a particular geometric element was evaluated qualitatively as either good, fair, or poor (Table 2.3). In the Table, V_i^{85} is the operating speed of the i^{th} geometric element and V_i^D is the design speed of the i^{th} geometric element. Fitzpatrick et al. (1997) have studied the relationships between design speed, operating speed, and posted speed on two-lane rural highways. They found that, V^{85} on the horizontal curves was less than V^D for all the curves with $V^D > 70$ km/h, and greater than V^D for most curves with $V^D < 70$ km/h. Similar to Lamm's design consistency criterion, Jacob et al. (2013) have proposed speed boundaries based on accident severity.

Operating Speed Deviation from Design Speed (ODD) was considered as a consistency metric, and Equivalent Property Damage Only (EPDO) crashes were considered for accident severity. Three ranges were proposed to evaluate a geometric element as good, fair and poor. The proposed ranges for design speed consistency are similar to Lamm's criterion. Using Lamm's safety criterion-I, few studies have evaluated the design speed consistency of highway elements located in plain, rolling, and mountainous terrains (Hassan et al. 2001; Richl and Sayed 2005; Castro et al. 2008; Zilioniene and Vorobjovas 2011; Wang et al. 2013; Chaudhari et al. 2022; Goyani et al. 2022). All these studies have considered speed at the center of the curve to estimate V^{85}.

Table 2. 3 Design speed consistency - safety criterion-I (Lamm et al. 1995)

Speed difference (km/h)	Design quality	Recommendations
$\|V_i^{85} - V_i^D\| \leq 10$	Good	Consistency; No corrections are required
$10 < \|V_i^{85} - V_i^D\| \leq 20$	Fair	Minor inconsistency; Traffic warning devices required
$\|V_i^{85} - V_i^D\| > 20$	Poor	Strong inconsistency; Redesign recommended

2.6.2 Operating speed consistency

Operating speed consistency evaluates two successive geometric elements based on the difference between the corresponding operating speeds (tangent to curve/ curve to tangent/ curve to curve). The basic hypothesis behind this criterion is that, a well-balanced operating speed sequence between successive geometric elements promotes a consistent and harmonized driving performance such that the drivers traverse the geometric elements safely (Fitzpatrick et al. 2000b; Lamm et al. 2007). Lamm et al. (1988) studied the operating speed difference between three combinations of successive geometric elements such as tangent to curve, curve to tangent, and curve to curve. Later, Lamm et al. (1995) defined speed difference ranges to evaluate successive geometric elements of a highway alignment. The successive geometric elements were evaluated qualitatively as either good, fair, or poor, based on the speed difference (Table 2.4). In the Table, V_i^{85} is the operating speed of the i^{th} geometric element and V_{i+1}^{85} is the operating speed of the $i+1^{th}$ geometric element. Using Lamm's safety criterion-II, a few studies have evaluated the operating speed consistency of successive geometric elements (tangent to curve) in a highway alignment located in plain, rolling, and mountainous terrains (Hassan et al. 2001; Richl and Sayed 2005; Castro et al. 2008; Zilioniene and Vorobjovas 2011; Wang et al. 2013).

Table 2. 4 Design speed consistency - safety criterion-II (Lamm et al. 1995)

Speed difference (km/h)	Design quality	Recommendations
$\lvert V_i^{85} - V_{i+1}^{85} \rvert \leq 10$	Good	Consistency; No corrections are required
$10 < \lvert V_i^{85} - V_{i+1}^{85} \rvert \leq 20$	Fair	Minor inconsistency; Traffic warning devices required
$\lvert V_i^{85} - V_{i+1}^{85} \rvert > 20$	Poor	Strong inconsistency; Redesign recommended

Similar to Lamm's operating speed consistency criterion, Jacob et al. (2013) have proposed speed boundaries based on accident severity. They considered Speed Reduction from the approach tangent to the midpoint of the curve ($SR_{AT\text{-}MC1}$) as a consistency metric and related it with Equivalent Property Damage Only (EPDO) crashes. Three ranges were proposed to evaluate the successive geometric elements as good, fair or poor. The proposed ranges for operating speed consistency are observed to have a speed increment of 5 km/h compared to Lamm's operating speed consistency criterion.

2.7 Consistency evaluation using operating speed profiles

Polus and Matter-Habib (2004) have developed two consistency measures using the operating speed profile data. The first was based on the normalized relative area (R_a) bounded between the speed profile and the average speed. Figure 2.1 shows the areas bounded between the speed profile and the average operating speed, denoted by a_i. Where, $\sum_{i=1}^{n} a_i$ is the sum of absolute areas bounded between the speed profile and the average operating speed (m^2/s); L is the entire segment length (m). The other measure was the standard deviation of operating speeds (σ) along the highway. The standard deviation is the most appropriate statistical measure of the data distribution around the mean value. The average operating speed, V_{avg}, was computed as the average weighted speed, by length, along the entire segment. This measure was proposed to complement the first measure (R_a) because, in a few cases, the R_a by itself provides similar results for different road characteristics.

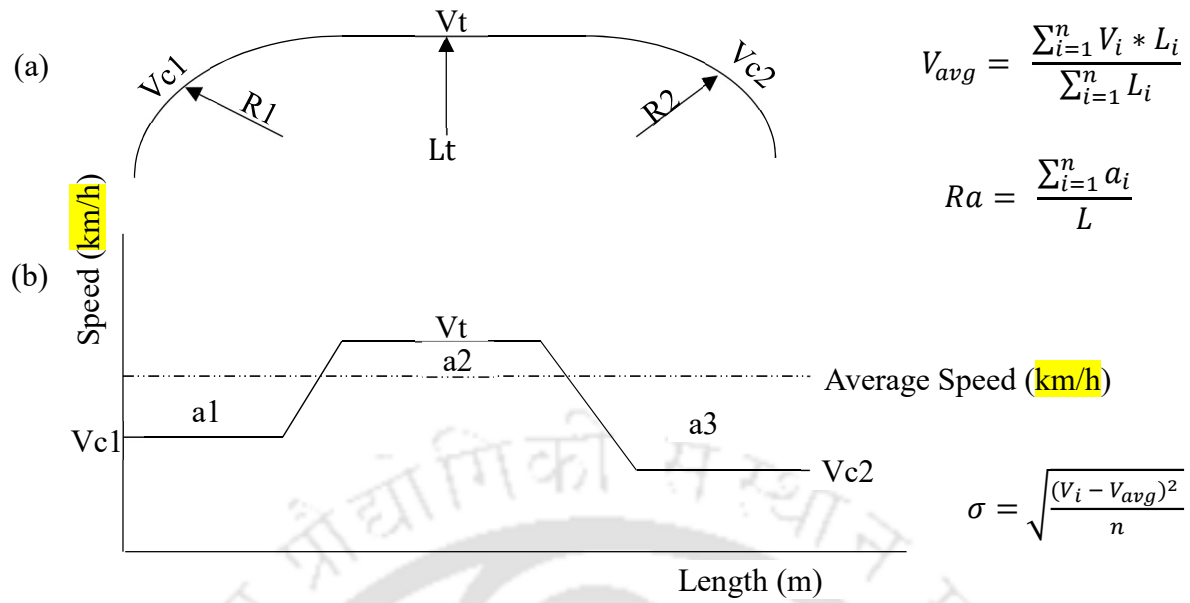

Fig. 2. 1 Speed profile-based consistency measures (a) Example road section; (b) Example speed profile (Polus and Mattar-Habib 2004)

The basic hypothesis behind these measures is that, for constantly changing geometric characteristics along any section of a road, there will be continuous changes in the speeds of vehicles. The main advantage of operating speed profile-based consistency measures is that they consider the operating speed corresponding to the overall road segment. However, the consistency measures and their thresholds proposed based on operating speed profile data have several issues. First, the consistency measures were developed based on the operating speed profile, where the speed profile was established using the previously developed operating speed models by Krammes et al. (1995) for curves and by Polus et al. (2000) for tangents. Second, the developed measures and thresholds were limited to highways in plain and rolling terrain. Third, the effect of vertical alignment on consistency was not considered. Further, the proposed consistency model (C_2) is far more restrictive in predicting crashes because it was developed based on an exponential function, in which C_2 decreases rapidly with the increase in consistency measures (Garach et al. 2014). Thus, Garach et al. (2014) developed a new consistency model (C_4) with hyperbolic function, and new thresholds were proposed to evaluate the highway alignment.

Similar to Polus and Matter-Habib (2004), Camacho-Torregrosa et al. (2013) developed several consistency measures based on the operating speed profile and proposed a design consistency index based on average operating speed ($\bar{\upsilon}_{85}^2$) and average speed reduction variables ($\overline{\Delta v_{85}}$). This consistency index was developed based on the operating speed and

acceleration/deceleration models proposed by Pérez-Zuriaga et al. (2010) and Pérez-Zuriaga et al. (2011). However, they have not proposed any consistency thresholds for evaluating the highway alignment. Another study by García et al. (2013) presented a consistency measure based on the hypothesis that design consistency may be defined as the difference between driver's expectations and road alignment behavior. The developed consistency measure was confined to the highways passing through plain terrain. In this study, the driver's expectations were estimated as the average operating speed in the previous 1km of the road segment (inertial operating speed), and road alignment behavior was estimated as operating speed at a point. Three thresholds were established based on the crash rates and consistency measure to evaluate the tangent to curve transitions as good, fair and poor. But, the effect of vertical alignment was not considered in developing the consistency index.

2.8 Consistency evaluation using individual speed profiles

In most of the earlier studies, geometric design consistency was evaluated using the speed data collected at specific locations on the geometric elements. The main reason for this is collecting the data at the curve center is relatively easier (Krammes et al. 1995; Passetti and Fambro 1999). Further, these studies primarily assume that the vehicle speed on the curve remains constant and the complete acceleration and deceleration take place on the tangents. However, Hirshe (1987) assessed ΔV_{85} and suggested that the driver corresponding to the 85th percentile speed on the approach tangent may not be the same as the driver corresponding to the 85th percentile speed on the curve. Thus, he has hypothesized that the 85th percentile speed reduction ($V_i^{85} - V_{i+1}^{85}$ i.e., ΔV_{85}) would underestimate the actual speed reduction experienced by each individual driver (Δ_{85}V).

McFadden and Elefteriadou (2000) have investigated the implications of using ΔV_{85} for geometric design consistency evaluation. For this, spot speed data were collected at nine locations on the approach tangent and curve. The study then estimated ΔV_{85}, $\Delta_{85}V$, $85S9$, and 85th percentile maximum speed reduction (85MSR) to compare the speed reduction based on data from two locations versus nine locations. The results have shown that Hirshe's hypothesis on the use of $\Delta_{85}V$ is valid. Further, collecting speed data at multiple locations has yielded the actual speed reduction (85MSR) experienced by the drivers as compared to the speed reduction ($\Delta_{85}V$) based on spot speed data collected at two specific locations on the curve and approach tangent. The speed reduction model (85MSR) was modeled using the speed at the approach tangent, curve radius, and length of the approach tangent. The speed reduction measures $\Delta_{85}V$,

and 85MSR works on the same principle, i.e., both measures calculate the speed difference between successive geometric elements based on each individual driver. The only difference between the two approaches is that $\Delta_{85}V$ is obtained only if the spot speeds corresponding to each vehicle were taken at the approach tangent and center of the curve. Whereas 85MSR can be obtained only if continuous speed profile data of individual vehicles are available from the approach tangent to the curve. The maximum speed difference between the approach tangent and curve corresponding to each individual vehicle was estimated by identifying the maximum speed on the approach tangent and the minimum speed on the curve. However, in some of the later studies, $\Delta_{85}V$ was estimated as the 85th percentile of individual difference between maximum speed on the approach tangent and minimum speed on the curve. ΔV_{85} was estimated as the difference between the 85th percentile of maximum speed on the approach tangent and minimum speed on the curve.

Considering the importance of speed data collection at multiple locations on a geometric element, several studies have collected individual speed profiles using either instrumented vehicles or driving simulators. The following subsections present the study of individual speed profile-based driver behavior through the 85th percentile of maximum speed reduction and 85th percentile of minimum and maximum speed models.

2.8.1 85th percentile of maximum speed reduction

Bella (2007) has collected continuous speed profile data using a driving simulator to evaluate $\Delta_{85}V$ and 85MSR. The $\Delta_{85}V$ was estimated from two fixed locations, one on the approach tangent and the other on the curve. Whereas 85MSR was estimated by considering the speed profile from 200m of the approach tangent to the curve and taking the difference between maximum speed on the approach tangent and minimum speed on the curve. The study found that 85MSR is statistically greater and more reliable than $\Delta_{85}V$. Length of the approach tangent, radius, and speed on the approach tangent was found to be significant in explaining the variability of 85MSR.

Pérez-Zuriaga et al. (2010) have evaluated the speed reduction variables (ΔV_{85}, $\Delta_{85}V$) using continuous speed profiles collected from cars equipped with GPS. The study section was a two-lane rural highway with longitudinal grades not exceeding 4%. The study found that ΔV_{85} underestimates the actual speed reduction from the tangent to the curve. Further, the deceleration rate was modeled from the tangent to the curve and found that the radius of the

curve and CCR as explanatory variables. The study also observed that the vehicles decelerate on an average upto 45% of the curve length.

Pérez-Zuriaga et al. (2013) evaluated the speed variation from tangent to curve transitions through speed reduction variables (ΔV_{85}, $\Delta_{85}V$) for the two-lane rural roads with longitudinal grades ranging from -6.3% to 5.7%. Continuous speed profiles corresponding to cars were collected using GPS. The study found that ΔV_{85} underestimates the actual speed reduction from the tangent to the curve by 0.9 times of $\Delta_{85}V$. Further, the estimated 85th percentile deceleration rates from the tangent-curve transition have ranged between 0.3 to 1.7 m/s^2. The analysis of the deceleration length and its location for all the drivers found that 24.68% of the drivers started deceleration before the curve and ended on the curve. Fifteen percent of the drivers started deceleration before the curve and ended it on the departing transition curve. Moreover, the study attempted to model the deceleration length with geometric characteristics, but none of the variables were found to be statistically significant.

Montella et al. (2014a) collected continuous speed profiles of cars using driving simulators corresponding to two-lane highways in level terrain. The test route consisted of twenty 1000m long tangents and twenty 400m long curves of 190m radius. This study investigated the constant speed assumption on the curve through operating speed profiles and individual speed profiles. The operating speed profile was developed by assuming a linear speed profile between the change points (starting/ending of deceleration and ending/starting of acceleration points). ΔV_{85} and $\Delta_{85}V$ were estimated after identifying the change points in the operating speed and individual speed profiles. Further, the estimated 85th percentile of deceleration and acceleration rates of individual drivers were found to be approximately double the deceleration (1.30 Vs 0.66m/s^2) and acceleration (0.85 Vs 0.37 m/s^2) rates corresponding to the operating speed profile. Further, they found that 29% and 74% of the drives have decelerated and accelerated on the curve, respectively.

Bella (2014) verified the assumption of constant speed using the simulated speed profiles corresponding to 26 configurations of 3 two-lane rural roads. The study found that the driver traveled at a constant speed from the point of curvature to the center of the curve and accelerated from the center of the curve to the point of transition. Then the study estimated the deceleration rates and acceleration rates for individual drivers as well as using the operating speed profiles. The results showed that the rates estimated using operating speeds are considerably lower than that were estimated using individual speed profiles. The speed profiles

showed that, 24% and 74% of the drivers completed their deceleration on the approach transition curve and the curve, respectively.

Montella et al. (2014b) developed operating speed reduction models ($\Delta_{85}V$) using the continuous speed profiles collected from instrumented cars. The study showed that individual driver's maximum speed reduction ($\Delta_{85}V$) was greater than the operating speed difference in the tangent to curve transition. Thus, $\Delta_{85}V$ was modeled as a function of geometric variables and found deflection angle, gradient, and CCR as explanatory variables. For the curves with a radius of less than 400m, they found that 52% of the drivers started deceleration on the approach tangent and ended on the curve; and 90% of the drivers started accelerating on the curve and ended on either departing transition curve or departing tangent. Thus, the study concluded that the speed on the curve is not constant.

Dhahir and Hassan (2019b) used instrumented vehicles to collect the speed data on horizontal curves of two-lane highways passing through rolling and mountainous terrains. Speed reduction models were developed corresponding to ΔV_{85}, $\Delta_{85}V$, and 85MSR as a function of geometric variables. They found that the radius of the curve, length of the curve, posted speed limit, and terrain type was statistically significant in modeling the speed variables. Further, they evaluated the speed reduction variables using the crash frequency models. $\Delta_{85}V$ was found to be relatively more significant in modeling the crash frequency compared to the other two variables. However, for developing these models, they combined the data collected from rolling and mountainous terrain.

Choudhari and Maji (2019) studied the effect of horizontal curve geometry on the 85MSR for plain terrain using a driving simulator. The maximum speed at the approach tangent (200m before the point of curvature) and minimum speed on the curve, corresponding to each individual driver was used to estimate the 85MSR. The curvature (1/R) and approach tangent length were found to be significant in modeling the 85MSR.

Malaghan et al. (2021) have explored the speed variability on a two-lane undivided rural highway located in plain terrain using individual speed profiles collected through cars and buses equipped with GPS. From the tangent, they have extracted the maximum speed and the speed corresponding to the location 200 m ahead of the PC. From the curve, the minimum speed (V_{Min}) and speed at the center of the curve (V_{CC}) were extracted. The study found that the maximum speed and minimum speed positions are distributed over the entire tangent and curve, respectively. Thus, Malaghan et al. (2020 & 2022a) considered maximum speed on the

tangent and minimum speed on the curve to estimate the operating speed reduction (ΔV_{85}, $\Delta_{85}V$). The study evaluated the two-speed reduction variables and developed an operating speed reduction model corresponding to $\Delta_{85}V$. The relation between the two-speed reduction variables found that $\Delta_{85}V$ for car and bus is higher than ΔV_{85} by 5.32 km/h and 5.01 km/h, respectively. Radius of the curve was found to be significant in modeling $\Delta_{85}V$ of cars. Radius, degree of curve and approach tangent length were found as explanatory variables for the bus.

From the above studies, it is clear that ΔV_{85} does not capture the actual speed reduction between successive geometric elements. Further, the 85th percentile of the speed difference between maximum speed on the approach tangent and minimum speed on the curve (85MSR/ $\Delta_{85}V$) yielded actual speed reduction. However, no study has evaluated the relevance of 85MSR/ $\Delta_{85}V$ in the geometric design consistency evaluation.

2.8.2 85th percentile of minimum and maximum speed

Dhahir and Hassan (2018) evaluated the constant speed assumption on the curve through minimum and maximum speed. They collected the data from the horizontal curves located in rolling and mountainous terrain using instrumented vehicles (cars and light trucks). The study concluded that the speed is not constant on the curve as there is a significant difference between the two-speed variables. However, in a later study, Dhahir and Hassan (2019a) found that there is no statistical difference between the speed at the center of the curve and the minimum speed on the curve. They also found that there is no difference in the speed at the beginning of the curve and the maximum speed on the curve. Further, three operating speed models were developed corresponding to speed at the center of the curve (V_{CC}), minimum speed on the curve (V_{Min}), and maximum speed on the curve (V_{Max}). The study also found that there is no effect of turning direction on the drivers traversing the curve. Further, they have suggested that the consistency evaluation needs to consider the speed variables, V_{Min} and V_{Max}.

Pérez-Zuriaga et al. (2010) have used minimum speed on the curve to develop operating speed models. The continuous speed profiles were collected using instrumented cars. The study found that the radius of the curve and curvature change rate (CCR) are significant in modeling the minimum operating speed. Bella and Agostini (2010) used continuous speed profiles from the driving simulators and developed operating speed models. The study modeled minimum operating speed and found CCR as an explanatory variable. Montella et al. (2014b) developed operating speed models using the continuous speed profiles of cars. The study was conducted on a four-lane divided highway with a longitudinal grade not exceeding ±6.35%. The minimum

speed on the curve was modeled as a function of geometric variables. The study found that curve radius, gradient, and CCR were significant in modeling the minimum operating speed.

Llopis-Castello et al. (2018) developed operating speed models for loaded and empty trucks on horizontal curves of two-lane rural roads using minimum speed on the curve. The study collected continuous speed profiles using instrumented vehicles on 11 road sections with average longitudinal grades ranging between -6% to +7.3%. The model results corresponding to loaded and empty trucks showed that the curve radius and gradient at the point of curvature significantly influence the operating speed. The study found that loaded trucks were more influenced by vertical alignment, and empty trucks were more influenced by horizontal alignment. Malaghan et al. (2020 & 2022a) have collected continuous speed profiles of cars and buses equipped with GPS from two-lane undivided rural highways in plain terrain. In this study, the minimum speed on the curve was used to estimate the operating speed on the curve. The study developed vehicle-specific operating speed models for cars and buses. The curve radius, length of the curve, and degree of the curve were significant in modeling the operating speed of a car. The curve radius, degree of curve and approach tangent length were significant in the case of a bus. All these studies have developed operating speed models based on the 85th percentile of minimum and maximum speed on the curve. However, no study has used these speed variables to evaluate the consistency of geometric elements.

2.9 Data collection approaches for geometric design consistency

Researchers used a wide variety of data collection approaches for carrying out geometric design consistency research. This section performs a comprehensive review of various approaches used for speed data collection.

2.9.1 Spot speed data collection approaches

In the geometric design consistency research, radar guns, LiDAR, electronic counters, and trap-length are commonly used to collect the spot speed of a vehicle. Several studies have used radar guns to collect speed at specific locations (Krammes et al. 1995; Andjus and Maletin 1998; Shallam et al. 2021; Chaudhari et al. 2022; Goyani et al. 2022). For instance, Krammes et al. (1995) collected spot speed data of cars using radar guns at specific locations on the approach tangent and curve, i.e., at the midpoint of the approach tangent and at the center of the curve. Andjus and Maletin (1998) have collected spot speed data of cars using radar guns at specific

locations on the curve, i.e., at the beginning of the transition curve, the midpoint of the curve and the end of the transition curve.

LiDAR guns are similar to that of radar guns but work by sending out pulses of light and measure vehicle speed based on the returned reflection pulses that bounce off the vehicle. McFadden and Elefteriadou (2000) have collected spot speed data of cars using LiDAR guns at every 50m on the approach tangent and at PC, CC and PT on the curve. However, Radar/LiDAR guns have several issues (Misaghi and Hassan 2005). First, the cosine errors are induced by the deviation between the beam of the radar/LiDAR gun and the actual driving direction. Second, human error while operating the guns for measuring speeds. Third, the presence of personnel and the equipment in the field could bias the actual driving behavior.

Electronic counters are also used to collect vehicle speed data at a particular location on the road section (Passetti and Fambro 1999; Fitzpatrick et al. 2000a; Misaghi and Hassan 2005). They are installed on the road such that vehicle speed is recorded based on the vehicle's wheelbase, the number of axles and axle spacing. Further, based on wheelbase and number of axles, vehicles are classified. For instance, Misaghi and Hassan (2005) collected vehicle speeds of cars, light trucks, and heavy trucks by installing electronic counters at the midpoint of the approach tangent, departing tangent, and center of the curve. Trap length is another approach used to collect spot speed data at specific locations (Al-Masaeid et al. 1995; Jacob and Anjaneyulu 2013; Sil et al. 2020). The speed at a particular location is measured as the time required to traverse a specific length of the road section. The trap length is marked on the field, and the time taken to traverse the trap length is recorded either by using a stopwatch or from a video footage. Al-Masaeid et al. (1995) used a 40 m trap length and measured the time taken to traverse with a stopwatch. Jacob and Anjaneyulu (2013) used a trap length of 15 to 20 m on the approach tangent and a trap length of 10 m on the center of the curve and measured the speed of various vehicle categories. Sil et al. (2020) used a 15m trap length and videography data to collect the speed of cars, light commercial vehicles, and heavy commercial vehicles at the center of the curve, point of curvature, and 50m before the point of curvature.

Thus, the above approaches allow the researchers to collect speed at specific locations, mostly at the midpoint of the approach tangent and the centre of the curve (Lamm and Choueiri 1987; Krammes et al. 1995; McFadden and Elefteriadou 2000; Park et al. 2003; Misaghi and Hassan 2005; Jacob and Anjaneyulu 2013; Shallam et al. 2019 and 2021). The analyses based on such data make assumptions such as the vehicles maintain a constant speed on the curve,

and deceleration and acceleration take place at approach and exit tangents (Lamm et al. 1999). McFadden and Elefteriadou (2000) revealed that the speed collected at specific points doesn't reveal the actual speed variability on any geometric element.

The limitations of the spot speed data can be overcome with continuous vehicle tracking using advanced data collection techniques such as instrumented vehicles, LiDAR (Light Detection and Ranging), driving simulators, and videography-based image-processing techniques (Fung et al. 2003; Bella 2008; Pérez-Zuriaga et al. 2010; Sun et al. 2018; Wu et al. 2019; Amrutsamanvar et al. 2021; Shallam et al. 2019; Malaghan et al. 2021).

2.9.2 Continuous speed data collection approaches

Collecting microscopic details of all the vehicles in a traffic stream without imposing any constraints on the driver/not attracting the driver's attention during the data collection process can be called Naturalistic Driving (ND) data (Fitch and Hanowski 2012; Bärgman 2016). Continuous vehicle tracking enables the researchers to collect microscopic details of the vehicle operation. Instrumented vehicles collect data on vehicle characteristics in the form of trajectories throughout the alignment. This data have been studied by the researchers to develop operating speed models on tangents and curves (Pérez-Zuriaga et al. 2010; Llopis-Castelló et al. 2018; Malaghan et al. 2020), determine the track patterns on the horizontal curves and its relevant risks (Xu et al. 2018), evaluate path radius adopted by driver traversing the horizontal curve with reference to the design radius of the curve (Shallam et al. 2019), and most importantly explore the speed variables and their positions on the horizontal curves and the tangent sections for geometric design consistency (Malaghan et al. 2021) etc. The driving simulators also produce similar data but in a closed and controlled environment by creating virtual highway alignment. Researchers have collected simulator-based vehicle trajectory data on a selected highway alignment and performed a consistency assessment on horizontal curves and tangents (Bella 2008; Montella et al. 2015; Choudhari and Maji 2019). A few studies have deployed LiDAR on the roadside to collect vehicle counts and trajectories at the intersections (Sun et al. 2018; Wu et al. 2019).

However, the studies based on the instrumented vehicles are limited to a specific category of vehicles. Moreover, with the presence of either the surveyor or the instrument installed in the vehicle, the actual driving behaviour could be biased (Farah et al. 2017; Xu et al. 2018; Malaghan et al. 2021). Similarly, the driving simulator studies are specific to controlled conditions and lack the realistic experience (Calvi and Bella 2014; Montella et al.

2015; Choudari and Maji 2019). On the other hand, LiDAR sensors are highly expensive and have a limited detection range (100m). Apart from these three approaches, image-processing (IP) techniques have been found to be useful in collecting naturalistic driving data and have become popular (Farah et al. 2017; Barmpounakis et al. 2019; Amrutsamanvar et al. 2021). Videography-based IP technique can capture the trajectory data of all the vehicles in a traffic stream. This enables the researchers to study both the vehicle to the road and vehicle-to-vehicle interactions, irrespective of the traffic conditions. Besides, this technique has a negligible impact on the driver's behavior. Videography-based IP involves certain mathematical operations for transforming the image coordinates into real-world coordinates (Ni 2015).

2.9.2.1 Videography-based trajectory extraction approaches

In videography-based trajectory extraction, the coordinate transformation is a major step for correcting the distortion and mapping the image coordinates to the real-world coordinates. Researchers have proposed various camera calibration techniques to correct the distortion in images and transform the coordinates (Tsai 1987; Wang and Tsai 1991; Fung et al. 2003; Schoepflin and Dailey 2003; He and Yung 2007). The camera calibration is done by computing both extrinsic and intrinsic parameters of the camera. The extrinsic parameters of a camera indicate the position and orientation with reference to the real-world coordinates. The intrinsic parameters indicate the inherent properties of the camera, such as focal length, optical length, image scaling factor, and lens distortion coefficients. In general, the intrinsic parameters remain the same except for the focal length as it may vary for different purposes. However, the intrinsic parameters can be calibrated prior to the use of the camera.

For computer vision applications such as video-based traffic analysis, it is essential to calibrate the extrinsic parameters for developing the relationship between any two images or image and real-world coordinates. The camera calibration techniques are numerous and are broadly classified into four categories. They are full-scale non-linear optimization, computing perspective transformation matrix using linear equations, two-plane method, and geometric technique (Tsai 1987). Among these techniques, the three-vanishing point technique proposed by Wang and Tsai (1991) uses a planar hexagonal pattern for calibration. The main assumption of this technique is that the target image or the real-world study region is a plane. The major disadvantage of this approach is that creating the hexagonal pattern with three pairs of parallel lines on the real field is practically difficult (Fung et al. 2003). Another problem with this approach is that, a priori parameter information is required for calibration. Schoepflin and

Dailey (2003) proposed a two vanishing point technique that identifies parallel and perpendicular lines in the image. Creating a square or rectangle pattern that has two vanishing points on the real-world field is easier than the hexagonal pattern. Fung et al. (2003) proposed a two vanishing point technique by using road lane markings. The major drawback of this approach is the ill-conditioning effect that occurs due to near-parallel lines. He and Yung (2007) proposed a calibration method using a single vanishing point from the lane markings to overcome the errors caused by ill-conditioning. This method doesn't assume any extrinsic parameters to be known a priori. Direct linear transformation (DLT) is a technique where internal parameters and orientation of the camera are represented by a group of coefficients and define a linear transformation between the 3D real world and image planes (Tsai 1987; Chen et al. 1994). This approach doesn't consider the lens distortion and solves the calibration problem using linear equations for homogeneous coordinates (Dubrofsky 2009). Thus, DLT is a relatively simple and accurate technique that permits great flexibility in camera setups, such as position and orientation. All the existing techniques perform camera calibration by considering the real-world region as a planar region. However, in the context of the study sections located in the non-planar region (mountainous terrain), the existing image processing tools have the following limitations:

1. The major pre-requisite for the existing tools is that the study location should be a planar region.
2. The developed tools for coordinate conversion from the image plane to the world plane are limited to straight-road sections.

Due to these limitations, very limited attempts have been made by the researchers to collect the trajectory data using videography on the non-planar horizontal curves (Farah et al. 2019; Farah et al. 2017).

2.10 Summary

In the geometric design consistency research, several consistency measures were developed and are broadly classified into alignment indices, driver workload, vehicle stability, and vehicle speed. Among various consistency measures that were developed, Lamm's safety criteria are the most widely accepted and used for consistency assessment (Anderson et al. 1999; Hassan et al. 2000; Castro et al. 2008; Zilioniene and Vorobjovas 2011; Wang et al. 2013; Goyani et al. 2022; Chaudhari et al. 2022). Lamm's criteria were developed using a large operating speed and accident data obtained from several countries, covering numerous

highways. These safety criteria support the design engineer in analyzing the compatibility of horizontal alignments and limit the risk of crashes on horizontal curves (Lamm et al. 1999).

Operating speed and operating speed reduction models play a vital role in evaluating the geometric design consistency. In this context, several operating speed and operating speed reduction models were developed (Krammes et al. 1995; Passetti and Fambro 1999). However, all these studies were based on speed collected at the curve center and the midpoint of the approach tangent with the assumption that speed on the curve is constant and deceleration and acceleration take place at the approach and departing tangent.

Several studies have used instrumented vehicles and driving simulators to investigate driver behavior along the curve and approach tangents (Bella 2007; Pérez-Zuriaga et al. 2010; Pérez-Zuriaga et al. 2013; Montella et al. 2014a; Llopis-Castello et al. 2018; Dhahir and Hassan 2019b; Malaghan et al. 2021). The analysis of continuous acceleration profiles revealed that a significant number of vehicles decelerate on the curve and accelerate before leaving the curve. The analysis of continuous speed profiles showed that the speed is not constant on the curve; further, the minimum speed doesn't occur at the center of the curve (Llopis-Castello et al. 2018; Dhahir and Hassan 2019b). In the evaluation of operating speed consistency for successive geometric elements (tangent to curve), the minimum speed on the curve plays a vital role. In this context, several vehicle-specific operating speed and operating speed reduction models were developed with minimum speed on the curve (Pérez-Zuriaga et al. 2010; Pérez-Zuriaga et al. 2013; Montella et al. 2014a; Llopis-Castello et al. 2018; Dhahir and Hassan 2019b; Malaghan et al. 2021).

Review of operating speed and operating speed reduction models indicates a huge scope for further research, specifically for hilly terrain. A majority of the studies were based on car (Pérez-Zuriaga et al. 2010; Pérez-Zuriaga et al. 2013; Montella et al. 2014a; Dhahir and Hassan 2019b; Malaghan et al. 2021). Moreover, a majority of speed reduction models developed are for rural highways in plain terrain (Pérez-Zuriaga et al. 2010; Jacob and Anjaneyulu 2013; Montella et al. 2014a; Choudari and Maji 2019; Malaghan et al. 2021), and these models are not applicable to rural highways passing through mountainous terrain. The existing studies were confined to the estimation of speed variability (operating speed reduction and operating speed), and none of these studies has attempted to evaluate the consistency of geometric elements using speed variability.

The continuous speed profiles collected from the GPS instrumented vehicles and the driving simulators have significant issues. The speed data corresponding to GPS instrumented vehicles are limited to a specific category of vehicles, and the actual driving behavior captured in this process could be biased (Farah et al. 2017; Xu et al. 2018; Malaghan et al. 2021). On the other hand, driving simulator studies are specific to controlled conditions (Calvi and Bella 2014; Montella et al. 2015; Choudari and Maji 2019). Thus, neither the GPS instrumented vehicles nor the driving simulators could collect the data necessary for a realistic evaluation of geometric design consistency. Videography-based image processing technique has potential advantages over instrumented GPS vehicles and driving simulators. This technique is widely used to collect trajectory data from straight tangent sections located in plain terrain (Farah et al. 2017; Barmpounakis et al. 2019; Amrutsamanvar et al. 2021). However, the existing techniques are not suitable for collecting trajectory data from the horizontal curves located in mountainous terrain.

Hence, the present study proposes an approach for collecting naturalistic vehicle trajectories using a videography-based image processing technique. Then, the vehicle-specific driver behavior on the horizontal curve will be analyzed through longitudinal acceleration and speed profiles. Necessary operating speed models were developed to understand the speed variability on the curve and to estimate essential speed variables (V_{Max}^{85} and V_{Min}^{85}) necessary for consistency evaluation. Finally, the role of V_{Max}^{85} and V_{Min}^{85}, as compared to that of V_{CC}^{85}, in the geometric design consistency will be assessed.

3 Multiple homography estimation and Data collection

3.1 Introduction

Video image-processing (IP) techniques are useful in collecting naturalistic driving data (Farah et al. 2017; Amrutsamanvar et al. 2019; Barmpounakis et al. 2019). Video image-processing technique can capture the trajectory data of all the vehicles in a traffic stream during the observation period. This enables the researchers to study both the vehicle-to-road and vehicle-to-vehicle interactions, irrespective of the traffic conditions. Besides, this technique has a negligible impact on the driver's behaviour. Videography-based IP involves certain mathematical operations for transforming the image coordinates into real-world coordinates (Ni 2015). The existing coordinate-transformation techniques assume that the road is planar (Fung et al. 2003; Wan et al. 2014; Munigety et al. 2014; Amrutsamanvar et al. 2019). Any road passing through mountainous terrain is expected to have grade changes and constituted by several horizontal and vertical curves. Many of the horizontal curves might also be superimposed by the vertical curves. Any horizontal curve superimposed with either a vertical curve or a constant grade is not planar. In non-planar terrains, the highway alignment might consist any of the following three combinations horizontal curve with a constant grade, horizontal curve superimposed with a hog/sag curve, or a straight tangent superimposed with a hog/sag curve. Figure 3.1 shows two scenarios of non-planar curves. Figure 3.1(a) shows a horizontal curve superimposed with a constant grade, and Figure 3.1(b) shows a straight road superimposed with a sag/hog curve. In these cases, the assumption of planarity is not valid and utilizing a single homography matrix for coordinate transformation leads to a significant error in the extracted microscopic data.

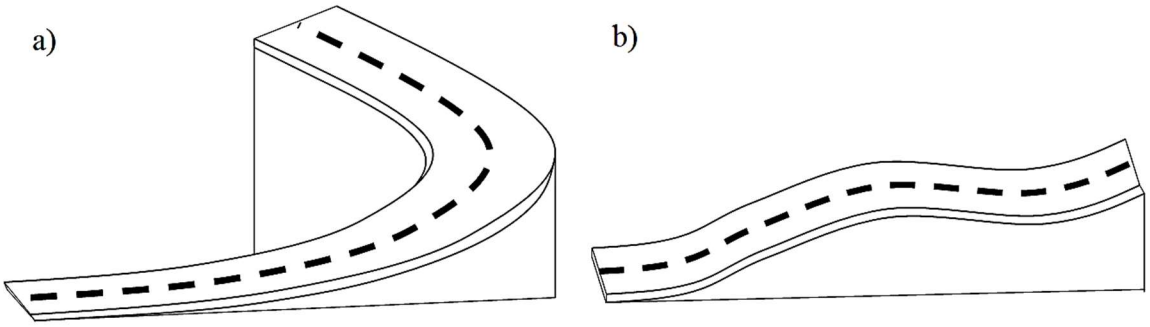

Fig. 3. 1 Non-planar highway alignments; a) Horizontal curve superimposed with a vertical grade b) Vertical curve

This chapter proposes a multiple homography approach based on Direct Linear Transformation (DLT) method to collect the trajectory data from non-planar horizontal curves. Then the proposed multiple homography approach for vehicle trajectory extraction is evaluated. Field data collection comprising site selection, videography data, and trajectory data extraction and processing are presented in the consequent sections. Section 3.6 presents the crash data corresponding to the study stretch.

3.2 Homography estimation for Coordinate Transformation

A homography is a matrix (***H***) that maps a given set of points from one plane to another plane. Often, homography is used in transportation studies to transform the pixel coordinates into real-world coordinates during image-processing-based traffic data collection. Figure 3.2 shows a pictorial representation of point-to-point correspondence between the real-world and image planes. A homography matrix maps this point-to-point correspondence as a transformation.

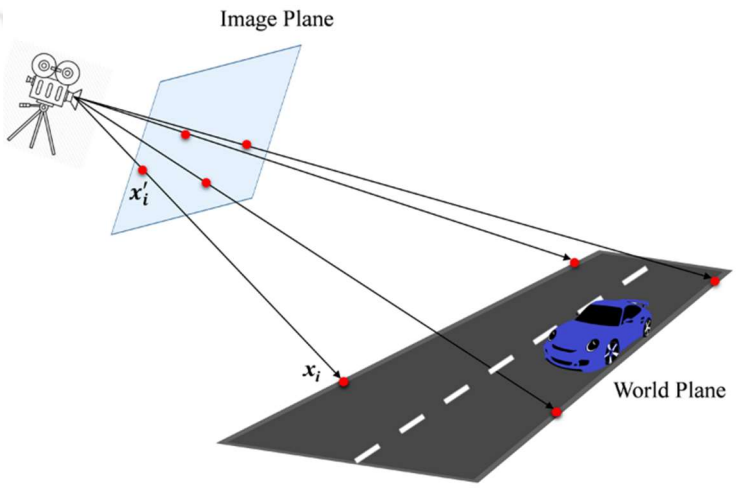

Fig. 3. 2 Illustration of homography for plain terrain

As shown in Figure 3.2, $\boldsymbol{x_i}$ and x_i' represent the vector of points on the real-world plane and in the image plane, respectively. The homography $\boldsymbol{H}$ maps the points in the following way:

$$x_i = Hx_i' \tag{3.1}$$

Where H is a 3×3 Homography matrix and can be written as follows:

$$H = \begin{bmatrix} h_{11} & h_{12} & h_{13} \\ h_{21} & h_{22} & h_{23} \\ h_{31} & h_{32} & h_{33} \end{bmatrix} \tag{3.2}$$

Where, h_{ij}, $\forall\, i, j = 1,2,3$ are the coefficients to be estimated.

The present study uses Direct Linear Transform (DLT) to calculate the homography matrix by assuming that the image plane and the real-world plane satisfy the collinearity condition (Dubrofsky 2009). Let x_i be $[x, y, 1]^T$ and x_i' be $[x', y', 1]^T$. The equations to be solved for estimating the homography matrix ($\boldsymbol{H}$) are,

$$x'(h_{31}x + h_{32}y + h_{33}) = h_{11}x + h_{12}y + h_{13} \tag{3.3}$$

$$y'(h_{31}x + h_{32}y + h_{33}) = h_{21}x + h_{22}y + h_{23} \tag{3.4}$$

For solving the above equations, coordinates of four known points are needed. Let (x_1, y_1), (x_2, y_2), (x_3, y_3), (x_4, y_4) be the known real-world coordinates and (x_1', y_1'), (x_2', y_2'), (x_3', y_3'), (x_4', y_4') be the corresponding pixel coordinates. Then the equations (3.3) and (3.4) can be rearranged as follows,

$$\begin{bmatrix} x_1 & y_1 & 1 & 0 & 0 & 0 & -x_1'x_1 & -x_1'y_1 & -x_1' \\ 0 & 0 & 0 & x_1 & y_1 & 1 & -y_1'x_1 & -y_1'y_1 & -y_1' \\ x_2 & y_2 & 1 & 0 & 0 & 0 & -x_2'x_2 & -x_2'y_2 & -x_2' \\ 0 & 0 & 0 & x_2 & y_2 & 1 & -y_2'x_2 & -y_2'y_2 & -y_2' \\ x_3 & y_3 & 1 & 0 & 0 & 0 & -x_3'x_3 & -x_3'y_3 & -x_3' \\ 0 & 0 & 0 & x_3 & y_3 & 1 & -y_3'x_3 & -y_3'y_3 & -y_3' \\ x_4 & y_4 & 1 & 0 & 0 & 0 & -x_4'x_4 & -x_4'y_4 & -x_4' \\ 0 & 0 & 0 & x_4 & y_4 & 1 & -y_4'x_4 & -y_4'y_4 & -y_4' \end{bmatrix} h = 0 \tag{3.5}$$

The above equation has the form $\boldsymbol{Ah} = 0$, with $\boldsymbol{A}$ as an 8×9 matrix. Given an estimate $\boldsymbol{h}$, the quantity $\|Ah\|$ is the algebraic error of the i^{th} datum. DLT minimizes the sum of squared algebraic errors as,

$$\hat{\mathbf{h}} = \underset{\mathbf{h}}{\operatorname{argmin}} \|\mathbf{Ah}\|^2 \qquad \text{s.t.} \|\mathbf{h}\| = 1 \tag{3.6}$$

A norm constraint is added to prevent trivial solutions since the homographic transformation has only 8 degrees of freedom. Here, the solution is the least significant right singular vector of $\boldsymbol{A}$ and is obtained through Singular Value Decomposition (SVD).

The estimated homography matrix can be used to relate the pixel coordinates on the image plane to the real coordinates on the world plane. As discussed, DLT primarily assumes a planar scene; thus, the applicability of estimated homography is limited only to the traffic videos collected from plain terrain. To extend the advantages of image-processing-based naturalistic driving data collection to a non-planar terrain, this study proposes a multiple-homography-based approach which is described in the following sub-section.

3.2.1 Cell-wise Direct Linear Transformation for Multiple Homographies

The present study hypothesizes that a non-planar terrain region can be effectively transformed into a combination of planar regions. A horizontal curve superimposed with a vertical grade (Figure 3.3), which represents a non-planar scene, was considered in the present study to illustrate the proposed multiple-homography approach. Figure 3.3 shows a change in the plane along the centerline due to both the gradient as well as the change of direction. However, due to design constraints, the change of plane would be gradual; thus, piecewise planar regions could be approximated.

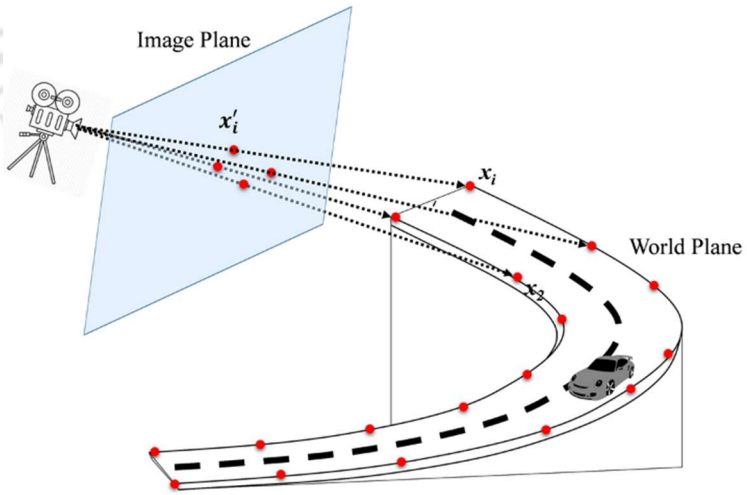

Fig. 3. 3 Illustration of Homography for non-planar region

In this study, the non-planar road section was divided into multiple plain sections (cells) using interconnected quadrilaterals (Figure 3.3). The point-to-point correspondence for each cell is represented as follows,

$$x_{C_i} = H_{C_i} x'_{C_i} \tag{3.7}$$

Where, $\boldsymbol{H_{C_i}}$ is the homography corresponding to i^{th} cell, x'_{C_i} is the corner of the quadrilateral composing cell i in the image plane, and x_{C_i} is the corresponding point in the real world. The homography was estimated for each planar region $C_i, (i = 1, 2, \ldots, n)$, using the procedure explained in the previous subsection. Trajectory data in pixel coordinates were transformed into real-world coordinates by applying the corresponding homography. Since the successive cells share the common corner points, the estimated homography gradually varies between the cells, thus ensuring a continuous trajectory. Table 3.1 shows the possible locations where the proposed multiple-cell homography is applicable.

Figure 3.4 shows the overall approach for collecting the trajectory data from mountainous terrain. The first step involves field data collection, which includes videography data, field reference points, and the road geometry. The second step involves pre-processing the collected videography data. The third and fourth steps deal with the vehicle tracking and coordinate transformation using the proposed DLT-based multiple homography, respectively. The fifth step deals with the extraction and smoothing of the vehicle trajectories.

Table 3. 1 Application scope of single and multiple homographies

Sl. No	Highway Alignment Detail	Homography Type
1	The horizontal curve superimposed with a constant grade	Multiple homography
2	The horizontal curve superimposed with the sag/hog curve	
3	Straight road superimposed with sag/hog curve	
4	The horizontal curve with no grade	Single homography
5	Straight road with no/constant grade	

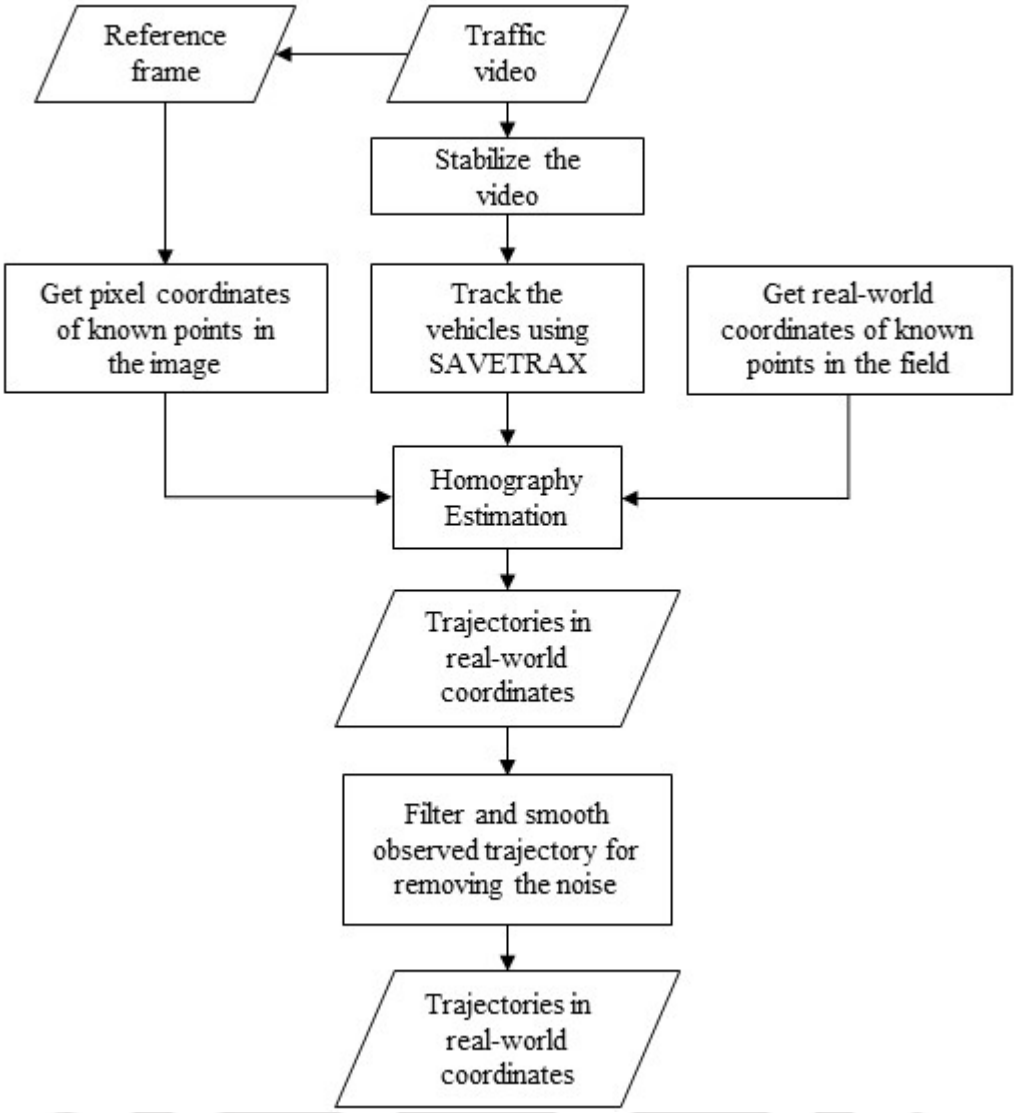

Fig. 3. 4 Illustration of trajectory data collection process from mountainous terrain

The proposed approach was evaluated on a horizontal curve superimposed with a sag curve. Further validation was done using the trajectory data collected from multiple horizontal curves located on the Shillong bypass highway. The details of the trajectory data collection framework and the evaluation results are presented in the following sections.

3.3 Evaluation of the proposed multiple homography approach

The present study evaluates the proposed multiple homography approach for the trajectory data collection from the horizontal curves located in mountainous terrain through a controlled experiment.

3.3.1 Details of the controlled experiment

A horizontal curve superimposed with a sag curve located in a residential campus was chosen for evaluating the multiple homography. Figure 3.5(a) shows the top view of the study region, and Figure 3.5(b) shows its contour map. The study region lies in mountainous terrain. The study section runs from a two-lane undivided road to a four-lane divided road. The length of the study section is 170 meters, and it consists of 3.5m wide lanes. The contour map was created using SRTM-DEM (The Shuttle Radar Topography Mission-Digital Elevation Model) file using the ArcGIS tool. The contour map with a 5-meter interval shows that the study area is non-planar, where the terrain of the study region changes continuously.

Fig. 3. 5 The study location of the four-legged roundabout in IIT Guwahati (a) Image from the drone (b) Contour map

3.3.1.1 Videography and instrumented vehicle data collection

The data were collected during the day and under dry weather conditions in 2019. A test vehicle (car) was used to make several trips on the study stretch during the observation period. Aerial footage (videography) of all the trips was captured using a drone (DJI Inspire 2) with a static position from an altitude of 50 meters (Figure 3.6). At an altitude of 50 m, the drone covered a distance of 220 meters, approximately. In this experiment, aerial footage was recorded with a resolution of 2704×1520 pixels and at a rate of 24 frames per second. The three-axis gimbal of the drone reduces minor roll rotation and drift by compensating sudden jerks or movement of the drone for capturing smooth motion videos.

Fig. 3. 6 Drone DJI Inspire2 Model-T650A

Table 3.2 presents the technical features of the drone used in the controlled experiment. The test vehicle (Maruti Suzuki Swift) was also instrumented with a high-end GPS device (V-Box). The V-Box data logger provides information such as speed, distance, acceleration, position, and many other derived data. The V-Box also has the facility to capture videos of the surrounding traffic. For each trip, speed, acceleration, and path, at a frequency of 10 Hz, were extracted from the V-Box data logger. On the study stretch, seven runs were made to compare the speed profile estimated using single and multiple homographies.

Table 3. 2 Technical specifications of the drone

Technical feature	Description	Technical feature	Description
Drone Model	T650A	Power	6000mAh 2S LiPo battery
Max. takeoff weight	4.25 kg	Operating temperatures	-20° to 40° C
Max. takeoff at sea level	2500 m	GPS	Yes
Max. flight time	20 mins approx.	Driving mode	Manual/ flight
Video quality	HD, 4K, 6K	Max. Speed	94 km/h in sports mode

In addition, the present study also collected tripod-based video film at a location on Shillong bypass road, located in the state of Meghalaya, India. Shillong bypass road is a two-lane undivided national highway (NH 6) located on mountainous terrain. The highway consists of several horizontal curves superimposed with either constant grade or sag and hog curves. The selected horizontal curve is located at 21+980 m chainage, has a length of 33.9 m, a radius of 100 m, and a constant gradient of 4.75 % (Figure 3.7). Figure 3.8 shows the plan and profile view of the corresponding horizontal curve. Video footage was collected using a GoPro Hero 5 camera. The camera is capable of recording videos with 4K resolution. The video footage was recorded with a resolution of 2704×1520 pixels and at a frame rate of 24 frames per second. The data were collected in the month of July 2019, for a duration of one hour during daylight and dry weather conditions.

Fig. 3. 7 The horizontal curve selected for validating the proposed multiple-homography approach

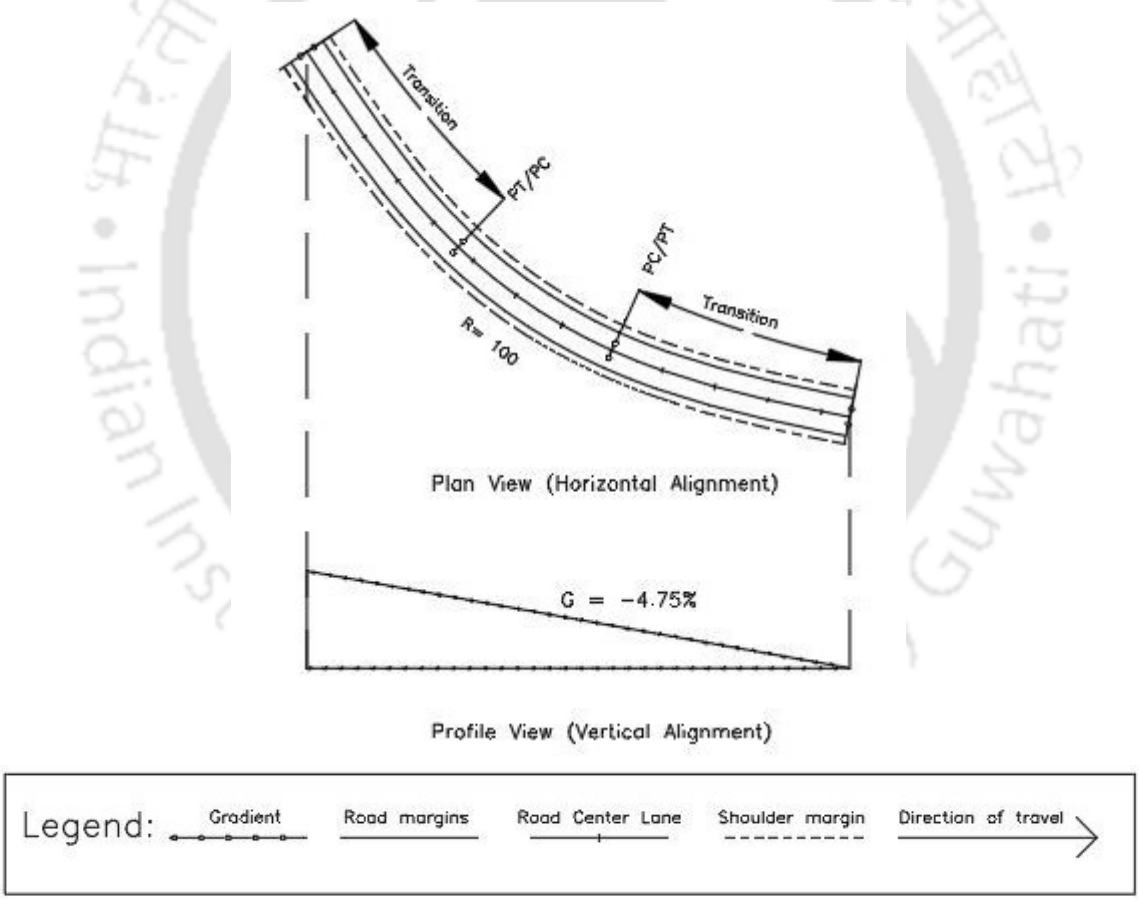

Fig. 3. 8 Plan and profile view of two horizontal curves with radius 100m and gradient -4.75%

3.3.1.2 Field data collection using Total Station

A field survey was conducted using the Total Station to geo-reference the field coordinates. In the survey, the field reference points were marked at an average distance of 10 to 20 meters

(Figure 3.9). Further, along with the field reference points, other geometric details such as road width, road length, gradient etc., were collected.

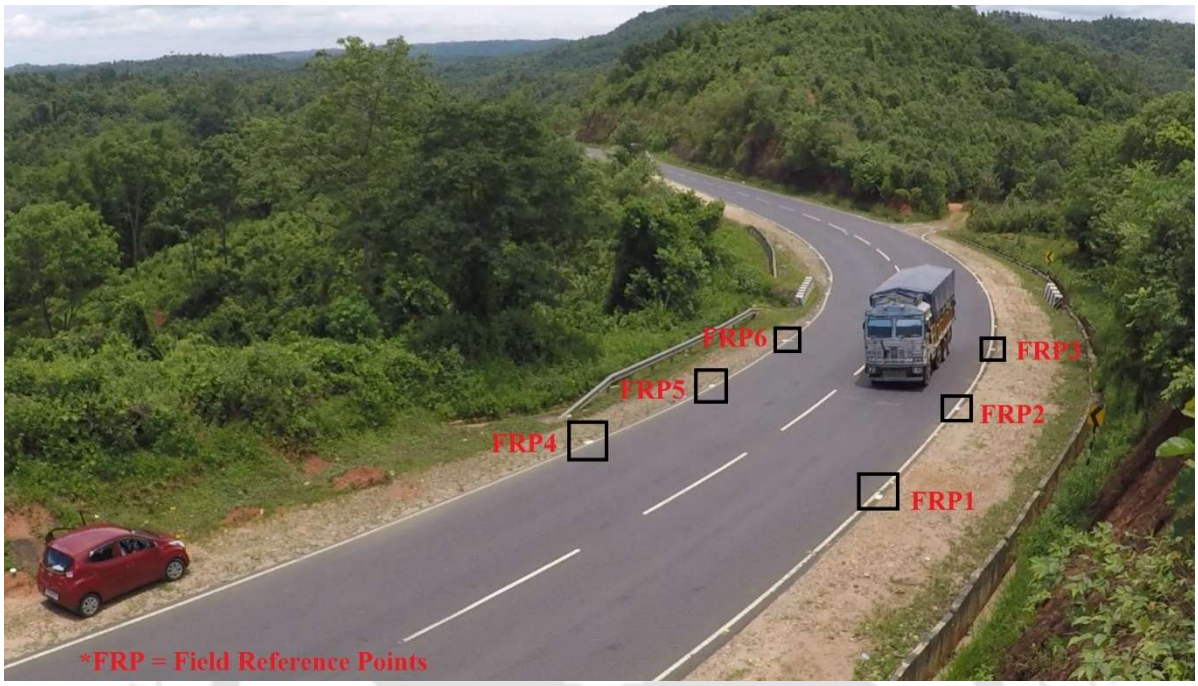

Fig. 3. 9 The study section with field reference points

3.3.2 Data extraction and Post-processing

Drones are not stable due to the presence of turbulence in the air while recording the videography data. Similarly, the tripod-based video films also may require stabilization, specifically when the data are collected during windy conditions. The vehicle trajectory extraction from these videos would result in erroneous data. Thus, drone videos need stabilization before extracting the trajectory data, and for this purpose, the present study used a video Stabilizer tool which is an integrated part of SAVETRAX.v01. It is an image-processing tool that takes the fixed reference points (pixels) on the first frame and stabilizes the subsequent frames of the video. The stabilizer tool removes any unwanted camera motion in the recorded video (Figure 3.10). In the next step, the vehicle trajectory data were tracked using a MATLAB-based SAVETRAX.v01 tool (Venthuruthiyil & Chunchu 2020a and 2020b). This is a semi-automated image-processing tool where each vehicle is annotated and then initialized for tracking. Figure 3.11(a-d) shows the snapshots of the semi-automated vehicle tracking tool and multiple cell homography estimation.

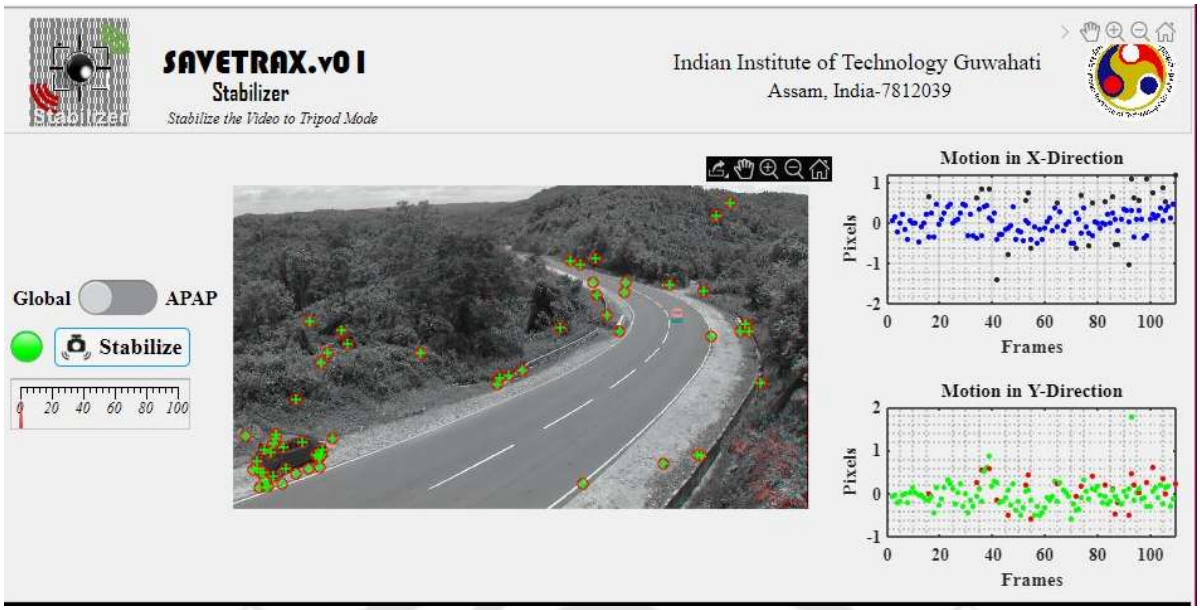

Fig. 3. 10 Video stabilizer showing the frame movement with time

Fig. 3. 11 Semi-automated vehicle tracking: (a) manual selection of tracking region, (b) manual vehicle identification and annotation, (c) automated vehicle tracking, and (d) multiple cell homography estimation

Figure 3.11(a) shows the tracking region, and Figure 3.11(b) shows the manual identification, classification, and annotation of the vehicle with a bounding box. The annotated vehicles were tracked automatically, and the trajectory data were extracted in pixel coordinates (Figure 3.11c). The proposed DLT-based multiple homography approach was used for coordinate transformation and extract the vehicle trajectories (Figure 3.11d). The extracted video processed vehicle trajectories have two noises. First, the heavy-tailed noise, and the other

is the error patterns that are dissimilar across vehicle types in both the longitudinal and lateral directions. The existing smoothing techniques, such as moving average, Kalman filter, simple low pass/high pass filters etc., are not suitable for smoothing video-processed trajectory data. Because they rely on invariant parameters that are only suitable for errors with the similar pattern. This study has used a smoothing technique proposed by Venthuruthiyil and Chunchu (2018 and 2020c). It is a Matlab-based smoothing tool that works based on a Recursively Ensembled Low-Pass (RELP) filter and an adaptive tri-cubic kernel smoother. The smoothing tool handles both the noises associated with the video-processed trajectory data. The smoothed trajectory data were used to derive other variables such as speed, longitudinal acceleration, lateral acceleration, and distance. The instrumented test vehicle data recorded by the V-Box tool were extracted using RACELOGIC 2.13.5 (Build 211) 2003 software. The extracted information from RACELOGIC includes the traveled path, speed, acceleration, and distance traveled by the test vehicle. The speed profiles from the instrumented vehicle were used as ground truth to evaluate the speed profiles of the same vehicle extracted from the video film.

3.3.3 Results and discussion

This sub-section evaluates the proposed multiple homography approach by comparing the speed profiles corresponding to single and multiple homographies. Trajectory data of the instrumented vehicle were used as the ground truth and compared with the results corresponding to single and multiple homographies. Figure 3.12(a) shows the drone image and plan & profile of the study location used for the comparative analysis.

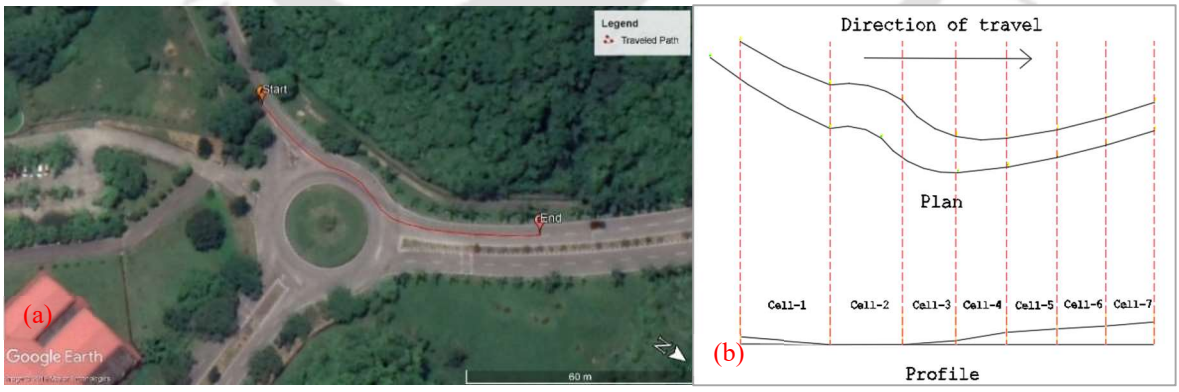

Fig. 3. 12 (a) Drone image; (b) Plan and profile view, of the study location

Figure 3.12 (b) shows the plan and profile view of the curve with the corresponding cells used for estimating multiple homographies. The gradient of the traveled path varies from -1.5% to + 6%, and the cell length ranges between 10 to 20 m. The proposed multiple

homography approach was also used to extract the trajectory data from a horizontal curve with a length of 33.9 m and a radius of 100 m, located in the Shillong bypass. The videography data collected at both locations were stabilized, and the vehicle trajectories were extracted. The vehicle trajectories were smoothed, and the speed and acceleration data were extracted.

3.3.3.1 Comparative analysis of the speed profiles estimated using single homography and V-Box

Considering the homography corresponding to four (Cell 1, 3, 5, and 7, shown in Figure 3.12b) of the seven different cells, four different speed profiles were extracted and compared with the ground truth data. Figure 3.13 (a) to (d) shows the speed profiles estimated using the single-cell homography matrix corresponding to four different cells of the traveled path.

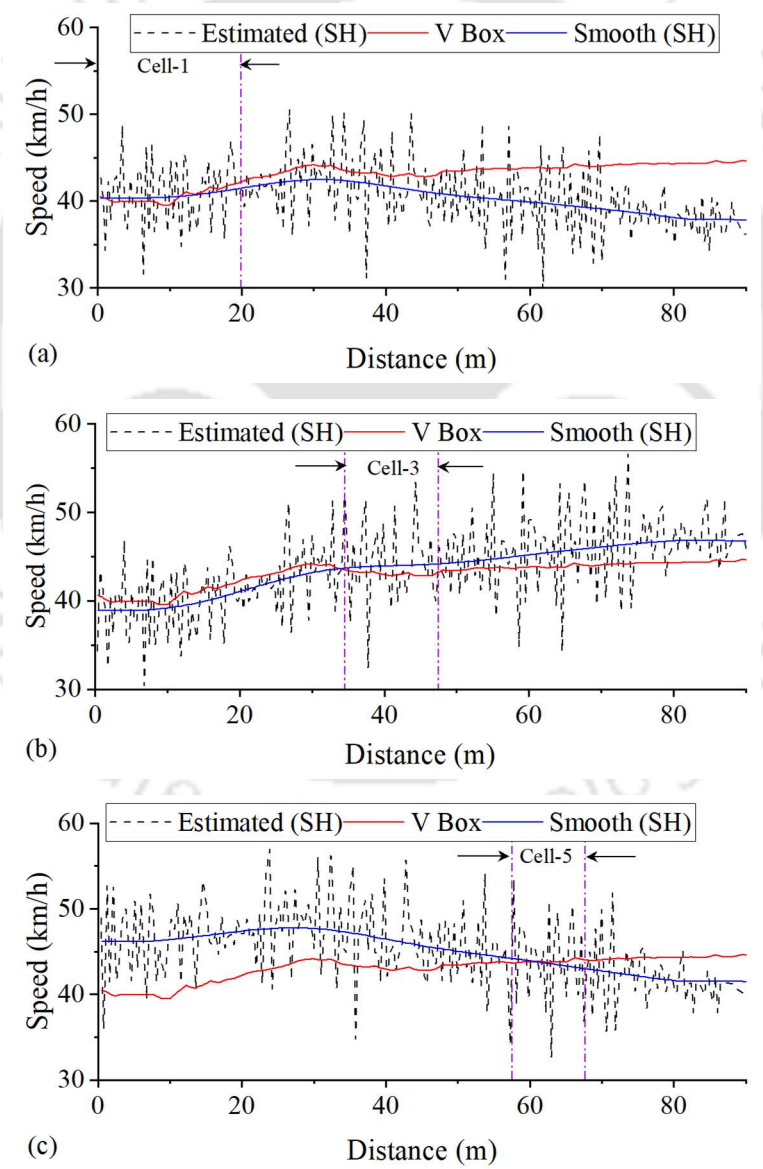

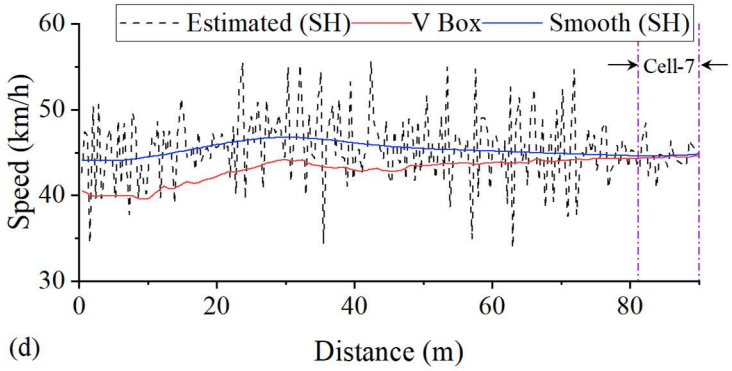

Fig. 3. 13 Comparison of speed profile estimated using single homography (SH) with the V-Box speed profile

Figure 3.13 indicates that the consideration of single homography has a significant impact on the estimated speed profile. This figure shows that the smoothed speed profiles match with the ground truth (V-Box) only near the cells that are used for homography estimation. As the vehicle moves away from the cell considered for the homography estimation, the difference in speed profiles increases (Figure 3.13a to 3.13d). The speed difference shows that the change in terrain resulted in a perspective distortion of the image filmed by the camera. This distortion, due to the 2D projection of the 3D scene, could be corrected using the proposed multiple-homography approach. The following sub-section compares the speed profiles estimated using the multiple-homography approach with the ground truth.

3.3.3.2 Comparative analysis of speed profiles estimated using the proposed multiple-homography approach and the ground truth

The proposed multiple-homography approach considers all the cells sequentially to estimate the vehicle trajectory. Figure 3.14 shows the speed profiles estimated using the proposed multiple-homography approach and the ground truth speed profile.

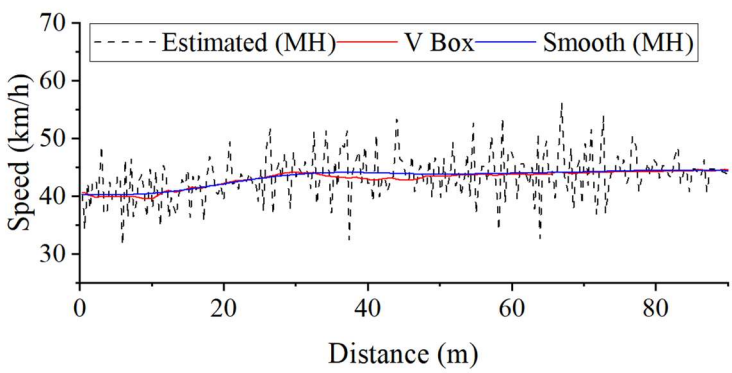

Fig. 3. 14 Comparison of speed profile estimated using multiple homography (MH) with the V-Box speed profile

Figure 3.14 shows that the estimated speed profile is comparable with the speed observed using V-Box. The error associated with the estimated speed was quantified in terms of Root Mean Square Error (RMSE).

$$RMSE = \sqrt{\frac{\sum_{i=1}^{n}(V_i - v_i)^2}{n}} \qquad i = 1, 2, 3, \ldots\ldots, n \tag{3.8}$$

Where, v_i is the speed of the test vehicle obtained from V-Box; V_i is the estimated speed of the test vehicle; n is the number of speed samples compared. The RMSE of the speed profiles estimated using single homography ranges between 1.5 to 3.53 km/h (Table 3.3). Moreover, the maximum difference between the ground truth and the estimated speed ranges between 2.5 and 7 km/h. With the proposed multiple-homography approach, the RMSE is less than 0.44 km/h, and the maximum speed difference between the speed profiles is 1 km/h.

Table 3. 3 Comparison of errors associated with single and multiple homographies

S. No	RMSE (km/h)	Max. Speed Difference	Homography
1	3.53	7 km/h	Single
2	1.5	2.5 km/h	Single
3	3.7	6.9 km/h	Single
4	2.73	5 km/h	Single
5	0.44	1 km/h	Multiple

The comparative analyses of the speed profiles have justified the significance of the proposed multiple-homography approach in real field application. Further, the present study analyzed the effect of single homography on the estimated vehicle paths. The following subsection compares the vehicular paths obtained from the single and multiple-homography approaches.

3.3.3.3 Comparative analysis of vehicle paths obtained from single and multiple homographies

The path followed by a vehicle on a horizontal curve plays a significant role in understanding the safety aspects of the driver's behaviour. Obtaining the vehicle path along a horizontal curve reveals many behavioural aspects of a driver negotiating the curve, such as cutting, drifting, swinging, normal, and ideal path (Spacek 2005). This study compares the paths adopted by cars while negotiating a horizontal curve, obtained from single and multiple homographies. The same trajectory dataset used for the speed profile comparison was used for this purpose.

For the single homography approach, the path was estimated based on a 10 m cell near the camera and transformed all the pixel coordinates to real-world coordinates. For the multiple-homography approach, eleven cells were considered to estimate the vehicle paths. In this case, the cell length varies between 5 to 10 m. Figure 3.15 shows the vehicular paths extracted using a single homography, and Figure 3.16 shows the corresponding paths estimated using multiple homographies.

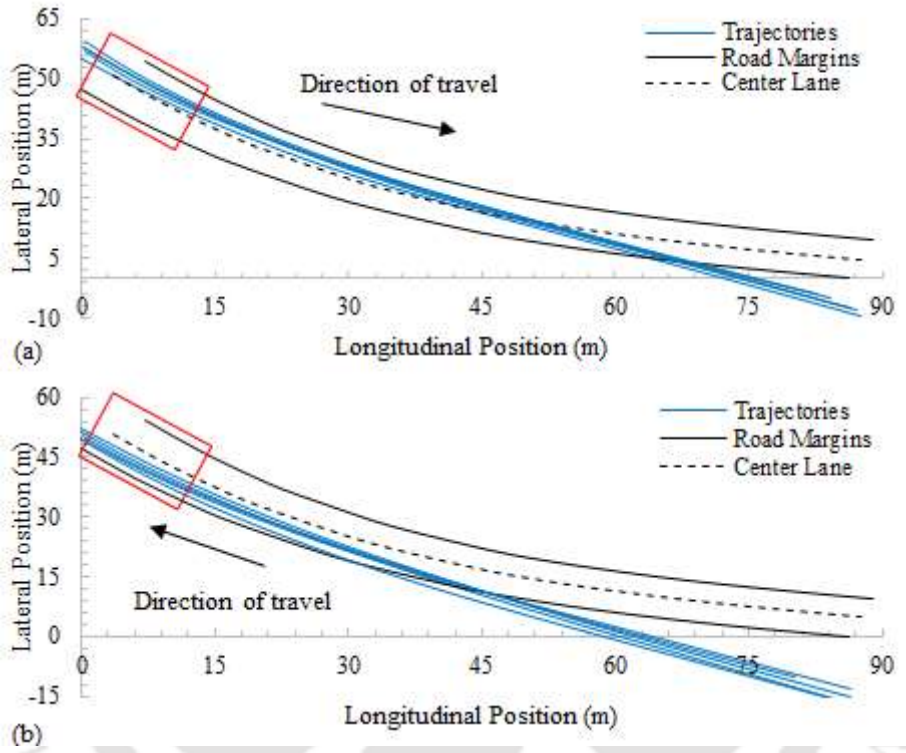

Fig. 3. 15 Paths adopted by cars, estimated using single homography: (a) left-turning cars, (b) Right turning cars

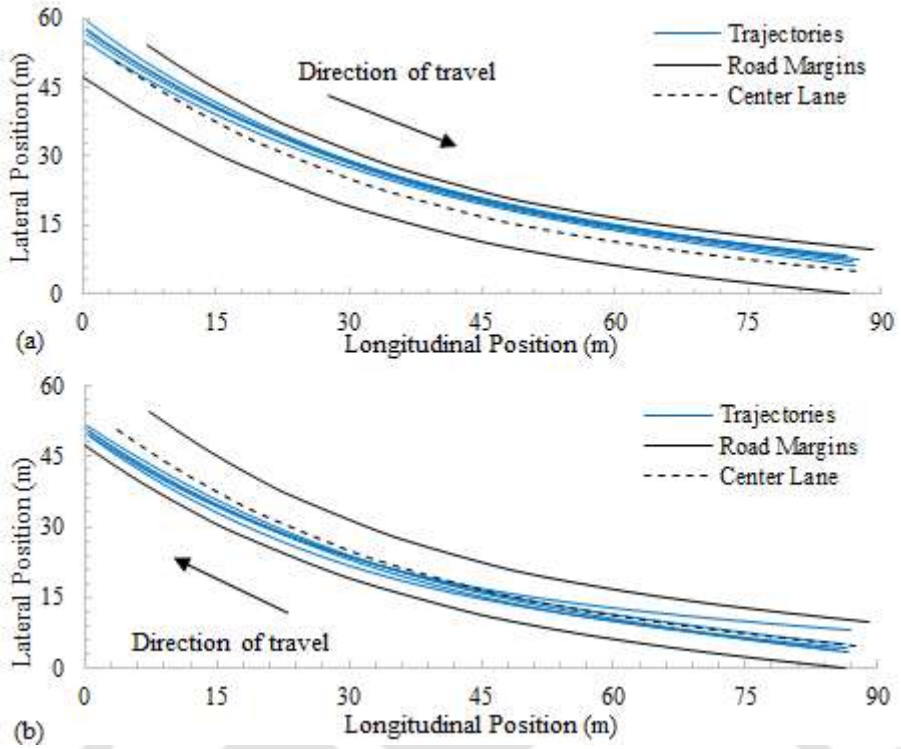

Fig. 3. 16 Paths adopted by cars, estimated using multiple homographies: (a) Left-turning cars, (b) Right-turning cars

Results indicate that the paths estimated using single homography fall outside the road boundaries. Whereas the trajectories estimated using the multiple-homography approach fall within the designated road boundaries for both directions (Figure 3.16). By assuming the vehicle path obtained from the multiple-homography approach as a proxy to the actual vehicle path, the RMSE for the path obtained using single homography was estimated. In the longitudinal direction, the error was 20.6 meters, whereas the average error corresponding to the lateral direction was 24 meters.

The comparative analysis of the speeds and paths adopted by the vehicles highlights the necessity of the proposed multiple-homography approach for collecting trajectory data from mountainous terrain. The multiple-homography approach was proposed for the road sections having complex road geometry where a single homography doesn't yield realistic speeds/paths. In summary, the proposed multiple homography approach benefits the researchers in collecting trajectory data from the locations having complex road geometry. The proposed approach would allow the researchers to analyze the design consistency and risk factors associated with driver behaviour in more detail.

3.4 Field data collection

In the present study, the Shillong bypass road was selected to explore the naturalistic driving behavior on the horizontal curves. Shillong bypass is a two-lane undivided national highway (NH-6) passing through mountainous terrain. The study highway starts at Umiam in Ri-Bhoi District and ends at Mawryngkneng in East Khasi Hills District, located in Meghalaya, a northeastern state of India.

3.4.1 Site description

The road stretch is 48.765 km long, with an elevation range of 871.577 to 1333.507m (Figure 3.17a). It begins at an altitude of 984.121m above sea level. The highway has 253 horizontal and 175 vertical curves, with gradients varying from -7 to +7% and curve radii from 35 to 1000m. Among the horizontal curves, 151 curves are superimposed with an upgrade or downgrade, and 97 curves are superimposed with either sag or hog curves. The design speed of the horizontal curves ranged between 30-65 km/h. Table 3.4 presents the alignment consistency assessment carried out using the alignment indices.

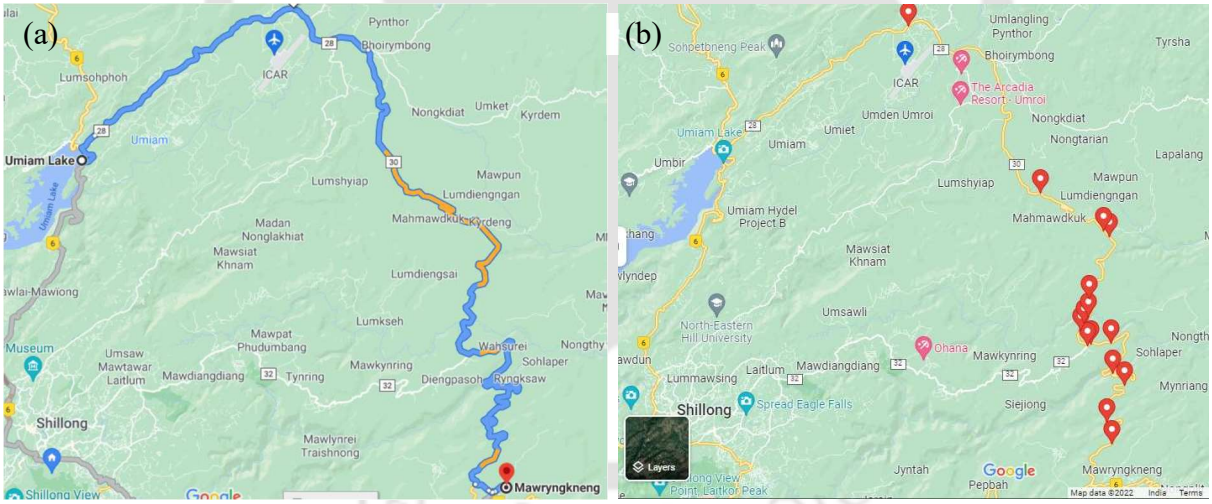

Fig. 3. 17 Study stretch details (a) Alignment; (b) Locations of data collection

Table 3. 4 Alignment indices of the selected road stretch

Alignment indices		
Average radius (AR)		174.7 m
Ratio of maximum radius to minimum radius (RR)		28.6
Average rate of vertical curvature (AVC)		33.5 m/%grade
Ratio of individual curve radius to average radius (CRR)	Min	0.2
	Max	5.7

Table 3.4 indicates that the radius corresponding to the horizontal curves in the highway alignment is right-skewed and unevenly distributed. For further assessing the consistency using the vehicle speed, this study selected fourteen horizontal curves from the road stretch (Figure 3.17b). The horizontal curves were selected based on the following criteria.

1. Availability of a clear vantage point from where the entire curve is visible.
2. There should not be any kind of roadside activity.
3. There shouldn't be any nearby barriers that could interrupt a vehicle's free-flowing speed, including intersections, speed breakers, and other road features.
4. The horizontal curves are superimposed with constant upgrades or downgrades.

Figure 3.18 show four locations of the selected horizontal curves. The alignment drawings and geometric details of the highway were obtained from the National Highway Authority of India (NHAI) regional office in Guwahati. All the geometric variables corresponding to the study were obtained from the alignment drawings. Table 3.5 shows the statistical summary of the geometric features corresponding to fourteen horizontal curves considered in the present study.

Fig. 3. 18 Sample photographs of the selected horizontal curves

Table 3. 5 Descriptive statistics of the geometric variables of the study locations

Parameter	Symbol	Minimum	Maximum	Mean	Standard deviation
Length of the curve (m)	L_C	29.765	113.407	61.46	21.38
Super elevation (%)	e	5.556	10	8.7	1.75
Deflection angle (degrees)	Δ	23.98	120.613	60.11	27.77
Curve radius (m)	R	80	200	113.21	43.66
Degree of curvature (degrees)	DC	8.73	21.84	17.17	4.98
Grade (%)	G	-6	6	0	4.53
Curvature Change Rate (degrees/km)	CCR	245.10	599.87	440.20	125.64
Design Speed (km/h)	V_D	40	50	49.29	2.67
Transition Length (m)	T_L	25	55	42.5	10.52
Tangent Length (m)	L_T	0.13	262.1	67	61.2

It is evident from the table that the geometry of the selected curves shows a significant variability. The mean, standard deviation, and range of various geometric variables show skewed distributions. Further, for a highway located in mountainous terrain, it is highly possible that the geometric variables of the horizontal curves would not be uniform. In mountainous terrain, the geometric design is constrained by the land availability. At the same time, due to lack of prior consistency assessment, the alignment might consist of a few tangents and flat horizontal curves. These aspects may inadvertently contribute to the inconsistent designs.

3.4.2 Trajectory data extraction

The videography data were collected from fourteen horizontal curves in the months of June 2019 and March 2020, with an average of 1-hour traffic data at each curve, during daylight and dry weather conditions. A GoPro Hero 5 camera was placed at a high vantage point using a tripod stand such that the entire horizontal curve could be captured. The camera is capable of recording stabilized videos with 4K resolution. The video footage was recorded with a resolution of 2704×1520 pixels and at a frame rate of 24 frames per second. In the field, various points corresponding to the curve such as the PC, CC, PT were identified using the alignment drawings. The vehicle trajectories were tracked using a Matlab-based SAVETRAX tool (Venthuruthiyil 2021). The proposed multiple homography was used for extracting the trajectory data. Then the extracted trajectories were smoothened to remove the noise using a smoothing technique proposed by Venthuruthiyil and Chunchu (2018 and 2020c). Figure 3.19

shows the composition of the traffic stream observed at various curves. Cars and trucks contributed 84 – 97% of the traffic volume.

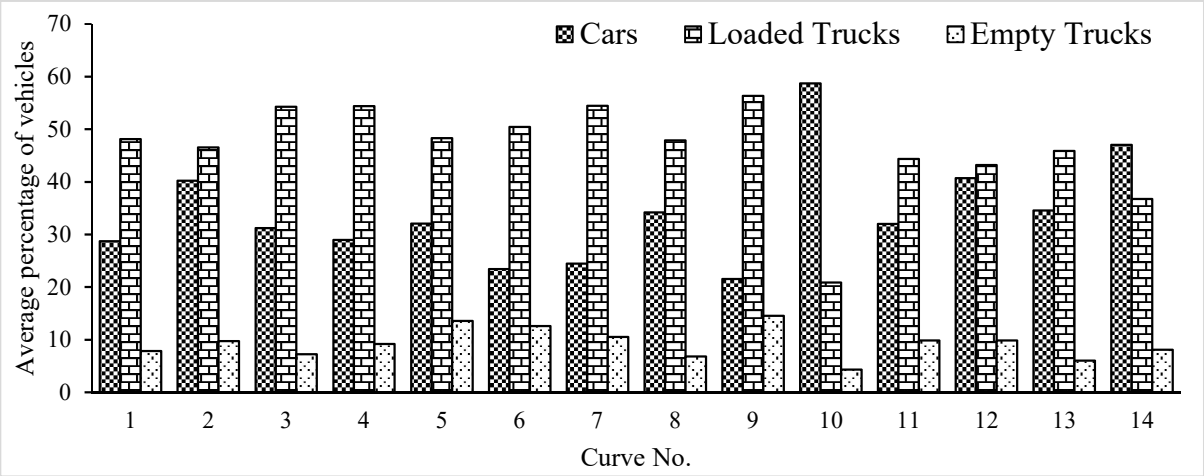

Fig. 3. 19 Average vehicle composition of the traffic stream at the study locations

Further, the trucks were classified into empty and loaded trucks through visual inspection of each truck in the recorded video footage. If the trailer of the truck is covered, the truck is classified as either a loaded or empty truck based on the speed profiles. On average, only 14% of the empty trucks were observed at the study locations. Thus, for further analysis, only cars and loaded trucks were considered. For geometric design consistency and safety evaluation, it is necessary to ensure that vehicles in the traffic stream are in free-flowing condition. Several researchers have recommended a time headway of 4 to 6 seconds between vehicles to define the free-flow condition (Lamm et al. 1990; Fitzpatrick et al. 2000a; Poe and Mason 2000; Misaghi and Hassan 2005; Maji et al. 2018; Malaghan et al. 2021). In this study, a time headway of 5 seconds was used to identify the free-flowing vehicles. Out of the total 2349 trajectories of the cars and trucks, 611 and 936 trajectories correspond to the free-flowing cars and loaded trucks, respectively. The average number of free-flowing cars and loaded trucks at each location are 47 and 70, respectively.

3.5 Extraction of microscopic data

The speed and longitudinal acceleration profiles were used to extract several variables that are used for the analysis and modeling of speed variability. Using the continuous profiles, spot speeds were extracted at PC, CC, and PT, for both the travel directions (Fig. 3.20). Several other variables required for further assessment of speed variability were also extracted.

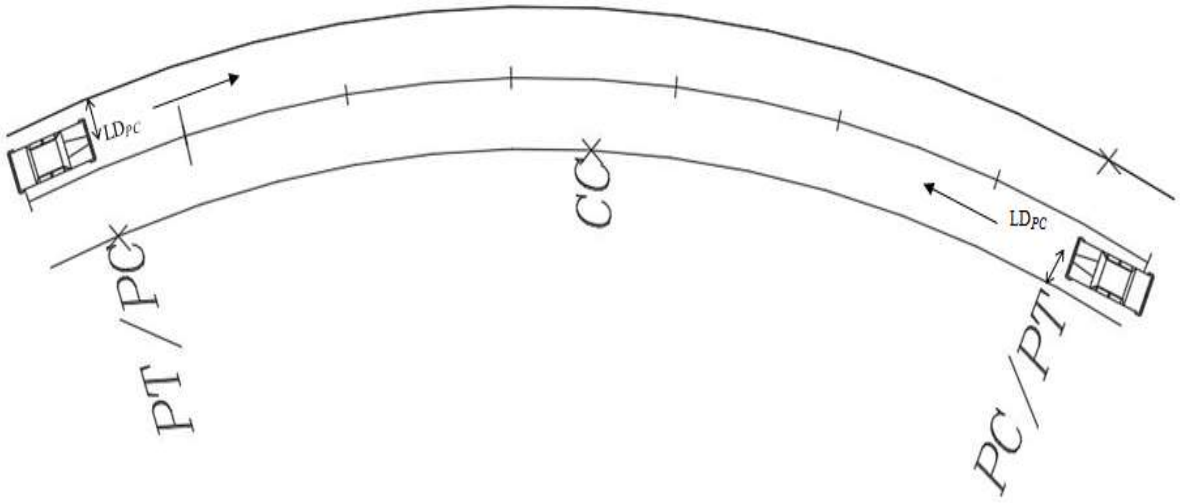

Fig. 3. 20 Schematic representation of the data collection points along the horizontal curve

From the speed profiles, the variables that were collected on the curve are mentioned below.

i. Speed at point of curvature (V_{PC})
ii. Speed at the center of the curve (V_{CC})
iii. Speed at point of transition (V_{PT})
iv. Speed at every one meter (V_{1m})
v. Minimum speed on the curve (V_{Min})
vi. Maximum speed on the curve (V_{Max})
vii. Average speed on the curve (V_{avg})

The vehicle trajectory data were also used to identify the lateral position with respect to the nearest outer edge of the curve and the location corresponding to V_{Min}, and V_{Max} on the curve for each vehicle. The following variables are obtained from the trajectory data.

i. Lateral distance of the vehicle at the point of curvature (LD_{PC})
ii. Lateral distance of the vehicle at the center of the curve (LD_{CC})
iii. Lateral distance of the vehicle at the point of transition (LD_{PT})
iv. Location of V_{Min} on the curve
v. Location of V_{Max} on the curve

Further, the longitudinal acceleration profiles were used to measure the following variables.

i. Deceleration length from the point of curvature
ii. Total deceleration length on the horizontal curve
iii. Acceleration length from the point of curvature

iv. Total acceleration length on the horizontal curve

Thus, considering vehicle trajectory in each travel direction, a total of 16 variables were extracted from each of the selected horizontal curve.

3.5.1 Removal of outliers

The outliers in each variable were identified and removed using the Quartile analysis. The outliers in the speed were defined as the speed values fall outside speed^{+} or speed^{-}, defined as follows.

$$speed^{+} = \max_{v_i}\{v_i | v_i < Q_3 + 1.5 \times IQR\} \quad (3.9)$$

$$speed^{-} = \min_{v_i}\{v_i | v_i > Q_1 - 1.5 \times IQR\} \quad (3.10)$$

Where Q_1, Q_3, and IQR are the 25th percentile speed, 75th percentile speed, and the interquartile range (IQR = $Q_3 - Q_1$) at each level, respectively. This procedure was adopted to remove outliers from all other variables corresponding to each vehicle type for all the horizontal curves.

3.6 Crash data collection

The crash data corresponding to the period December 2013 to March 2021 was collected from the NHAI regional office in Guwahati. The crash data includes detailed information about the crash, type of collision, nature of the injury, location, cause, and direction of vehicle movement. A total of 464 crashes, with an annual rate of 66 crashes, were observed between 2013 and 2021. Many of these crashes have occurred on or nearby the curve. Crashes that occurred on the transition curves and on tangents that are 10-20m away from the transition curves have also been attributed to the nearest horizontal curve. More than one crash has been observed on 158 curves, with a maximum of 30 crashes on curve no. 145. Figure 3.21 illustrates the nature, classification, vehicles involved, and severity of the crashes.

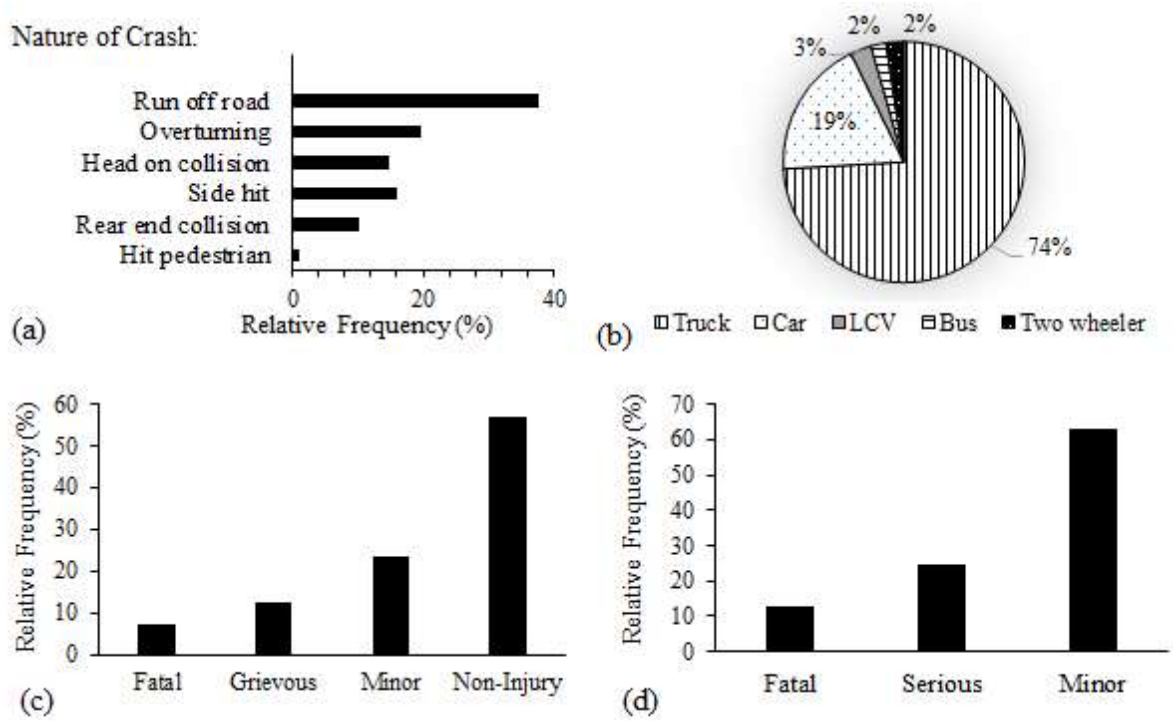

Fig. 3. 21 Analysis of the crash data a) Type of crash; b) Percentage of various types of vehicles involved in crashes; c) No. of crashes classified as per the severity; d) No. of injured persons classified as per the injury severity

The figure shows that run-off-road and overturning are the leading types of crashes observed on the study stretch. The figure also shows that in a majority of the crashes, the truck is the primary vehicle causing the crash and followed by the car. Run-off-road and overturning crashes (i.e., crashes involving single vehicles) are linked to free-flowing vehicles, and they comprise the majority of the crashes. Both these crashes signify the relevance of operating speed and design consistency in the crash occurrence. Crash data indicates that, close to 60% of crashes involve a single vehicle.

3.7 Summary and conclusions

This chapter proposes a multiple-homography-based coordinate transformation technique for collecting the trajectory data from a non-planar horizontal curve using video image-processing technique. The primary assumption behind this approach was that a non-planar region could be converted into a sequence of planar regions, and a separate homograph matrix needs to be estimated for each planar region. The proposition was verified using the trajectory obtained using V-box equipment. The speed profiles estimated using the proposed approach and the data from an instrumented vehicle were compared. The comparative analysis shows that the speed profiles estimated using the multiple-homography approach were more accurate (RMSE of

0.44 km/h) compared to that of a single homography approach (RMSE varied between 1.5 and 3.7 km/h). The systematic deviation in the estimated path using a single homography was also tested. It was found that the path estimated using a single homography deviates from the original path depending on the proximity of the cells considered for homography estimation. The findings highlight the necessity of using the multiple-homography approach to collect more realistic trajectory data on non-planar geometric elements.

Further, videography data corresponding to fourteen locations was collected from a two-lane undivided national highway (NH-6) passing through mountainous terrain. The vehicular composition from the study locations shows that trucks and cars are the major constituents of the traffic stream. Among the trucks, the composition of empty trucks is very low; thus, further analysis was carried out only for cars and loaded trucks. Several variables were extracted from the vehicle trajectories to carry out the analysis of speed variability on the horizontal curves with a view to assess the geometric design consistency.

4 Analysis and modelling of speed variability on horizontal curves

4.1 Introduction

Operating speed and operating speed reduction models play a vital role in assessing the consistency of geometric elements. In this context, a majority of the studies used spot speed data collected at specific locations, mostly at the midpoint of the curve and tangent (Leisch and Leisch 1977, Lamm and Choueiri 1987, and Krammes et al. 1995; Gibreel et al. 1999; Misaghi and Hassan 2005; Jacob and Anjaneyulu 2013; Pérez-Zuriaga et al. 2013; Shallam el at. 2021), for assessing the operating and design speed consistencies. This could be due to the fact that the spot speed data collection techniques are suitable to collecting data at the center of the curve (Krammes et al. 1995; Passetti and Fambro 1999). Further, the primary assumption in these studies is that the vehicle speed on the curve remains constant, and the complete acceleration and deceleration take place on the tangents.

On the other hand, continuous speed profiles obtained using either GPS instrumented vehicles or driving simulators provide a detailed understanding of speed variability along a geometric alignment (Pérez-Zuriaga et al. 2013; Calvi and Bella 2014; Montella et al. 2014b; Choudhari and Maji 2019). Several studies used continuous speed profiles to investigate the constant speed assumption on the curve and assess the speed variables (V_{Min}, V_{Max}, ΔV_{85}, $\Delta_{85}V$, Maximum Speed Reduction (MSR)) that were estimated using the spot speed data (Pérez-Zuriaga et al. 2010; Jacob and Anjaneyulu 2013; Pérez-Zuriaga et al. 2013; Montella et al. 2014a; Dhahir and Hassan 2018; Llopis-Castelló et al. 2018; Malaghan et al. 2020). They found that the speed is not constant on the curve, and the minimum and maximum speeds do not occur at the center of the curve. Therefore, considering the speed variability on the curve would reveal the possible locations of minimum and maximum speeds on the curve. Considering speed variability along the curve in developing operating speed and operating speed reduction models, and in consistency evaluation, would also reflect the actual driving behavior (Dhahir and Hassan 2018). However, most of the existing studies on speed variability correspond to the two-lane highways located in plain/rolling terrain. Very few studies have assessed the speed variability on the horizontal curves located in mountainous terrain.

Besides, the continuous speed variables obtained using instrumented vehicles and driving simulators have several issues. The instrumented vehicles are limited to a specific category of vehicles, and the actual driving behavior captured in this process could be biased (Farah et al. 2017; Xu et al. 2018; Malaghan et al. 2021). On the other hand, driving simulator studies are specific to controlled conditions (Montella et al. 2014a; Calvi and Bella 2014; Choudari and Maji 2019). Thus, neither the GPS instrument vehicles nor the driving simulators can collect naturalistic driving (ND) data.

Since higher speed variability is correlated with safety, understanding speed variability within and between the geometric elements could assist researchers and designers in improving the highway geometric elements. Further, investigating the speed variables, i.e., maximum speed and minimum speed on the curve, would play a crucial role in the appropriate evaluation of operating speed consistency and design consistency. This chapter investigates the speed variability and identifies the factors leading to the maximum speed difference of a vehicle while moving on a horizontal curve constituting a two-lane rural highway passing through mountainous terrain. Trajectory data, discussed in the previous chapter, were used in this analysis.

4.2 Preliminary analysis of speed variability

This section presents the preliminary analysis of the speed and acceleration data corresponding to free-flowing vehicles on the horizontal curves. Figures 4.1 and 4.2 present the speed profiles, acceleration profiles, and the locations of V_{Min} and V_{Max} corresponding to the car and loaded trucks observed on four horizontal curves. The four horizontal curves differ from one another with respect to geometric characteristics such as radius, length of the curve, gradient, length of the approach tangent, etc. The speed profiles in Figures 4.1 and 4.2 indicate that the driver's speed adoption depends on the gradient and travel direction. Figures indicate that the vehicular speeds are higher on the downgrade than those traveling on the upgrade. These differences in speed and acceleration with respect to travel direction and gradient may also reflect the changing drivers' perception of the other geometric parameters. Further, a majority of the cars exceed the design speed, whereas the loaded trucks travel at lower speeds. In addition, for the curves with the similar gradient (Fig 4.1 and 4.2 (b) and (c)), more variations in the speed and acceleration profiles of both cars and loaded trucks are observed. The variations corresponding to the figures can be attributed to difference in radius of the curve besides various other factors such as length of the approach tangent, length and radius of the previous curve.

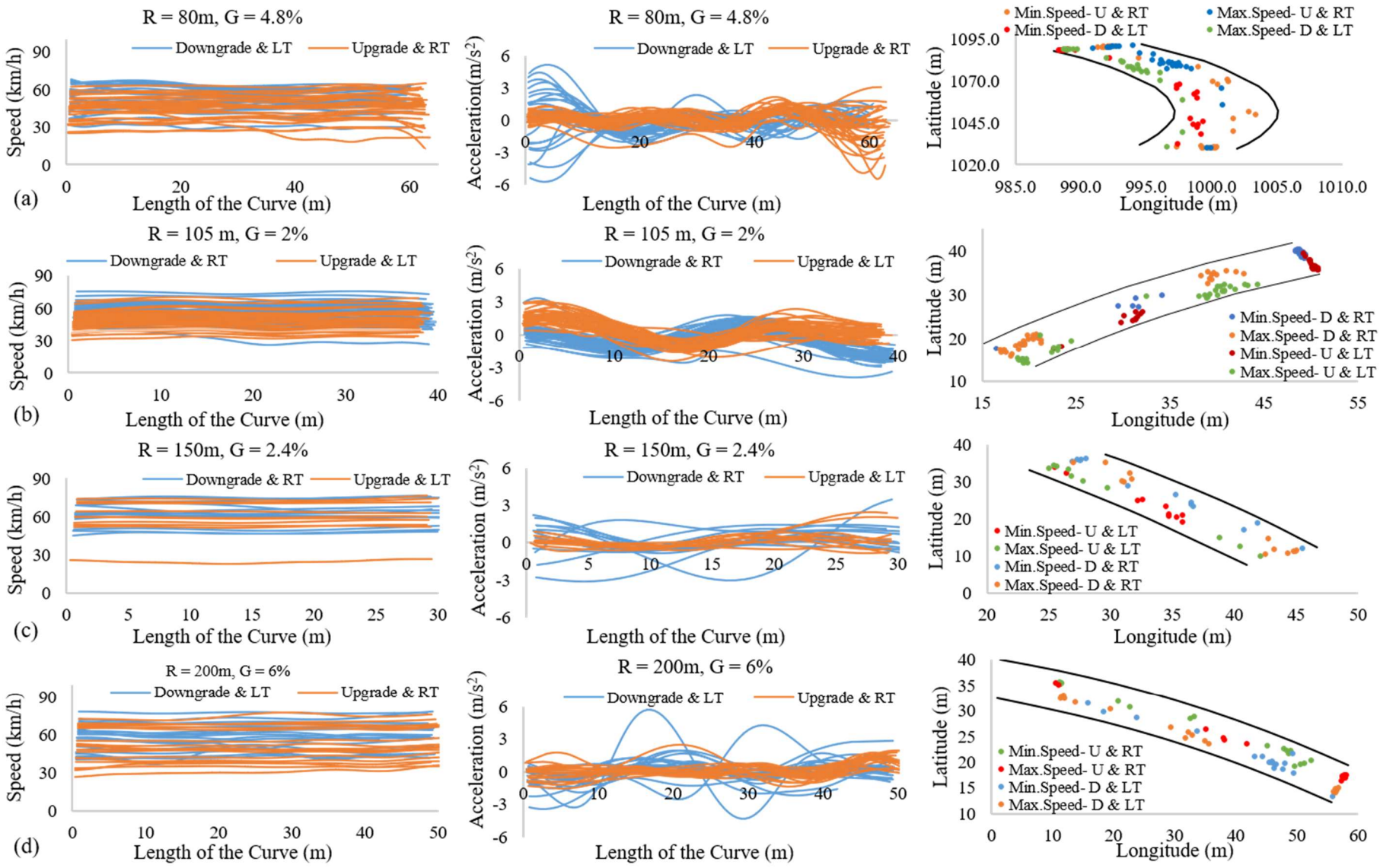

Note: RT – Right Turning; LT – Left Turning; U – Upgrade; D- Downgrade

Fig. 4. 1 Speed and acceleration profiles and locations of minimum & maximum speeds of car, corresponding to four different curves

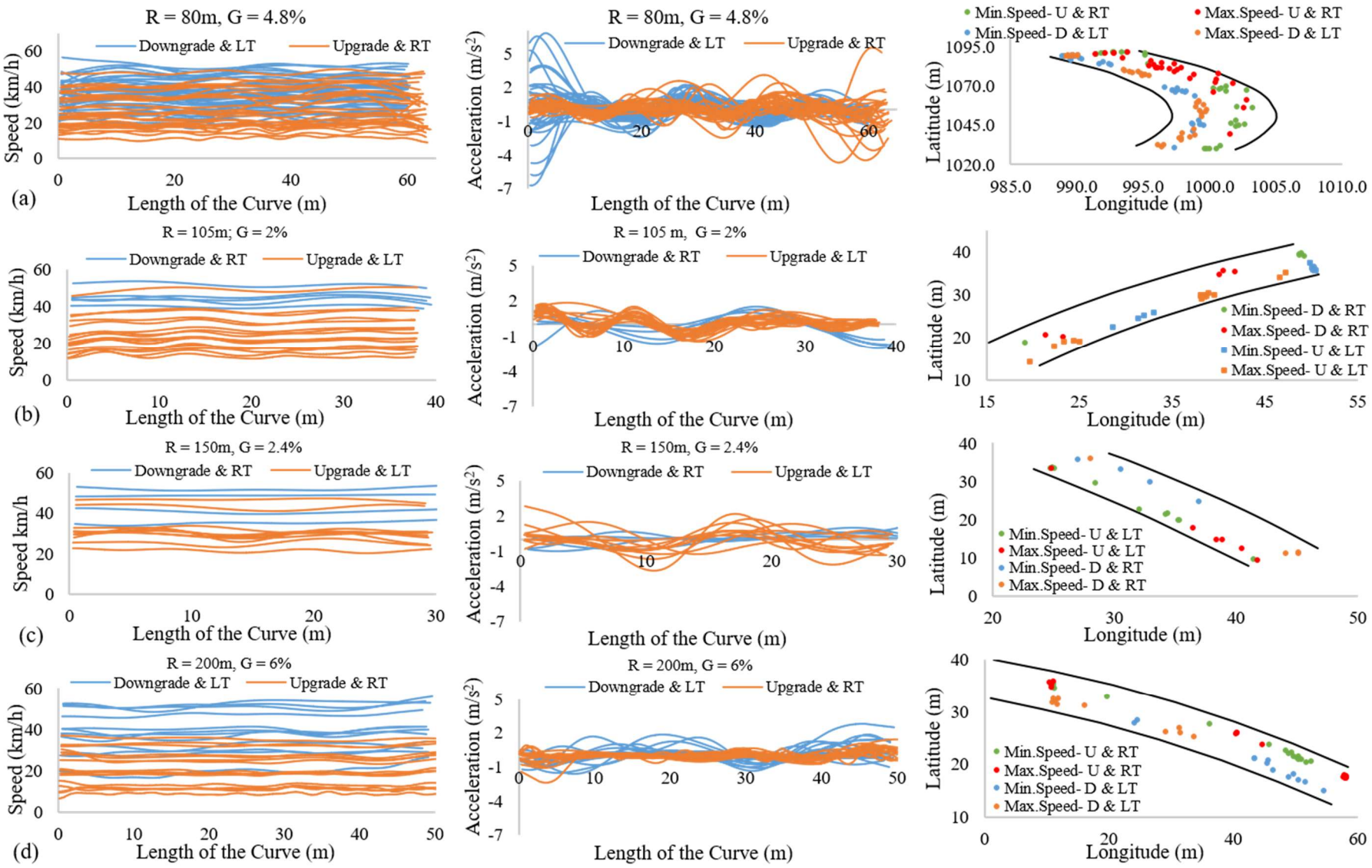

Fig. 4. 2 Speed & acceleration profiles and locations of minimum & maximum speeds of loaded truck, corresponding to four different curves

It is also observed that, as radius increases, the fluctuations in the speed and acceleration profiles decreases. Acceleration profiles indicate a significant variability in the speeds of car and loaded trucks, irrespective of the curve geometry. The figures also indicate that the locations corresponding to minimum and maximum speeds of car and loaded truck spread all along the curve.

4.3 Analysis of acceleration profiles

This section analyzed the speed variability on the curve through acceleration profiles of cars and loaded trucks. Figures 4.1 and 4.2 show that accelerations and decelerations occur on the curve for both vehicle types. Further, the vehicles are observed to traverse the curve in four different driving patterns (Figure 4.3).

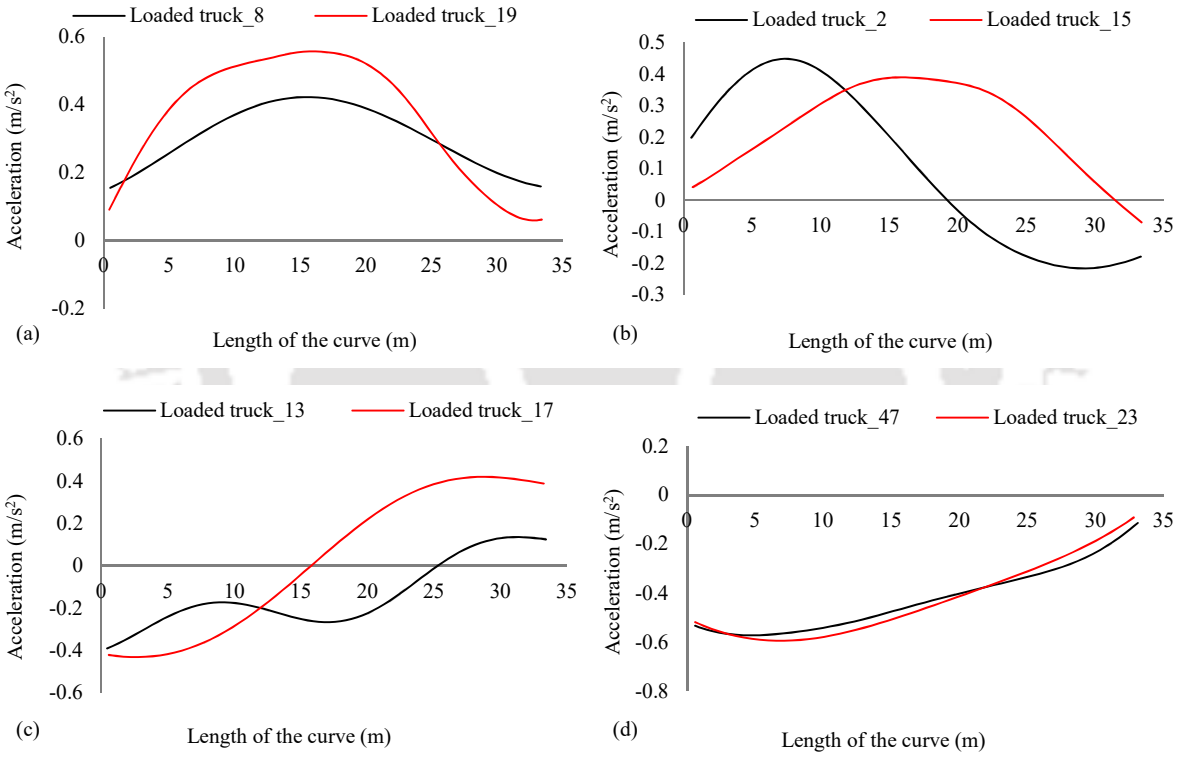

Fig. 4. 3 Four driving patterns of the vehicles (a) Continuous acceleration (b) Initially accelerating then decelerating (c) Initially decelerating then accelerating (d) Continuous deceleration

First, the vehicle enters the curve in deceleration mode and accelerates before departing the curve. Second, the vehicle traverses the entire curve in deceleration mode. Third, the vehicle enters the curve in acceleration mode and decelerates on the curve. Fourth, the vehicle

accelerates throughout the curve. Table 4.1 presents the proportion of four driving patterns of cars and loaded trucks corresponding to the 14 curves.

Table 4. 1 Proportion of cars and loaded trucks accelerating and decelerating on the curve

Curve. No	Direction	Percentage decelerating vehicles				Percentage accelerating vehicles			
		Entering the curve		On the entire curve		Entering the curve		On the entire curve	
		Car	Loaded truck	Car	Loaded truck	Car	Loaded truck	Car	Loaded truck
1	Right	40.54	20.00	5.41	0.00	59.46	80.00	0.00	0.00
	Left	0.00	0.00	0.00	0.00	100.00	100.00	0.00	0.00
2	Left	89.29	90.00	7.14	6.67	10.71	10.00	7.14	3.33
	Right	7.14	14.63	7.14	0.00	92.86	85.37	28.57	2.38
3	Left	50.00	30.00	0.00	0.00	50.00	70.00	0.00	0.00
	Right	23.08	75.00	0.00	0.00	76.92	25.00	0.00	0.00
4	Left	33.33	28.57	0.00	0.00	66.67	71.43	0.00	0.00
	Right	0.00	5.56	0.00	0.00	100.00	94.44	0.00	0.00
5	Left	12.50	4.55	0.00	0.00	87.50	95.45	0.00	0.00
	Right	75.00	42.86	0.00	0.00	25.00	57.14	12.50	0.00
6	Left	68.75	72.22	0.00	1.85	31.25	27.78	0.00	0.00
	Right	37.50	39.29	0.00	0.00	62.50	60.71	0.00	0.00
7	Right	44.44	71.43	0.00	0.00	55.56	28.57	0.00	0.00
	Left	6.67	7.69	0.00	0.00	93.33	92.31	0.00	0.00
8	Right	52.63	56.25	0.00	0.00	47.37	43.75	5.26	0.00
	Left	82.35	83.33	0.00	0.00	17.65	16.67	0.00	0.00
9	Left	60.00	42.31	0.00	0.00	40.00	57.69	0.00	0.00
	Right	84.62	91.84	0.00	0.00	15.38	8.16	0.00	0.00
10	Left	33.33	4.35	0.00	0.00	66.67	95.65	0.00	0.00
	Right	80.00	36.59	0.00	0.00	20.00	63.41	0.00	2.44
11	Right	20.69	42.86	0.00	0.00	79.31	57.14	0.00	0.00
	Left	34.62	41.03	0.00	0.00	65.38	58.97	0.00	0.00
12	Right	32.00	40.91	0.00	0.00	68.00	59.09	0.00	0.00
	Left	76.00	91.11	0.00	0.00	24.00	8.89	0.00	0.00
13	Right	33.33	48.48	0.00	0.00	66.67	51.52	0.00	0.00
	Left	37.50	20.34	0.00	0.00	62.50	79.66	0.00	0.00
14	Right	53.57	65.12	0.00	0.00	46.43	34.88	0.00	0.00
	Left	53.33	48.08	0.00	0.00	46.67	51.92	0.00	0.00

The table shows that the majority of vehicles (98%) are either accelerating or decelerating from the point of curvature and then either decelerating or accelerating before leaving the curve. At almost 12 locations, a majority of the cars (>50%) are decelerating on the curve from the point of curvature. Whereas at 9 locations, a majority of the loaded trucks (>50%) have decelerated on the curve from the point of curvature. Several factors, such as the road geometry in the vicinity of the curve and vehicle operations on the curve, might affect the acceleration and deceleration behavior of the vehicles. If the road geometry within the vicinity of the curve is not conforming to the driver's expectations, there could be deceleration and acceleration manoeuvres after entering the curve. A vehicle might decelerate after entering the curve at a speed higher than the design speed and realizing that the geometry of the downstream road stretch is not conforming to the driver's expectation. However, the acceleration/deceleration behavior of such vehicles might also be affected by the presence of the vehicles in the opposing traffic stream. If there is no vehicle in the opposing stream, the vehicle could encroach onto the opposite lane and maintain a radius larger than the curve radius to sustain the higher speed or even further accelerate. If there is a vehicle in the opposing lane, the deceleration process would continue until reaching the perceived safe speed corresponding to the curve geometry. Similarly, a vehicle might decelerate on the second half of the curve due to non-conformity of geometry or due to the presence of a vehicle in the opposing traffic stream.

The effect of vehicle operations on the curves is even more significant on the speed variability when there is no restriction/lack of enforcement of restriction on the passing or overtaking maneuvers. Encroachment of the opposite lane was observed near all fourteen curves. Hence, the acceleration-deceleration behavior is not only affected by the highway geometry but also by the individual vehicle operations on the curve.

Further, the extent of decelerating and accelerating length from the point of curvature was measured for each vehicle. Deceleration and acceleration length reflect the speed variability on the curve. Figures 4.4 and 4.5 present the deceleration and acceleration length of cars and loaded trucks. Figure 4.4 shows the cars, and loaded trucks decelerate up to 70% and 40% of the curve length, respectively. Figure 4.5 shows the cars, and loaded trucks accelerate up to 50% and 30% of the curve length, respectively.

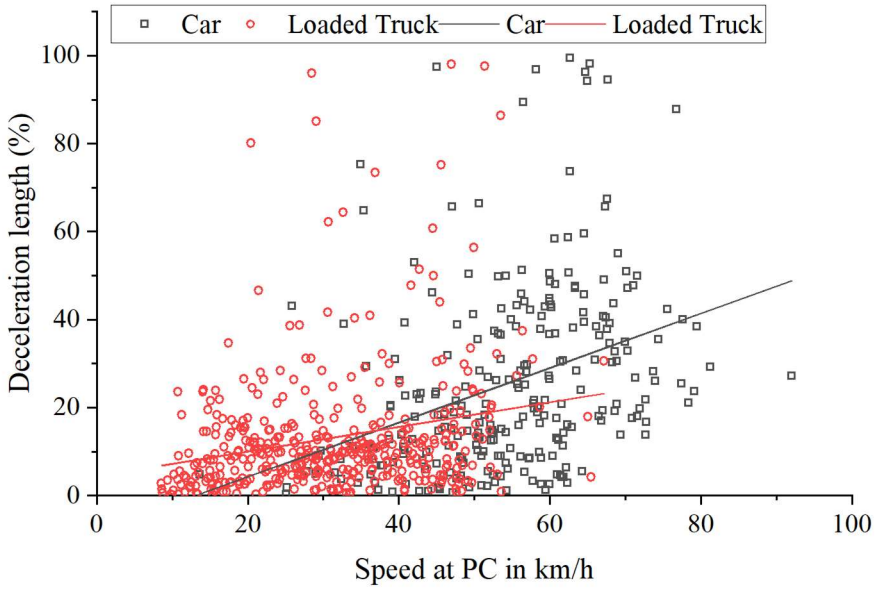

Fig. 4. 4 Vehicle's deceleration length on the curve from the point of curvature

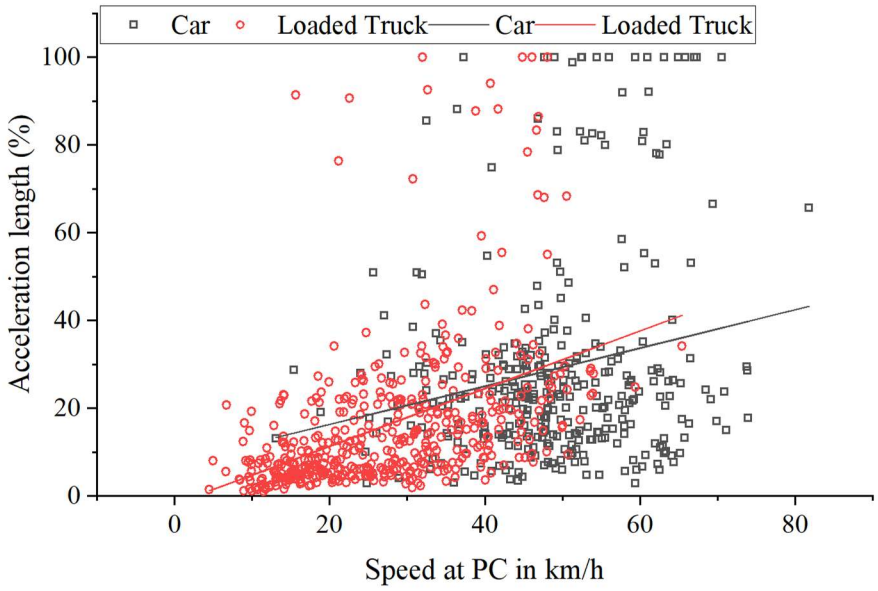

Fig. 4. 5 Vehicle's acceleration length on the curve from the point of curvature

Figure 4.4 shows that the deceleration length corresponding to the cars is higher than that of loaded trucks. This is obvious since cars traveling at higher speed require more length to complete the deceleration. Figure 4.5 shows that the slope of acceleration length corresponding to the cars is lower than that of loaded trucks. This could be due to the differences in the mechanical characteristics of cars and loaded trucks. Figure 4.5 also shows that the deceleration and acceleration length corresponding to the car and loaded trucks increases with speed at the point of curvature. Figure 4.6 presents the percentage frequency of accelerating and decelerating cars and loaded trucks corresponding to various curve lengths

expressed in multiples of ten percent. The percentage frequency of accelerating and decelerating cars and loaded trucks shows the differences in driving patterns of these two vehicle types. This figure also shows that irrespective of vehicle class, neither maximum nor minimum speed occurs at the center of the curve.

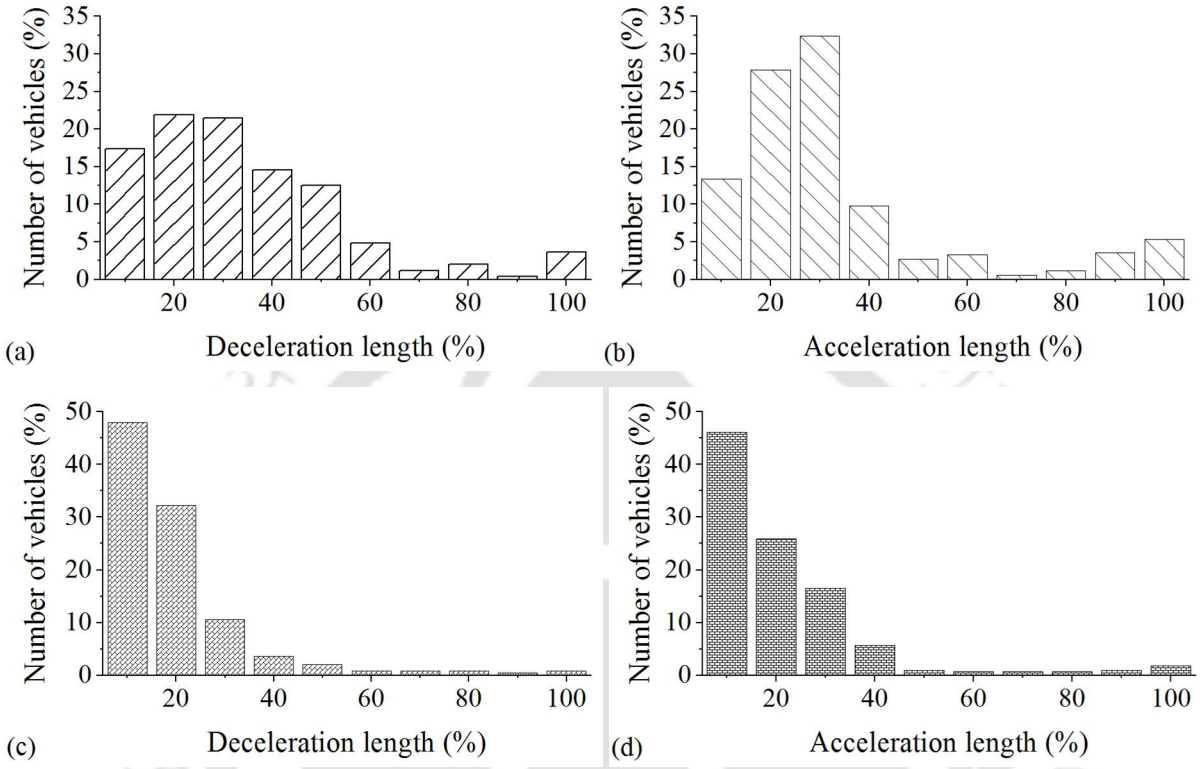

Fig. 4. 6 Percentage frequency of deceleration and acceleration length at every ten percent of the curve length for (a-b) car and (c-d) loaded truck

Besides, the percentage of total deceleration length (PTDL) and percentage of total acceleration length (PTAL) of car and loaded truck were also extracted. The 85th percentile values of PTDL and PTAL corresponding to car and loaded truck show a linear dependence (Figure 4.7). This observation could be specific to the horizontal curves falling in the mountainous terrain.

The above analysis shows that the vehicular speed varies on the horizontal curves falling in mountainous terrain. Both the geometry and the vehicle operations affect the speed variability. Hence, it is necessary to understand the factors affecting the speed variability and analyze its effect on the speed-based consistency assessment. The following sections present the analysis corresponding to the operating speed at the curve center, and maximum and minimum operating speeds.

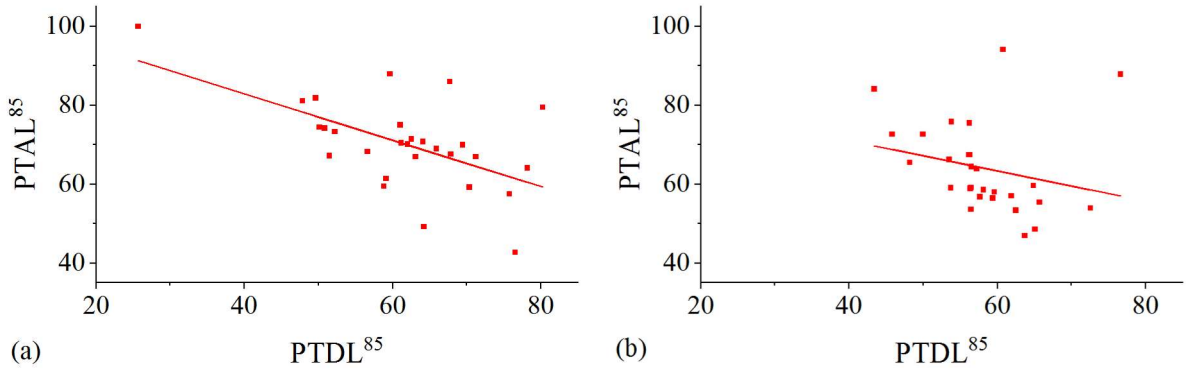

Fig. 4. 7 Scatterplots corresponding to $PTDL^{85}$ and $PTAL^{85}$ for (a) cars; (b) loaded trucks

4.4 Analysis of speed variability on horizontal curves

This section presents a detailed analysis of the speed variability using the data collected from fourteen curves. Since the vehicles vary their speeds on the curve, the data collection location significantly impacts the estimated operating speed. This phenomenon is illustrated by extracting the operating speeds of cars and loaded trucks at five different locations on the curve. The five locations on the curve are PC, CC, PT, a midpoint between PC and CC, and a midpoint between CC and PT. The considered curve is flat (<3%), 60.96m long, and has a radius of 80m. Figure 4.8 shows significant variability in the operating speed among the five different locations, for both vehicles, in each travel direction.

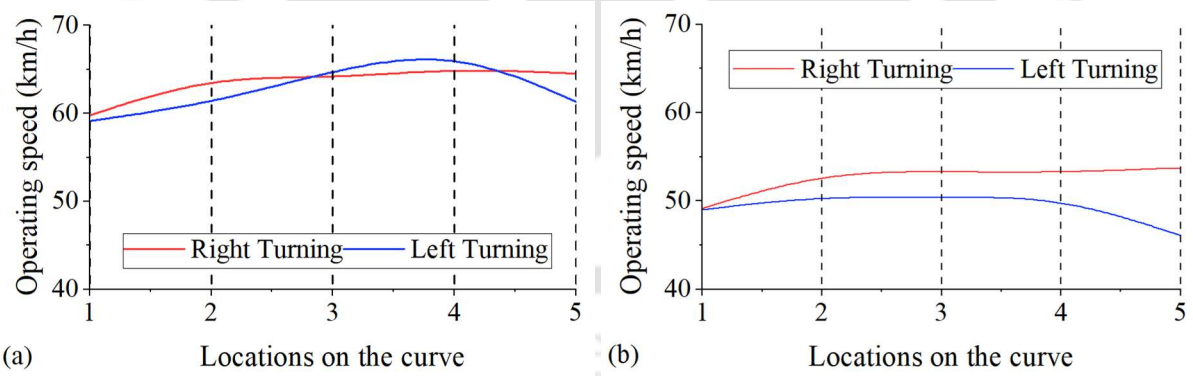

Note: 1 is at PC; 2 is at midpoint of PC and CC; 3 is at CC; 4 is at midpoint of CC and PT; and 5 is at PPT

Fig. 4. 8 Operating speed at various locations on the horizontal curve (a) car and (b) loaded truck

Further considering the speed at every one-meter, operating speed profile models were developed using quantile regression to assess the speed variability on the horizontal curve. Quantile regression models the conditional quantiles of the response variable Y given the set of covariates X (Koenker and Bassett 1978; Xiao 2009; Li et al. 2011). This approach is more flexible for modeling the data with heterogeneous conditional distributions and robust to the

outliers in Y than the least square regression (Li et al. 2011). The linear model for the τ^{th} quantile is as follows:

$$Y_i = \alpha + \beta_1 X_i + z_i^T \gamma + e_i \quad i = 1,2,....,n \tag{4.1}$$

Where Y_i is the i^{th} response, X_i is the independent variable, z_i is the q-dimensional vector of linear covariates with constant slopes, α is the Y-intercept, β_1 is the slope and e_i is the error term whose τ^{th} quantile is zero conditional on (X_i, z_i). Let $\eta = (\alpha, \beta_1, \gamma^T)$. The τ^{th} quantile of Y_i given X_i and z_i is $Q(X_i, z_i; \eta)$. The coefficients of the τ^{th} quantile can be obtained by solving the following equation.

$$\min_{\eta \in R^3 + q} \sum_{i=1}^{n} \rho_\tau (Y_i - Q(X_i, z_i; \eta)) \tag{4.2}$$

Where $\rho_\tau(w) = w(\tau - I(w < 0))$, $0 < \tau < 1$. Here, I(·) denotes the indicator function. In this study, quantile regression models were developed with $\tau = 0.85$ (85^{th} percentile) and obtained operating speed profiles. Figure 4.9 shows the operating speed profiles of two curves obtained through quantile regression. Figure 4.9 (a-b) shows the operating speed profiles of car and loaded truck corresponding to a curve of 80m radius. The estimated acceleration/deceleration rates corresponding to car for the horizontal curve was 0.75m/s^2. The estimated acceleration/deceleration rates corresponding to loaded truck for the horizontal curve was 0.33m/s^2. Figure 4.9 (c-d) shows operating speed profiles of car and loaded truck corresponding to a curve of 200m radius. The estimated acceleration/deceleration rates corresponding to car for the horizontal curve was -0.87m/s^2. The estimated acceleration/deceleration rates corresponding to loaded truck for the horizontal curve was -0.65m/s^2. Figure also shows the models of operating speed profile as a function of curve length. The coefficient of L_C in the models are statistically significant at a 5% significance level.

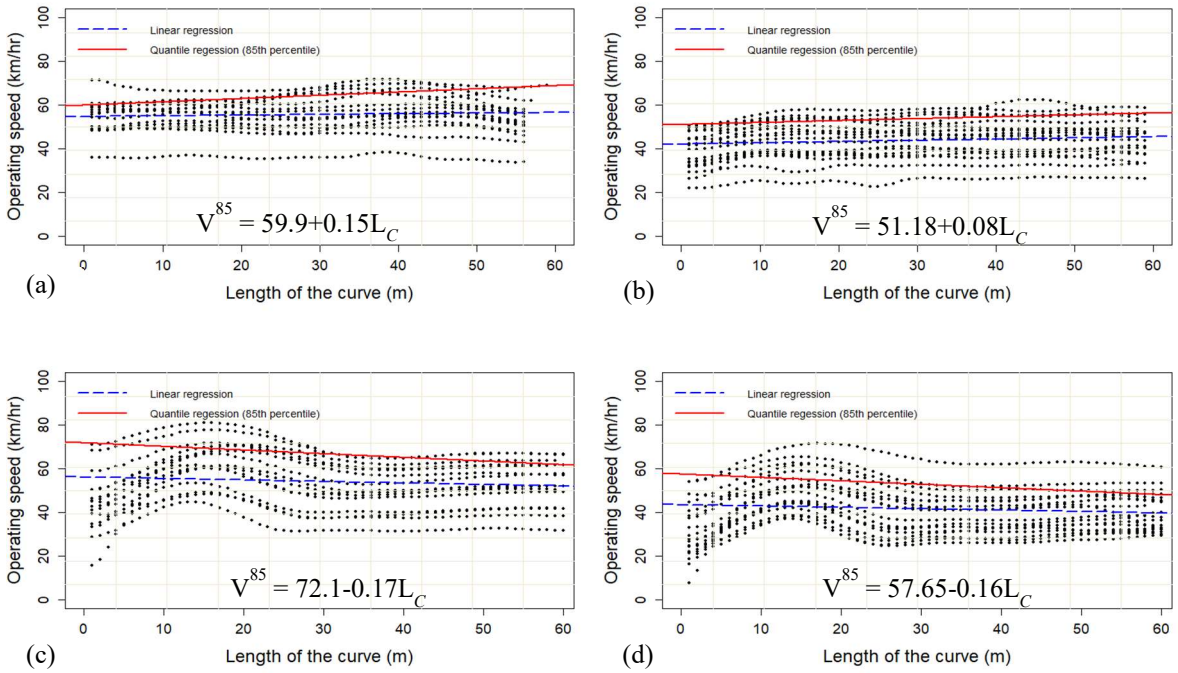

Fig. 4. 9 Operating speed profiles corresponding to the horizontal curve with radius 80m for (a) car and (b) loaded truck; and 200m for (c) car and (d) loaded trucks

The figure shows that the operating speed either linearly increasing or decreasing from the point of curvature to the point of transition, indicating that accelerations and decelerations take place on the curve. Considering the speed variability on the curve, the variables such as V_{Min}, V_{Max}, and V_{CC} are further investigated in the following sub-sections.

4.4.1 Comparison of V_{Min} and V_{Max} on the curve

The locations of V_{Min} and V_{Max} on the curve were investigated by dividing the curve into three equal segments (Figure 4.10). Based on the locations of V_{Min} and V_{Max} on each curve, the frequency of vehicles having V_{Min} and V_{Max} was determined for each segment. Figures 4.11 and 4.12 show the frequency distributions of V_{Min} and V_{Max} corresponding to the car and loaded truck, for fourteen horizontal curves, in both left and right turning directions. Figure 4.11 shows that V_{Min} and V_{Max} of the car mostly occur either at the first or third segment of the curve.

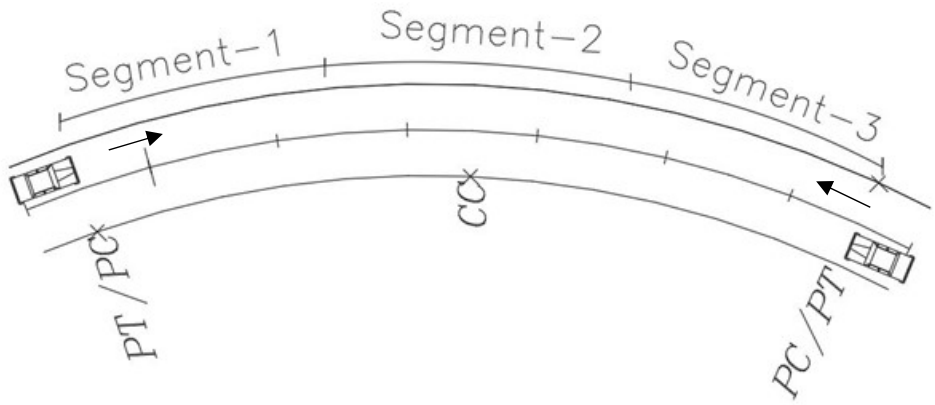

Fig. 4. 10 Typical horizontal curve segmented into three equal sections

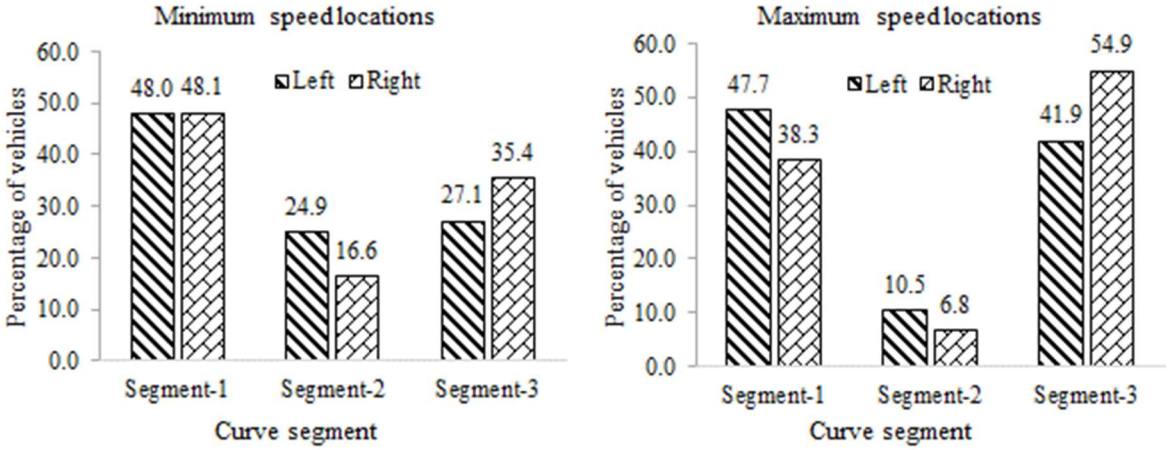

Fig. 4. 11 Distribution of minimum and maximum speed locations for car, on left and right turning curves

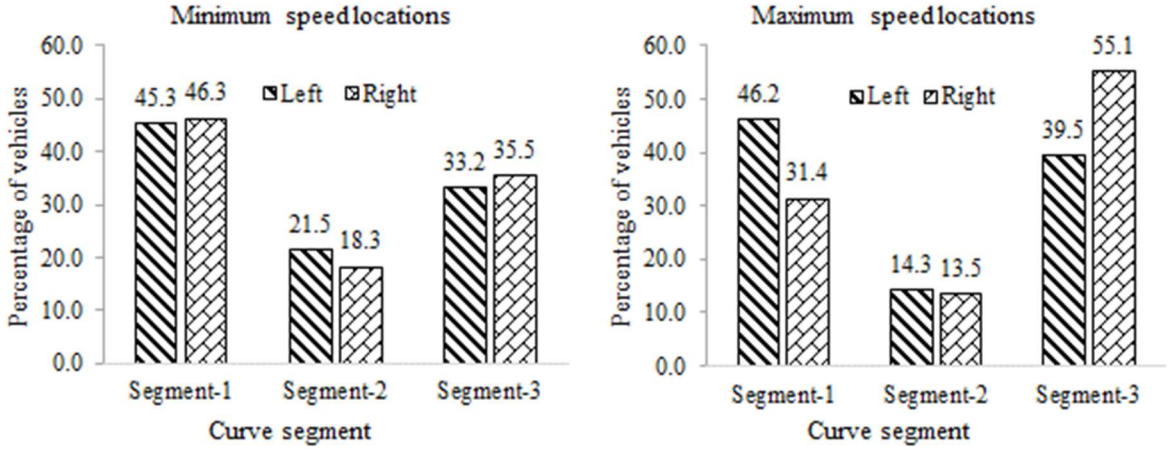

Fig. 4. 12 Distribution of minimum and maximum speed locations for loaded trucks, on left and right turning curves

Two types of driving behavior could be interpreted from the frequencies of V_{Min} and V_{Max}. First, the drivers do not often complete their deceleration on the approach tangent and enter into the curve in deceleration mode, then accelerates while departing the curve. Second,

the drivers accelerate upon entering the curve from the approach tangent, reach maximum speed, decelerate, and then accelerate while departing the curve. It can be postulated from the figure that the speed of the car is not constant in both travel directions. The figure also shows that neither the V_{Min} nor the V_{Max} occurs at the center of the curve. Similar patterns were observed for the loaded trucks as well.

Further, the speed variability of both car and loaded truck were assessed through statistical comparison of V_{Min}, V_{Max}, and V_{CC}. Tables 4.2 and 4.3 show the statistics of V_{Min}, V_{Max}, and V_{CC} of cars and loaded trucks, corresponding to fourteen locations and both travel directions. Table 4.2 shows that the average V_{Min} of the car exceeds the design speed (50 kmph) in 36% of the locations, in both left and right turning directions. Whereas the average V_{Max} of the truck is lower than the design speed on all the curves (Table 4.3). The mean and variance of V_{Min}, V_{Max}, and V_{CC} are different for both car and loaded trucks, on all the horizontal curves.

Table 4. 2 Statistics of V_{Min}, V_{Max}, and V_{CC} for the car with respect to the travel direction, in km/h

	Left Turning Car						Right Turning Car					
Curve No.	V_{Min}		V_{Max}		V_{CC}		V_{Min}		V_{Max}		V_{CC}	
	μ	σ^2	μ	σ^2	μ	σ^2	μ	σ^2	μ	σ^2	μ	σ^2
1	46.7	58.53	51.6	67.52	49.0	66.61	52.5	85.45	58.3	71.56	54.8	86.56
2	59.2	65.07	61.2	52.95	59.7	54.81	57.3	88.31	61.3	70.87	59.7	77.16
3	57.4	208.9	59.8	207.0	57.8	209.1	56.8	266.0	61.8	185.1	58.3	247.4
4	51.6	63.05	58.9	87.15	55.3	75.55	50.4	73.32	57.7	91.49	55.8	88.17
5	53.0	105.2	57.4	116.2	54.6	121.6	51.0	70.32	56.0	80.11	52.5	65.37
6	45.6	115.1	49.6	104.6	46.8	107.9	43.4	47.42	48.7	55.16	45.2	54.13
7	45.3	127.9	63.1	124.5	51.7	145.1	45.9	133.8	61.7	81.36	49.1	100.5
8	55.0	133.6	60.9	104.0	58.2	109.5	48.1	270.3	53.3	188.2	50.4	202.6
9	44.1	28.90	51.1	41.16	47.1	28.65	39.1	76.01	48.0	61.18	43.7	64.81
10	46.7	172.5	51.3	179.4	48.9	174.7	46.9	104.7	52.2	102.8	49.4	102.1
11	47.5	113.4	57.7	101.7	53.1	82.44	42.5	131.1	51.7	128.2	46.8	95.77
12	44.7	59.24	52.6	38.93	49.3	36.33	44.2	126.5	56.1	99.11	50.3	51.67
13	40.3	79.79	49.8	75.82	44.6	52.96	43.4	89.57	55.1	82.04	50.2	56.78
14	48.8	140.3	61.3	135.7	54.0	90.50	45.0	95.20	56.0	106.4	48.7	64.54

Table 4. 3 Statistics of V_{Min}, V_{Max}, and V_{CC} for loaded trucks with respect to travel direction, in km/h

	Left Turning Loaded Truck						Right Turning Loaded Truck					
Curve No.	V_{Min}		V_{Max}		V_{CC}		V_{Min}		V_{Max}		V_{CC}	
	μ	σ^2	μ	σ^2	μ	σ^2	μ	σ^2	μ	σ^2	μ	σ^2
1	23.2	84.95	27.1	89.39	24.5	88.93	42.9	15.65	46.8	19.85	43.7	17.94
2	44.7	30.98	47.1	25.57	45.7	28.04	23.4	132.6	25.8	136.9	24.5	136.6
3	29.6	57.77	33.5	52.86	30.5	61.84	43.2	61.55	45.6	55.21	43.8	57.82
4	39.0	69.46	44.9	71.72	43.5	73.52	38.6	71.69	45.2	75.33	43.9	75.77
5	13.5	13.73	17.0	14.82	14.2	14.74	30.6	155.7	34.7	158.0	32.4	164.4
6	16.8	61.89	21.3	67.74	18.7	63.55	38.9	61.29	44.1	59.82	40.5	55.35
7	32.8	146.5	50.3	125.3	38.8	124.2	14.7	65.54	28.5	79.21	19.4	58.52
8	36.3	109.3	41.4	96.22	39.0	106.3	19.7	73.86	22.9	78.08	20.9	74.11
9	23.3	70.08	30.0	103.2	26.6	81.95	29.2	65.36	34.9	73.27	32.9	69.87
10	33.3	80.65	37.6	76.39	35.6	77.42	16.9	75.87	20.8	87.78	19.1	78.87
11	30.9	75.81	39.0	76.22	35.8	75.16	24.4	94.76	31.0	122.5	28.2	104.3
12	22.2	68.91	28.2	63.83	25.6	62.70	29.3	79.58	39.3	82.67	35.1	63.79
13	17.8	70.07	25.5	63.10	21.3	53.36	27.6	77.95	36.4	57.50	33.2	68.81
14	24.1	74.15	37.1	73.96	30.6	41.00	16.7	75.88	26.7	89.95	21.1	53.78

Further, a statistical test was performed at a 5% significance level to ascertain whether the average V_{Min} is less than the average V_{Max}. Table 4.4 shows the summary of the t-test, i.e., t-statistic and *p*-values, for each location, for the Null hypothesis, H_o: Avg.V_{Min} ≥ Avg.V_{Max}. The *p*-values for cars and loaded trucks corresponding to all the locations in both travel directions are less than 0.05. The null hypotheses for cars and loaded trucks, with respect to travel direction, were rejected for all the curves indicating that both car's and loaded truck's Avg.V_{Min} is statistically less than the Avg.V_{Max}. Thus, it can be concluded that the speeds of cars and loaded trucks vary along the horizontal curve in both the travel directions of a curve. The following sub-section presents the analysis pertaining to the occurrence of V_{Min} and V_{Max} at the centre of the curve.

Table 4. 4 Summary of t-test on the difference b/w V_{Min} and V_{Max}, at 5% significance, for car and loaded truck

Curve No	Left Turning Car		Right Turning Car		Left Turning Loaded Truck		Right Turning Loaded Truck	
	t stat	*p*-value	*t* stat	*p*-value	*t* stat	*p*-value	*t* stat	*p*-value
1	-18.66	<0.000	-10.31	<0.000	-18.50	<0.000	-8.41	0.001
2	-4.21	<0.000	-5.08	<0.000	-6.73	<0.000	-9.82	<0.000
3	-5.49	<0.000	-4.26	<0.000	-7.16	<0.000	-6.59	0.007
4	-9.48	<0.000	-12.93	<0.000	-12.87	<0.000	-10.70	<0.000
5	-11.18	<0.000	-6.43	<0.000	-20.85	<0.000	-10.92	<0.000
6	-7.12	<0.000	-7.78	<0.000	-11.98	<0.000	-12.69	<0.000
7	-12.71	<0.000	-21.65	<0.000	-14.95	<0.000	-21.22	<0.000
8	-6.54	<0.000	-4.17	<0.000	-7.48	<0.000	-9.77	<0.000
9	-6.71	<0.000	-6.94	<0.000	-10.56	<0.000	-18.50	<0.000
10	-10.50	<0.000	-8.81	<0.000	-16.57	<0.000	-12.46	<0.000
11	-6.86	<0.000	-7.18	<0.000	-8.59	<0.000	-9.27	<0.000
12	-7.11	<0.000	-7.93	<0.000	-10.17	<0.000	-9.23	<0.000
13	-5.78	<0.000	-8.83	<0.000	-13.48	<0.000	-10.18	<0.000
14	-8.75	<0.000	-6.14	<0.000	-11.70	<0.000	-8.93	<0.000

4.4.2 Comparison of V_{Min}, V_{Max}, and V_{CC}

Constant speed assumption facilitated the data collection at the center of the curve for developing operating speed and speed reduction models that are later used to evaluate the design and operating speed consistencies. Both these measures may not represent the geometric consistency if the V_{Min} and V_{Max} do not occur at the center of the curve. This subsection statistically verifies whether the V_{CC}, V_{Max}, and V_{Min}, of both the cars and loaded trucks, are statistically the same or not. The statistics of V_{Min} and V_{CC} (Tables 4.2 and 4.3) show that the average V_{Min} is relatively smaller than the average V_{CC}, for both the car and loaded trucks, near all the locations.

A two-tailed t-test was performed at 5% significance level to determine whether the V_{Min} and V_{CC} are statistically the same. Table 4.5 shows the summary of the t-test, i.e., t-statistic and *p*-values, for each location, for the Null hypothesis, H_o: Avg.V_{Min} = Avg.V_{CC}.

Table 4. 5 Summary of t-test on the difference b/w average V_{Min} and average V_{CC} at 5% significance, for car and loaded truck

Curve No	Left Turning Car		Right Turning Car		Left Turning Loaded Truck		Right Turning Loaded Truck	
	t stat	*p*-value	t stat	*p*-value	t stat	*p*-value	t stat	*p*-value
1	-9.99	0.000	-5.52	0.000	-5.59	0.000	-3.32	0.029
2	-2.03	0.053	-3.85	0.001	-5.43	0.000	-6.92	0.000
3	-2.34	0.044	-3.05	0.010	-3.40	0.008	-2.14	0.122
4	-6.21	0.000	-9.72	0.000	-9.71	0.000	-7.93	0.000
5	-4.21	0.004	-2.72	0.030	-4.58	0.000	-6.39	0.000
6	-4.42	0.001	-2.87	0.012	-9.16	0.000	-5.68	0.000
7	-3.65	0.003	-5.37	0.000	-4.88	0.000	-7.32	0.000
8	-6.27	0.000	-2.68	0.015	-6.98	0.000	-6.99	0.000
9	-8.04	0.000	-5.61	0.000	-9.20	0.000	-14.88	0.000
10	-5.80	0.000	-7.82	0.000	-8.15	0.000	-8.89	0.000
11	-3.78	0.001	-4.48	0.000	-5.34	0.000	-8.72	0.000
12	-4.47	0.000	-4.81	0.000	-7.54	0.000	-6.12	0.000
13	-4.00	0.001	-5.48	0.000	-9.09	0.000	-6.74	0.000
14	-4.59	0.000	-3.01	0.006	-7.19	0.000	-5.86	0.000

The table shows that the *p*-values for cars and loaded trucks, corresponding to all the locations, in both travel directions, are less than 0.05. Thus the null hypotheses for cars and loaded trucks, with respect to travel direction, were rejected for all the curves indicating that both car's and loaded truck's average V_{Min} are statistically different from the respective average V_{CC}. Therefore, it can be concluded that V_{Min} doesn't occur at the center of the curve for cars and loaded trucks. Likewise, Avg.V_{CC} and Avg.V_{Max} were statistically compared using the Null hypothesis, H_o: Avg.V_{Max} = Avg.V_{CC}, at a 5% significance level. Table 4.6 shows the summary of the t-test, i.e., t-statistic and *p*-values, for each location and travel direction, corresponding to the car and loaded truck, respectively.

Table 4. 6 Summary of t-test on the difference b/w average V_{Max} and average V_{CC} at 5% significance, for car and loaded truck

Curve No	Left Turning Car		Right Turning Car		Left Turning Loaded Truck		Right Turning Loaded Truck	
	t stat	*p*-value	*t* stat	*p*-value	*t* stat	*p*-value	*t* stat	*p*-value
1	-14.61	<0.00	-10.03	<0.00	-16.14	<0.00	-7.61	<0.00
2	-5.99	<0.00	-7.11	<0.00	-6.45	<0.00	-9.88	<0.00
3	-4.44	<0.00	-3.92	<0.00	-5.43	<0.00	-3.88	0.03
4	-7.03	<0.00	-4.75	<0.00	-8.55	<0.00	-4.48	<0.00
5	-10.16	<0.00	-5.35	<0.00	-21.73	<0.00	-5.99	<0.00
6	-5.36	<0.00	-7.45	<0.00	-10.11	<0.00	-10.44	<0.00
7	-18.37	<0.00	-31.62	<0.00	-21.57	<0.00	-26.30	<0.00
8	-3.67	<0.00	-5.67	<0.00	-3.31	0.01	-5.69	<0.00
9	-3.94	<0.00	-3.58	<0.00	-6.09	<0.00	-7.12	<0.00
10	-4.78	<0.00	-5.39	<0.00	-11.08	<0.00	-7.37	<0.00
11	-8.55	<0.00	-5.13	<0.00	-8.19	<0.00	-5.16	<0.00
12	-8.86	<0.00	-4.51	<0.00	-6.10	<0.00	-7.26	<0.00
13	-6.52	<0.00	-5.97	<0.00	-8.97	<0.00	-8.37	<0.00
14	-5.64	<0.00	-5.75	<0.00	-9.17	<0.00	-6.11	<0.00

The *p*-values are less than 0.05 for cars and loaded trucks corresponding to all the locations, in both travel directions. Thus the null hypotheses for cars and loaded trucks, with respect to travel direction, were rejected for all the curves indicating that both car's and loaded truck's average V_{Max} is statistically different than the average V_{CC}. Hence, it can be concluded that V_{Max} doesn't occur at the curve center, for both vehicles, and in both the travel directions.

4.5 Development of maximum speed difference model

The above analysis shows that neither the maximum nor the minimum speed occurs at the center of the horizontal curve. The maximum speed difference on the curve based on the V_{Min} and V_{Max} was measured for each car and loaded truck, for all the locations (Figure 4.13). The 85th percentile of maximum speed difference ($Max\Delta_{85}V$) ranged between 2.1 to 22.9 km/h and 2.2 to 22.48 km/h, for cars and loaded trucks, respectively. The average values of $Max\Delta_{85}V$ for cars and loaded trucks are 9.7 km/h and 8.4 km/h, respectively. The standard deviations of $Max\Delta_{85}V$ for cars and loaded trucks are 5.4 km/h and 4.98 km/h, respectively. The 85th percentile of maximum speed difference ($Max\Delta_{85}V$) on the curve was modeled using several geometry and speed-related parameters.

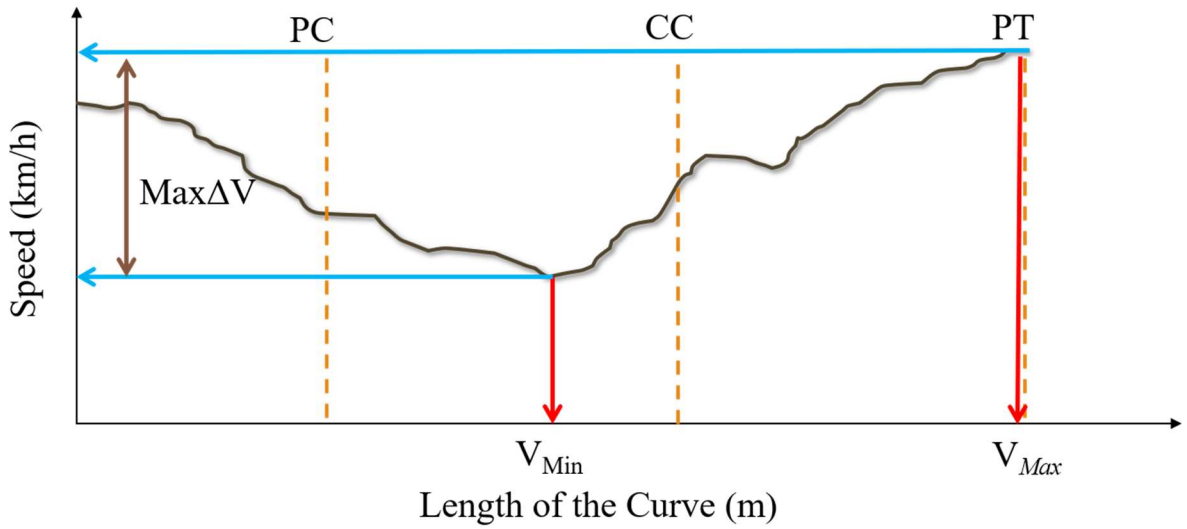

Fig. 4. 13 Schematic representation of maximum speed difference on the curve

The independent variables include the geometric parameters of the curve, approach tangent, and departing tangent of the curve. The independent variables also include the parameters such as the speed at the point of curvature (V_{PC}) and the vehicle's lateral distance, measured at the PC (LD_{PC}), from the vehicle's centerline to the nearest edge of the road (Figure 3.20). The inclusion of these speed parameters was possible only due to the availability of high-fidelity vehicle trajectories. Independent variables influencing the MaxΔ_{85}V were identified based on the Pearson correlation analysis. The influencing variables were identified based on the strength of the correlation (correlation greater than 0.3) and used in further regression modeling (Cohen et al. 2003; Akoglu 2018). Tables 4.7 & 4.8 present the Pearson correlation matrices for car and loaded trucks, respectively.

Tables 4.7 & 4.8 indicate that the correlation of independent variables with the MaxΔ_{85}V is different for cars and loaded trucks. Correlation analysis also shows that the linear association between MaxΔ_{85}V and the lateral distance at the point of curvature (LD_{PC}) is very low. The independent variables were selected based on the correlation coefficients and linear regression models were estimated using the Ordinary Least Square (OLS) Method.

Table 4. 7 Pearson correlation matrix corresponding to MaxΔ_{85}V for cars

	MaxΔ_{85}V	*R*	Δ	L_{at}	L_C	L_{et}	*G*	$R \times L_w$	*DC*	*CCR*	V_{PC}	LD_{PC}
MaxΔ_{85}V	1											
R	0.37	1										
Δ	0.04	-0.81	1									
L_{at}	0.07	-0.36	0.42	1								
L_C	0.4	-0.27	0.78	0.24	1							
L_{et}	-0.1	-0.36	0.42	0.16	0.24	1						
G	-0.14	0	0	-0.41	0	0.41	1					
$R \times L_w$	0.3	0.95	-0.81	-0.38	-0.33	-0.33	0.02	1				
DC	-0.23	-0.98	0.89	0.43	0.42	0.43	0	-0.94	1			
CCR	-0.46	-0.94	0.61	0.35	-0.02	0.35	0	-0.85	0.89	1		
V_{PC}	-0.56	0.14	-0.46	0.03	-0.66	-0.11	-0.12	0.14	-0.24	0.08	1	
LD_{PC}	-0.11	-0.05	0.08	-0.12	0.11	0	0.08	0.06	0.03	0.04	0.12	1

Table 4. 8 Pearson correlation matrix corresponding to MaxΔ_{85}V for loaded trucks

	MaxΔ_{85}V	*R*	Δ	L_{at}	L_C	L_{et}	*G*	$R \times L_W$	*DC*	*CCR*	V_{PC}	LD_{PC}
MaxΔ_{85}V	1											
R	0.27	1										
Δ	0.16	-0.81	1									
L_{at}	0.08	-0.36	0.42	1								
L_C	0.51	-0.27	0.78	0.24	1							
L_{et}	0.01	-0.36	0.42	0.16	0.24	1						
G	-0.05	0	0	-0.41	0	0.41	1					
$R \times L_W$	0.19	0.95	-0.81	-0.38	-0.33	-0.33	0.02	1				
DC	-0.12	-0.98	0.89	0.43	0.42	0.43	0	-0.94	1			
CCR	-0.39	-0.94	0.61	0.35	-0.02	0.35	0	-0.85	0.89	1		
V_{PC}	-0.15	-0.04	-0.09	0.56	-0.25	-0.1	-0.75	-0.01	0.02	0.15	1	
LD_{PC}	-0.03	-0.05	0	-0.17	-0.03	-0.04	-0.08	0.11	0.04	0.1	0.08	1

Shallam et al. (2021) found that driver perception varies based on the gradient and the turning direction, and both these parameters have a significant impact on the adopted speed. Hence, this study analyzed the impact of these two parameters on the way the other curve characteristics affect speed adoption through variable interaction. For this, two dummy variables corresponding to travel direction (D) and gradient (G) interacting with other geometric and speed parameters were considered. This allows testing the hypothesis that the effect of the other curve characteristics on MaxΔ_{85}V is significantly different based on the direction and the gradient. In modeling MaxΔ_{85}V, a backward stepwise regression was used

and found that none of the independent variables was found to be statistically significant at a 5% significance level. This could be due to the fact that, in a highway alignment passing through mountainous terrain, the geometric variables considered for operating speed modeling are unevenly distributed, leading to selection bias (Shallam et al. 2021). Apart from the selection bias, heteroscedasticity was also observed in the data. In such situations, modeling $Max\Delta_{85}V$ using the OLS technique might lead to insignificant coefficient estimates. Heteroscedasticity in the data causes OLS regression to underestimate the standard errors of the coefficients, which means that the t-statistics of the coefficients will be inflated. This, in turn, can increase the probability of rejecting a true null hypothesis (Greer 2012). Thus, to overcome the issues due to heteroscedasticity and selection bias, the weighted multivariate linear regression approach proposed by Qu et al. (2015) and Shallam et al. (2021) was used for modeling $Max\Delta_{85}V$.

Considering the selection bias and heteroscedasticity, weights were estimated based on the proximity of observations in the multi-dimensional space. Qu et al. (2015) proposed a multi-dimensional extension of the weight estimation procedure for calibrating the fundamental macroscopic diagram of the traffic stream. Qu et al. (2015) used the one-dimensional Euclidean distance between a pair of points to assign weights. Later, Shallam et al. (2021) extended the procedure for multi-dimension, and the details of the proposed method are as follows.

Let (X_1, v_1), (X_2, v_2), ……., (X_n, v_n) be the observations where v_i is the operating speed and X_i be the vector of independent variables. In the case of ordinary least squared regression, the model function $v = f(X_i, \hat{\beta})$ is estimated by minimizing the standard deviation:

$$\min_{\hat{\beta}} \sum_{i=1}^{n} (v_i - f(X_i, \beta))^2 \tag{4.3}$$

In this case, the assumption was that all the observations were equally weighted while estimating the model parameters. However, the assumption is not valid for the data that has significant selection bias. The weighted linear regression can handle such bias if the weights are properly assigned to the observations. Weighted linear regression minimizes:

$$\min_{\hat{\beta}} \sum_{i=1}^{n} \varpi_i (v_i - f(X_i, \beta))^2 \tag{4.4}$$

Where the weights ϖ_i are estimated as follows.

Let $X_i = [x_i^1, x_i^2, \ldots\ldots, x_i^n]^T$ be the n-dimensional vector of the independent variables corresponding to the i^{th} curve of the highway alignment considered in the study. The weight corresponding to a particular observation is estimated based on the proximity of the other observations in the n-dimensional space. The proximity between a pair of observations x_i and x_j is measured as Euclidean distance $D_{(i),(j)}$ in n-dimensional space, as shown in Equation 4.5,

$$D_{(i),(j)} = \sqrt{\sum_{p=1}^{n} (x_i^p - x_j^p)^2} \tag{4.5}$$

In the equation 4.5, 'p' represents the number of independent variables. Now, the weight estimation is performed similarly to Qu et al. (2015), as follows;

Step-1: Rank the observations based on the distance from the origin $D_{(i)} = \sqrt{\sum_{p=1}^{n} x_i^{p^2}}$. Thus we have, $(v_1, X_1) \ldots\ldots, (v_i, X_i) \ldots\ldots, (v_n, X_n)$, where $X_{(1)} \leq X_{(2)} \leq \ldots..\leq X_{(i)} \leq \ldots\ldots..\leq X_{(n)}$ are the observations corresponding to independent variables and $v_{(i)}$ is the observation of the dependent variable corresponding to the i^{th} geometry.

Step-2: Define (u) as the largest index (i) that corresponds to the same vector as $X_{(1)}$, i.e.,

$$u := argmax\{i = 1, 2, \ldots\ldots n | X_{(i)} = X_{(1)}\} \tag{4.6}$$

Then,

$$\varpi_i = \frac{D_{(u+1),(1)}}{u},\ i = 1,2, \ldots., u \tag{4.7}$$

Step-3: Define $u = u+1$. Define (u) as the largest index (i) that corresponds to the same vectors as $X_{(u)}$, i.e.,

$$u := argmax\{i = u, u+1, u+2, \ldots\ldots n | X_{(i)} = X_{(u)}\} \tag{4.8}$$

If $u < n$, set

$$\varpi_i = \frac{D_{(u+1),(u-1)}}{2(u-u+1)},\ i = u,\ u+1,\ u+2,\ \ldots.,\ u \quad (4.9)$$

and repeat Step 3. Else,

$$\varpi_i = \frac{D_{(n),(u-1)}}{n-u+1},\ i = u,\ u+1,\ u+2,\ \ldots.,\ n \quad (4.10)$$

and stop.

The OLS regression approach assumes that the error follows a normal distribution and the extreme values (known as outliers) are rare (Ghosh 2018). However, these values still occur, and the main disadvantage of the OLS method is its sensitivity to outliers. The outliers significantly influence the fit because squaring the residuals magnifies the effects of these extreme data points. Thus, to minimize the outliers, the data can be fitted with robust weighted least square regression. The robust regression works on the principle that less weight is assigned to the observations lying far from the group of data and vice-versa that uses an iteratively reweighted least-squared algorithm (Chatterjee and Mächler 1997; Ghosh 2018). Table. 4.9 shows the models developed for each vehicle category using Robust Weighted Least Square (RWLS) Method.

Table 4. 9 Summary of RWLS estimates of MaxΔ_{85}V models

Vehicle	Regression models	R^2	R^2_{Adj}	RMSE (km/h)	MAD (km/h)
Car	34.491 - 0.00214CCR + 0.0021CCR × G - 0.0057CCR × D - 0.44V_{PC} - 0.073V_{PC} × G + 0.0953V_{PC} × D	0.99	0.99	7.42	5.78
Loaded Truck	2.989 + 0.13L_C + 0.028L_C × G - 0.075L_C × D - 0.0023CCR - 0.0016CCR × G+0.0028CCR × D	0.99	0.99	6.42	4.26

Note: D = Direction; G = Gradient

For cars, curvature change rate (CCR) and speed at the point of curvature (V_{PC}) are significant in explaining the variability of MaxΔ_{85}V. The maximum speed difference on the curve increases with the decreasing CCR and speed at the point of curvature. Whereas for loaded trucks, the length of the curve (L_C) and CCR are significant in explaining the variability in MaxΔ_{85}V. The MaxΔ_{85}V increases with the increasing curve length but decreases with the increasing CCR. Unlike cars, the speed at the point of curvature has not shown any influence on the loaded trucks, and this could be because the loaded truck travels at a lower speed, and its speed variability on the curve completely depends on the curve characteristics. However,

the interaction variables in the model corresponding to both the vehicles have shown that gradient and travel direction significantly influence the explanatory variable's effect on MaxΔ_{85}V. The direction and magnitude of the interaction with the variable's coefficients show the effect of differences in gradient and travel direction.

The effect of interaction variables was analyzed using the interaction plots shown in Figures 4.14 and 4.15. Figure 4.14a shows that the up and downward gradients have a different impact on the way CCR affects the MaxΔ_{85}V of cars. The upward gradient has a positive effect on the coefficient of CCR, whereas the downward gradient has a negative impact. In contrast, for loaded trucks, both the upward and downward gradients have a negative effect on the way CCR is affecting the MaxΔ_{85}V (Figure 4.15a). However, the effect of the upgrade is relatively higher than the downgrade. This differential impact could be because of the positive impact of the downward gradient on the speed variability of the loaded trucks.

Turning direction of the curve was also found to have a differential impact on the way CCR and V_{PC} influence the speed variability of cars (Figure 4.14b & 4.14d). CCR has a relatively higher negative impact on the speed variability of left-turning cars. However, the V_{PC} has a relatively higher impact on the speed variability of right-turning cars. Similarly, the effect of CCR and L_C on the speed variability of loaded trucks changes with turning direction (Figure 4.15b & 4.15d). One of the reasons for this differential impact could be the left-side driving adopted in India. For the vehicles taking a left turn, the drivers will have more visibility of the opposite lane than the right-turning. To traverse the curve safely, the driver's visibility of the opposite lane is an important aspect, especially for the two-lane undivided highways passing through mountainous terrain. Thus, the interaction variables from both models suggest that the effect of CCR, V_{PC}, and L_C on the dependent variable varies depending on the gradient and travel direction.

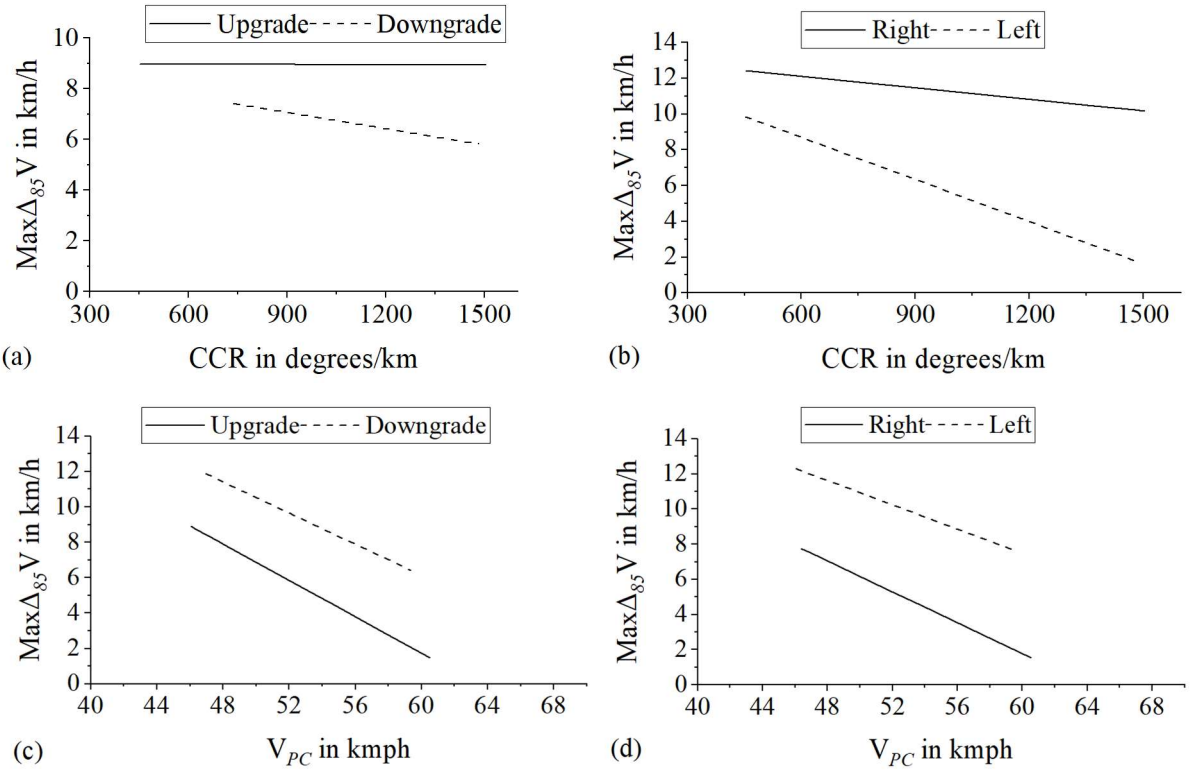

Fig. 4. 14 Interaction plots for the car showing the effect of (a & c) gradient on CCR and V_{PC} and (b & d) travel direction on CCR and V_{PC}

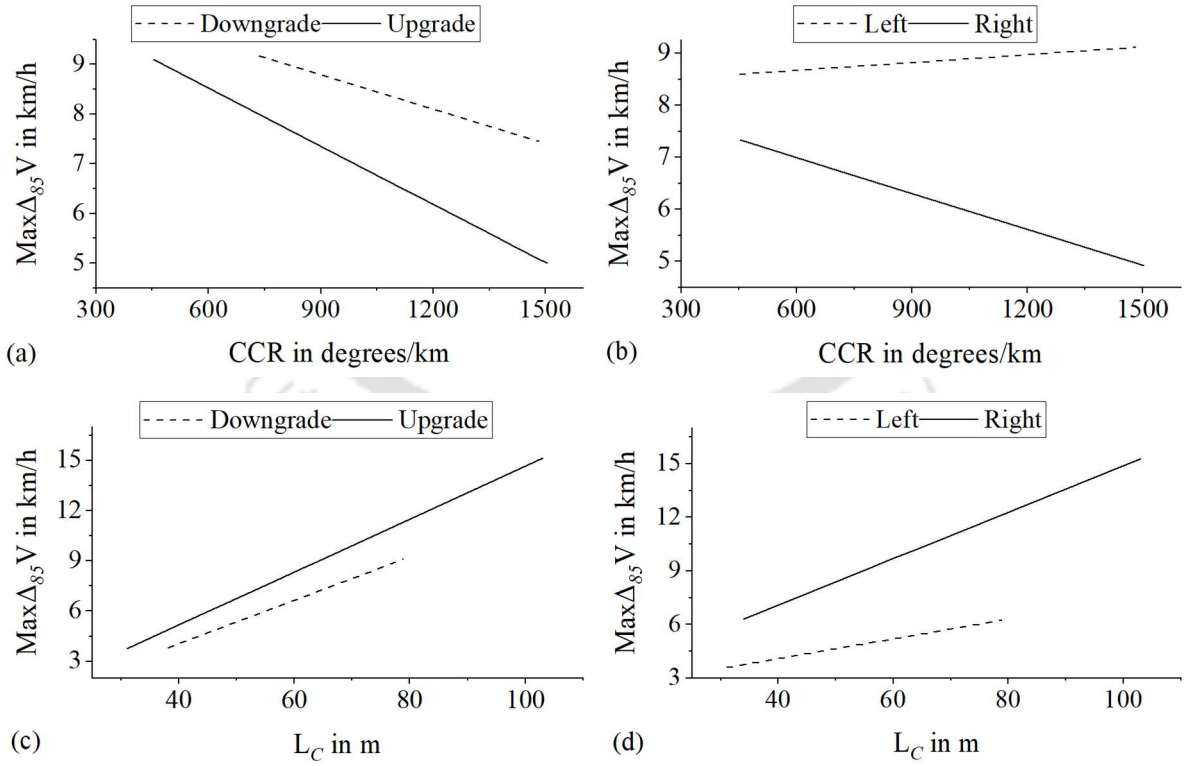

Fig. 4. 15 Interaction plots for loaded trucks showing the effect of (a & c) gradient on CCR and L_C and (b & d) travel direction on CCR and L_C

Further, the obtained regression models were validated using the data collected at six other locations on the same highway. The RWLS models were validated using Root Mean Square Error (RMSE) and Mean Absolute Difference (MAD) metrics (Eqs. 4.11 & 4.12).

$$\text{Root mean square error (RMSE)} = \sqrt{\frac{\sum_{i=1}^{n}(observed_i - predicted_i)^2}{n}} \quad (4.11)$$

$$\text{Mean absolute difference (MAD)} = \frac{\sum_{i=1}^{n}|observed_i - predicted_i|}{n} \quad (4.12)$$

Where, n is the number of observations.

Table. 4.9 shows the model validation measures (RMSE and MAD). The RMSE corresponding to the car and loaded trucks is 7.42 km/h and 6.42 km/h, respectively. The MAD corresponding to the car and loaded trucks is 5.78 km/h and 4.26 km/h, respectively.

4.5.1 Sensitivity analysis

This section presents the sensitivity analysis of the independent variables that are significant in modeling MaxΔ_{85}V. Since the geometric variables are in different dimensions, the magnitudes of the coefficients corresponding to the predicted variables are different. Thus, to compare the variables in the model, the regression coefficients are standardized to a single, standard set of statistically reasonable units (Siegel, 2016). Consider the following regression equation

$$Y = a + b_i X_i, \qquad i = 1,2,3, \ldots \ldots, n \quad (4.13)$$

In the eq. (4.13) the regression coefficient b_i represents the effect of the geometric variable X_i on Y, with all other X_{i+1} to X_n variables unchanged. The standardized coefficients are calculated as follows:

$$\beta_i = b_i \frac{S_{X_i}}{S_Y} \quad (4.14)$$

Where, β_i is the standardized coefficient of b_i; S_{X_i} is the standard deviation of the variable X_i; S_Y is the standard deviation of the response (dependent) variable; and $b_i$is the coefficient of the variable X_i. In each model, the absolute values of the standardized regression coefficients can be compared to have an indication of the relative importance of the variables.

Table 4.10 shows the standardized coefficients of the explanatory variables. In the model corresponding to the car, the interaction variables CCR×D and CCR×G, and V_{PC}×D are

relatively more sensitive than CCR and V_{PC}, respectively. This finding signifies that the effect of CCR on MaxΔ_{85}V of car varies depending on the gradient and turning direction of the curve. The most significant aspect is that the effect of CCR has an opposing effect on MaxΔ_{85}V of cars depending on the turning direction. For both left and right turning curves, the MaxΔ_{85}V reduces with the CCR. But, with the increasing CCR, the rate of decrease in MaxΔ_{85}V is relatively higher for the cars taking left turn.

Similarly, the effect of V_{PC} on the MaxΔ_{85}V varies depending on the turning direction of the curve. In the model corresponding to the loaded truck, the interaction variables CCR×D and CCR×G, and L_C are relatively more sensitive. The effect of CCR on the MaxΔ_{85}V varies depending on the gradient and turning direction of the curve. In the case of gradient, the MaxΔ_{85}V decreases with the CCR for both upgrade and downgrade. But, with the increasing CCR, the rate of change in MaxΔ_{85}V is relatively higher for the loaded trucks traveling on upgrade. In the case of turning direction, the MaxΔ_{85}V increases with the CCR for left turning curves. Whereas for the right turning curves, the MaxΔ_{85}V decreases with the CCR.

Table 4. 10 Degree of sensitivity for explanatory variables in MaxΔ_{85}V models

Vehicle	β_1(Std β_1)	β_2(Std β_2)	β_3(Std β_3)	β_4(Std β_4)	β_5(Std β_5)	β_6(Std β_6)
Car	CCR (-0.16)	CCR × G (0.28)	CCR × D (-0.75)	V_{PC} (-0.48)	V_{PC} × G (-0.4)	V_{PC} × D (0.53)
Loaded truck	L_C (0.66)	L_C × G (0.22)	L_C × D (-0.58)	CCR (-0.19)	CCR × G (-0.23)	CCR × D (-0.41)

4.6 Discussion

Studies related to the geometric design consistency assessment assume that the vehicles maintain a constant speed on the curve and the acceleration/deceleration takes place only on the approach/departing tangents. This study has analyzed the speed variability of cars and loaded trucks on the horizontal curves located in mountainous terrain through acceleration and speed profiles. The acceleration/deceleration behavior of cars and loaded trucks (Figures 4.1 & 4.2), is similar to the results obtained by Xu et al. (2017). Further, the acceleration profiles corresponding to the car and loaded truck showed that accelerations and decelerations take place on the curve. Besides, the analyses of speed profiles have clearly shown that the V_{Min} and V_{Max} are significantly different, and the results corresponding to the car are similar to the study of Dhahir and Hassan (2018).

Further, V_{Min}, and V_{Max}, were found to be statistically different from V_{CC}. Llopis-Castello et al. (2018) have found that the V_{Min} and V_{CC} are not the same for both the loaded and empty trucks on the horizontal curves with gradient less than 10%. Dhahir and Hassan (2018) found a statistically significant difference between V_{Min} and V_{Max} on 81% of the curves; however, in a later study (Dhahir and Hassan 2019a), they found that there is no significant difference between V_{Min} and V_{CC} of the cars moving on rolling and mountainous highways. The present study found that the speed variability is present across all the observed curves and the vehicle types. Based on the results of this study, it can be postulated that measuring the speed at the center of the curve could lead to erroneous estimation of design and operating speed consistencies.

In addition, considering the speed variability on the curve, $Max\Delta_{85}V$ was modeled for both cars and loaded trucks, respectively. For cars, curvature change rate (CCR) and speed at the point of curvature (V_{PC}) are significant in explaining the variability of $Max\Delta_{85}V$. Whereas for loaded trucks, the length of the curve (L_C) and CCR are significant in explaining the variability in $Max\Delta_{85}V$. Further, the interaction variables in the model corresponding to both vehicles have shown that gradient and travel direction significantly influence the explanatory variable's effect on $Max\Delta_{85}V$. On curves superimposed with downgrade, CCR has a negative impact on $Max\Delta_{85}V$ and a positive impact on $Max\Delta_{85}V$ for the curves with upgrade for cars. Whereas for loaded trucks, CCR has negative impact on $Max\Delta_{85}V$ for curves with both upgrade and downgrade. However, the impact for the curves with upgrade is observed to be more than the curves with downgrade. The reason could be due to the fact that drivers tries to accelerate more on the upgrades to maintain their speeds. In terms of turning direction, CCR has negative impact on $Max\Delta_{85}V$ for cars in both travel directions. Whereas for loaded trucks, turning direction has differential impact on the way CCR and $Max\Delta_{85}V$ are related. This could be because, the left-turning vehicles could have more visibility as compared to that on right-turning curves.

For cars with curves superimposed with both downgrade and upgrade, V_{PC} has a negative impact on $Max\Delta_{85}V$. Further, it is observed that, the curves with downgrade have more $Max\Delta_{85}V$ with respect to V_{PC} as compared to that of curves with upgrade. The reason could be that, cars travel aggressively on downgrade curves as compared to upgrade curves. Similarly, the curves with both left and right travel direction, V_{PC} has negative impact on $Max\Delta_{85}V$. Further, it is observed that curves with left turning have more $Max\Delta_{85}V$ with respect to V_{PC} as compared to that of curves with right turning. The reason for differences in travel

direction is that left turning curves have more visibility, thus leading to have more $Max\Delta_{85}V$ with decreasing V_{PC}. Unlike cars, the V_{PC} has not shown any influence on the loaded trucks, and this could be because the loaded truck travels at a lower speed, and its speed variability on the curve completely depends on the curve characteristics. Further, the sensitivity analysis has shown that travel direction has more impact on determinants than gradient for both vehicle types.

4.7 Summary

This chapter investigated the speed variability of the cars and loaded trucks while traversing the horizontal curves of a two-lane undivided rural highway passing through mountainous terrain and identified the important determinants. All the necessary data were extracted from the trajectory data obtained from the video film. The acceleration and deceleration length, measured from the point of curvature for cars and loaded trucks, were estimated from the acceleration profiles. The deceleration and acceleration length reflected the speed variability on the curve and the possible minimum and maximum speed locations. Based on the speed variables V_{CC}, V_{Max}, and V_{Min}, and their locations of occurrence, it was observed that neither the minimum nor the maximum speed occurs at the center of the curve. $Max\Delta_{85}V$ on the curve was modeled, and important determinants were identified. CCR and the V_{PC} are significant in explaining the maximum speed difference of the car. The L_C and CCR are significant in explaining the speed variability of the loaded trucks. Another important finding of this study is that the gradient and the turning direction have a differential impact on the way the above determinants influence speed variability.

Given the speed variability on the curve, consistency evaluation based on the operating speed corresponding to the curve center could lead to erroneous results. For a realistic evaluation, it is necessary to estimate V_{Max} and V_{Min}, which can be used for assessing the design and operating speed consistencies. However, always it is not possible to collect videography data and use the speed profile data to obtain the maximum and minimum operating speeds on the curve. Hence, a sample of speed profile data (or a sequence of spot speeds at several points on the curve) may be used to correct the operating speeds obtained from the center of the curve before using the latter for assessing the geometric design consistency. In future, considering the vehicle trajectory before the curve, curve portion and after the curve would reveal the starting and ending points of the acceleration/ deceleration that helps to understand driving patterns over long stretches.

5 Development of operating speed correction models

5.1 Introduction

In evaluating the design and operating speed consistencies, most existing studies collect the speed data at the center of the curve, with the assumption that the vehicle speed remains constant on the curve. Several operating speed and operating speed reduction models were developed using the speed data collected at the center of the curve (Leisch and Leisch 1977, Lamm and Choueiri 1986, Krammes et al. 1995; Gibreel et al. 1999; Misaghi and Hassan 2005; Jacob and Anjaneyulu 2013; Perez-Zuriaga et al. 2013; Shallam el at. 2021). However, the continuous speed profile data collected using either the instrumented vehicle or driving simulator have shown that the speed is not constant on the curve (Pérez-Zuriaga et al. 2013; Calvi and Bella 2014; Montella et al. 2014; Dhahir and Hassan 2018; Llopis-Castello et al. 2018; Choudhari and Maji 2019; Malaghan et al. 2020). Considering the speed variability on the curve, some of these studies have developed operating speed reduction models based on the maximum speed reduction of individual vehicles.

Identifying and capturing the minimum and maximum speed occurrence on the curve is not possible without having continuous speed profile data. At the same time, collecting naturalistic vehicle trajectories through videography approach on the horizontal curves in mountainous terrain is not possible in all the scenarios as it depends on the availability of clear vantage points. Hence, this chapter models the correction factors for the operating speed corresponding to the center of the curve, for estimating the maximum and minimum 85th percentile speeds.

5.2 Correction models for maximum operating speed

Continuous speed profile data were used to develop the correction factors for estimating the 85th percentile of maximum speed on the curve (V_{Max}^{85}). The correction factors refers to the modeling 85th percentile of the speed difference between maximum speed on the curve and speed at the center of the curve ($\Delta V_{Max,CC}^{85}$). The difference between maximum speed on the

curve and speed at the center of the curve ($\Delta V_{Max,CC}$) was measured for each vehicle using the speed profile data. Figure 5.1 shows a typical speed profile and the difference in maximum speed and the speed at the curve center.

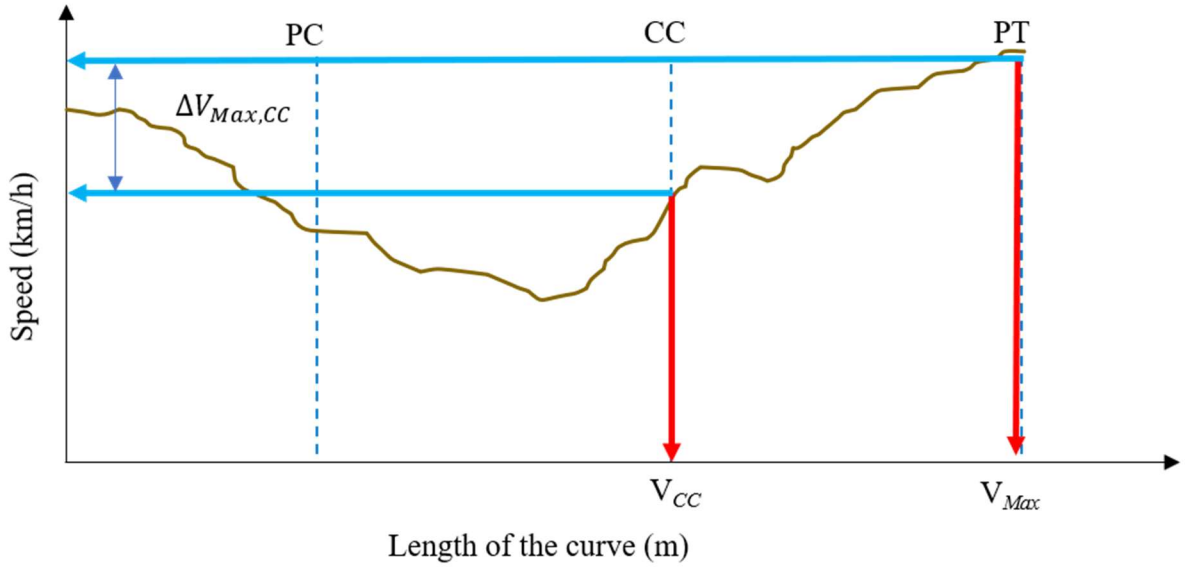

Fig. 5. 1 Illustration of the difference between maximum speed on the curve and speed at the curve center

The 85th percentile of the speed difference between maximum speed and speed at the center of the curve ($\Delta V^{85}_{Max,CC}$), corresponding to all the locations, range between 1.5 to 14 km/h, and 1.6 to 13.4 km/h, for cars and loaded trucks, respectively. The average values of $\Delta V^{85}_{Max,CC}$ for car and loaded truck are 4.84 km/h and 4.34 km/h, respectively. The standard deviations of $\Delta V^{85}_{Max,CC}$ for car and loaded truck are 2.97 km/h and 2.67 km/h, respectively.

5.2.1 Identification of independent variables

The $\Delta V^{85}_{Max,CC}$ was modeled as a function of the geometric parameters of the curve, the approach tangent, and the departing tangent. The independent variables also include the parameters such as the speed at the point of curvature (V_{PC}) and the vehicle's lateral distance (LD_{PC}), measured at PC, from the vehicle's centerline to the nearest edge of the road (Figure 3.20). Independent variables that influence the $\Delta V^{85}_{Max,CC}$ were identified using the Pearson correlation analysis. The influencing variables were identified based on the strength of the correlation (correlation greater than 0.3) and used in further regression modeling (Cohen et al. 2003; Akoglu 2018). Tables 5.1 & 5.2 present the Pearson correlation matrices for car and loaded trucks, respectively.

Table 5. 1 Pearson correlation matrix corresponding to $\Delta V_{Max,CC}^{85}$ for cars

	$\Delta V_{Max,CC}^{85}$	e	T_L	R	Δ	R_{PC}	L_{PC}	L_{AT}	L_C	L_{ET}	L_W	$R \times L_W$	DC	CCR	V_{PC}	LD_{PC}
$\Delta V_{Max,CC}^{85}$	1															
e	-0.4	1														
T_L	-0.31*	0.9*	1													
R	0.4*	-0.92*	-0.98*	1												
Δ	-0.03	0.76*	0.87*	-0.81*	1											
R_{PC}	-0.06	0.13	0.17	-0.21	-0.03	1										
L_{PC}	0.1	-0.02	-0.17	0.16	-0.11	-0.45	1									
L_{AT}	-0.17	0.36*	0.42*	-0.36*	0.42*	0.27	-0.34*	1								
L_C	0.33*	0.3	0.38*	-0.27	0.78*	-0.28	0.04	0.24	1							
L_{ET}	-0.17	0.36*	0.42*	-0.36*	0.42*	-0.05	-0.22	0.16	0.24	1						
L_W	-0.14	0.28	0.14	-0.19	0.02	0.38*	0.11	-0.06	-0.16	0.1	1					
$R \times L_W$	0.36*	-0.84*	-0.95*	0.95*	-0.81*	-0.09	0.2	-0.38*	-0.33*	-0.33*	0.12	1				
DC	-0.29	0.91*	1*	-0.98*	0.89*	0.15	-0.14	0.43*	0.42*	0.43*	0.15	-0.94*	1			
CCR	-0.47*	0.85*	0.91*	-0.94*	0.61*	0.32*	-0.15	0.35*	-0.02	0.35*	0.29	-0.85*	0.89*	1		
V_{PC}	-0.5*	-0.2	-0.29	0.24	-0.47*	0.01	-0.13	0.06	-0.56*	-0.12	-0.16	0.2	-0.32*	-0.07	1	
LD_{PC}	-0.1	0.08	0.03	-0.06	0.08	0.2	0.16	-0.05	0.11	0	0.35*	0.05	0.03	0.04	0.02	1

* Indicates correlation

Table 5. 2 Pearson correlation matrix corresponding to $\Delta V_{Max,CC}^{85}$ for loaded trucks

	$\Delta V_{Max,CC}^{85}$	e	T_L	R	Δ	R_{PC}	L_{PC}	L_{AT}	L_C	L_{ET}	L_W	$R\times L_W$	DC	CCR	V_{PC}	LD_{PC}
$\Delta V_{Max,CC}^{85}$	1															
e	-0.47*	1														
T_L	-0.45*	0.9*	1													
R	0.42*	-0.92*	-0.98*	1												
Δ	-0.16	0.76*	0.87*	-0.81*	1											
R_{PC}	-0.25	0.13	0.17	-0.21	-0.03	1										
L_{PC}	0.33*	-0.02	-0.17	0.16	-0.11	-0.45*	1									
L_{AT}	-0.21	0.36*	0.42*	-0.36*	0.42*	0.27	-0.34*	1								
L_C	0.29	0.3	0.38*	-0.27	0.78*	-0.28	0.04	0.24	1							
L_{ET}	-0.47*	0.36*	0.42*	-0.36*	0.42*	-0.05	-0.22	0.16	0.24	1						
L_W	-0.25	0.28	0.14	-0.19	0.02	0.38*	0.11	-0.06	-0.16	0.1	1					
$R\times L_W$	0.44*	-0.84*	-0.95*	0.95*	-0.81*	-0.09	0.2	-0.38*	-0.33*	-0.33*	0.12	1				
DC	-0.43*	0.91*	1	-0.98*	0.89*	0.15	-0.14	0.43*	0.42*	0.43*	0.15	-0.94*	1			
CCR	-0.31*	0.87*	0.97*	-0.93*	0.96*	0.07	-0.11	0.44*	0.59*	0.44*	0.09	-0.9*	0.98*	1		
V_{PC}	-0.03	-0.06	-0.04	0.06	-0.11	0.08	-0.19	0.59*	-0.17	-0.14	0.19	0.12	-0.04	-0.08	1	
LD_{PC}	-0.08	0.21	0.09	-0.12	0.06	0.35*	-0.05	-0.18	0.02	-0.03	0.49*	0.02	0.11	0.1	0.08	1

* Indicates correlation

5.2.2 Results

In modeling $\Delta V_{Max,CC}^{85}$, the independent variables were selected based on the correlation coefficients and estimated the linear regression models using the robust weighted least square (RWLS) method. The RWLS method proposed by Qu et al. (2015) and Shallam et al. (2021) handles the selection bias and heteroscedasticity in the data. A backward stepwise regression approach was used to eliminate insignificant variables and the other independent variables that have multi-collinearity. Table 5.3 shows the operating speed correction models developed for estimating the 85th percentile of maximum speed on the curve corresponding to the cars and loaded trucks.

Table 5. 3 Summary of correction models for the 85th percentile of maximum speed on the curve ($\Delta V_{Max,CC}^{85}$)

Vehicle	Regression models	R^2	R^2_{Adj}	RMSE (km/h)	MAD (km/h)
Car	$4.14 + 0.02L_C + 0.085L_C \times G - 0.059L_C \times D - 0.0013CCR - 0.0036CCR \times G + 0.0029CCR \times D$	0.99	0.98	1.81	1.36
Loaded Truck	$3.72 - 0.01L_{et} + 0.0071L_{et} \times G + 0.0106L_{et} \times D$	0.82	0.79	2.23	1.57

For cars, the length of the curve (L_C) and curvature change rate (CCR) are significant in explaining the variability of $\Delta V_{Max,CC}^{85}$. The $\Delta V_{Max,CC}^{85}$ on the curve increases with the increasing L_C and decreasing CCR. Whereas, for loaded trucks, L_{et} is significant in explaining the variability of $\Delta V_{Max,CC}^{85}$. The $\Delta V_{Max,CC}^{85}$ increases with the decreasing L_{et}. The interaction variables in the model corresponding to both the vehicles have shown that the gradient and travel direction significantly influence the explanatory variable's effect on $\Delta V_{Max,CC}^{85}$. The direction and magnitude of the interaction with the variable's coefficients show the differences in the effect of gradient and travel direction. The explanatory variables shown in Table 5.3 are statistically significant at a 5% significance level. Further, the models were validated using the data collected at six different locations on the same highway. The Mean absolute difference (MAD) and Root mean square error (RMSE) were used to validate the models (Eqs. 4.11 & 4.12). Table 5.3 shows the RMSE and MAD statistics corresponding to the developed models. The table shows that, for cars, RMSE and MAD are 1.81 km/h and 1.36 km/h. Whereas the operating speed correction model corresponding to the loaded truck can estimate the correction factor with an RMSE and MAD of 2.23 km/h and 1.57 km/h, respectively.

5.2.2.1 Analysis of the interaction variables

The effect of interaction variables on the $\Delta V_{Max,CC}^{85}$ was analyzed for cars and loaded trucks using the interaction plots (Figures 5.2 and 5.3). Figure 5.2a shows that the upward and downward gradients have a different impact on the way the L_C and CCR affect the $\Delta V_{Max,CC}^{85}$. Both the upward and downward gradients have a positive effect on the coefficient of L_C. But, the effect of L_C on the $\Delta V_{Max,CC}^{85}$ of cars traveling on the upward gradient is relatively higher than that of the downward gradient. The upward and downward gradients have a negative effect on the coefficient of CCR, but their slopes are significantly different (Figure 5.2b). The effect of CCR is relatively higher on the upward gradient than on the downgrade. The effect of the L_C and CCR on the $\Delta V_{Max,CC}^{85}$ of cars also depends on the turning direction of the curve (Figure 5.2c & 5.2d). As L_C increases, $\Delta V_{Max,CC}^{85}$ increases for the left-turning curves. Whereas for the right turning curves, $\Delta V_{Max,CC}^{85}$ decreases with the increasing L_C. $\Delta V_{Max,CC}^{85}$ increases with CCR for left-turning curves. But, for the right turning curves, the $\Delta V_{Max,CC}^{85}$ decreases with the increasing CCR.

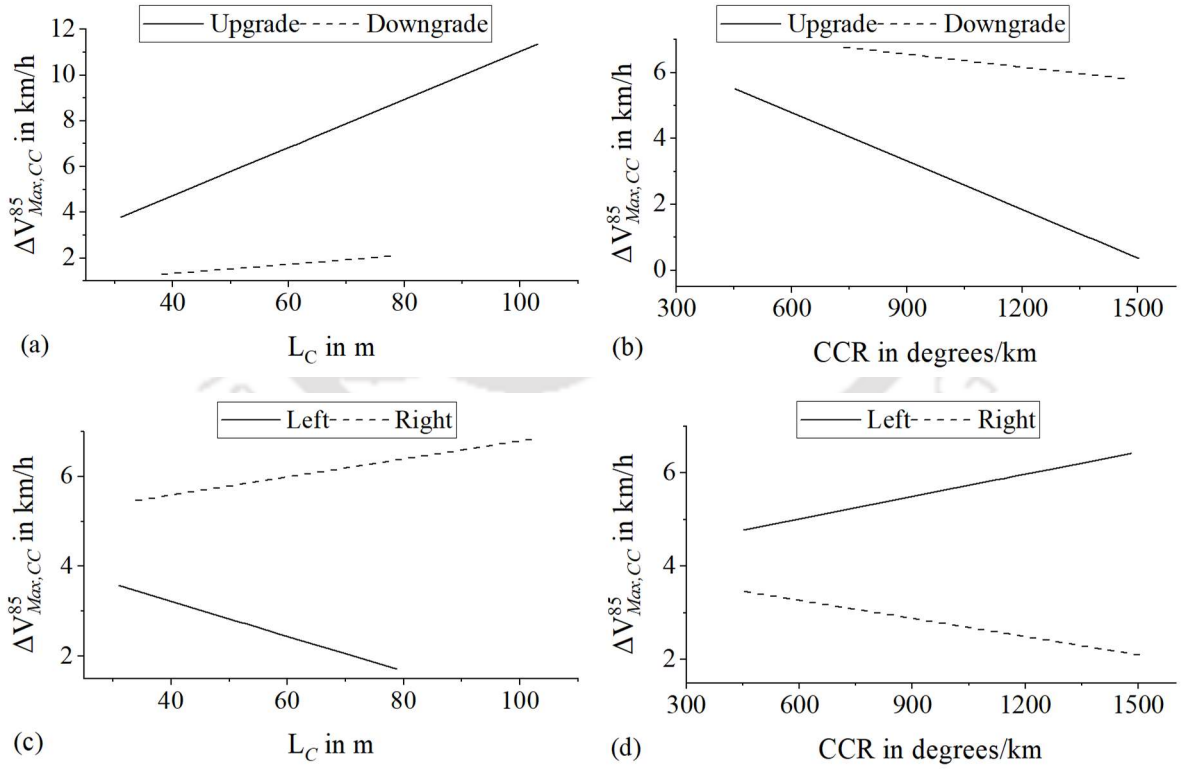

Fig. 5. 2 Interaction plots for the car showing the effect of (a & b) gradient on L_C and CCR; (c & d) travel direction on L_C and CCR

For loaded trucks, the effect of L_{et} on the $\Delta V_{Max,CC}^{85}$ depends on the gradient direction (Figure 5.3a). L_{et} has a negative effect on $\Delta V_{Max,CC}^{85}$ in the case of both the upward and downward gradient. However, L_{et} has a relatively higher negative effect on $\Delta V_{Max,CC}^{85}$ in the case of the downward gradient compared to the upward gradient. the effect of length of the exit tangent on the $\Delta V_{Max,CC}^{85}$ also depends on the turning direction of the curve (Figure 5.3b). For the loaded trucks taking left turn, L_{et} has a positive impact on the $\Delta V_{Max,CC}^{85}$. Whereas for the loaded trucks taking right turn, L_{et} has a negative impact on $\Delta V_{Max,CC}^{85}$ Further, a small change in L_{et} will have more effect on $\Delta V_{Max,CC}^{85}$ for the right-turning loaded trucks.

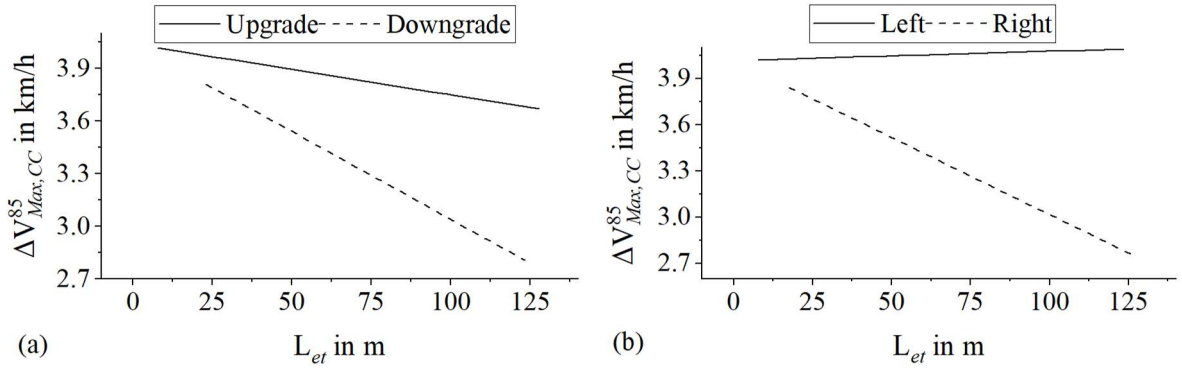

Fig. 5. 3 Interaction plots for loaded truck showing the effect of (a) gradient on L_{et}; (b) travel direction on L_{et}

5.2.2.2 Sensitivity analysis of the independent variables

This section presents the sensitivity analysis of the independent variables that are significant in modeling $\Delta V_{Max,CC}^{85}$. The standardized coefficients of the explanatory variables in the models corresponding to $\Delta V_{Max,CC}^{85}$ were estimated using Eq. 4.14. Table 5.4 presents the standardized coefficients of the explanatory variables of the developed models. For each model, the absolute values of the standardized coefficients were compared to assess the relative importance of the variables. In the model corresponding to the car, the interaction variables $L_C \times G$ and $L_C \times D$ are relatively more sensitive than L_C. Similarly, the interaction variables CCR × G and CCR × D are relatively more sensitive than CCR. This indicates that the drivers' perception of CCR varies based on the gradient and the turning direction of the curve. For the loaded trucks, the L_{et} is relatively more sensitive than the interaction variables. In this case, the drivers' perception of L_{et} doesn't depend on the gradient and the turning direction.

Table 5. 4 Degree of sensitivity for explanatory variables in $\Delta V_{Max,CC}^{85}$ models

Vehicle	β_1(Std β_1)	β_2(Std β_2)	β_3(Std β_3)	β_4(Std β_4)	β_5(Std β_5)	β_6(Std β_6)
Car	L_C (0.13)	L_C × G (0.87)	L_C × D (-0.61)	CCR (-0.14)	CCR × G (-0.69)	CCR × D (0.55)
Loaded truck	L_{et} (-0.17)	L_{et} × G (0.13)	L_{et} × D (0.16)	-	-	-

5.3 Correction models for minimum operating speed

Similar to the previous section, continuous speed profile data were used to develop the correction factors for estimating the V_{Min}^{85} on the curve. The correction factors refer to the modeling 85th percentile of the speed difference between minimum speed on the curve and speed at the center of the curve ($\Delta V_{Min,CC}^{85}$). The difference between minimum speed and speed at the center of the curve ($\Delta V_{Min,CC}$) was estimated for each vehicle, for all the fourteen horizontal curves. Figure 5.4 shows a typical speed profile and the difference in minimum speed and the speed at the curve center.

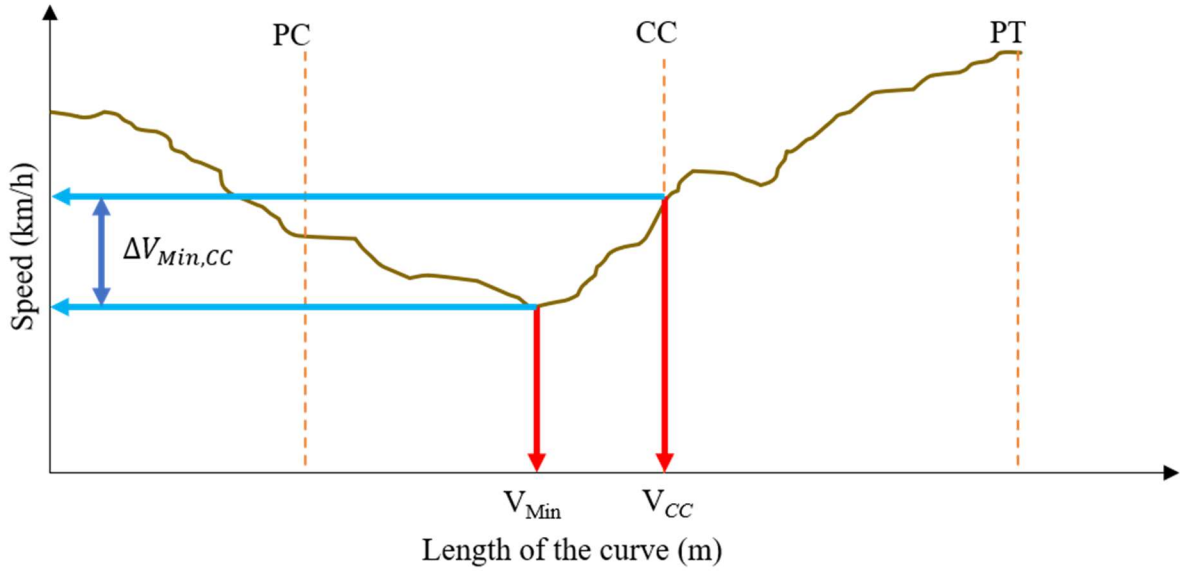

Fig. 5. 4 Illustration of the difference between minimum speed on the curve and speed at the center of the curve

$\Delta V_{Min,CC}^{85}$ corresponding to all the locations, range between 1 to 12 km/h, and 1 to 11 km/h, for cars and loaded trucks, respectively. The average values of $\Delta V_{Min,CC}^{85}$ for cars and loaded trucks are 5 km/h and 4.7 km/h, respectively. The standard deviations of $\Delta V_{Min,CC}^{85}$ for cars and loaded trucks are 2.9 km/h and 2.7 km/h, respectively.

5.3.1 Identification of independent variables

The $\Delta V_{Min,CC}^{85}$ was modeled using the geometric parameters of the curve, approach tangent, and departing tangent. The independent variables also include the parameters such as the speed at the center of the curve and the vehicle's lateral distance, measured at PC from the vehicle's centerline to the nearest edge of the road (Figure 3.20). Independent variables that influence the $\Delta V_{Min,CC}^{85}$ were identified based on the Pearson correlation analysis. The influencing variables were identified based on the strength of the correlation (correlation greater than 0.3) and used in further regression modeling (Cohen et al. 2003; Akoglu 2018). Tables 5.5 & 5.6 present the Pearson correlation matrices corresponding to the car and loaded trucks, respectively.

Table 5. 5 Pearson correlation matrix corresponding to $\Delta V_{Min,CC}^{85}$ for cars

	$\Delta V_{Min,CC}^{85}$	e	T_L	R	Δ	R_{PC}	L_{PC}	L_{AT}	L_C	L_{ET}	L_W	$R \times L_W$	DC	CCR	V_{PC}	LD_{PC}
$\Delta V_{Min,CC}^{85}$	1															
e	-0.14	1														
T_L	0	0.9*	1													
R	0.1	-0.92*	-0.98*	1												
Δ	0.26	0.76*	0.87*	-0.81*	1											
R_{PC}	-0.05	0.13	0.17	-0.21	-0.03	1										
L_{PC}	-0.01	-0.02	-0.17	0.16	-0.11	-0.45*	1									
L_{AT}	0.27	0.36*	0.42*	-0.36*	0.42*	0.27	-0.34*	1								
L_C	0.48*	0.3	0.38*	-0.27	0.78*	-0.28	0.04	0.24	1							
L_{ET}	0.1	0.36*	0.42*	-0.36*	0.42*	-0.05	-0.22	0.16	0.24	1						
L_W	-0.23	0.28	0.14	-0.19	0.02	0.38*	0.11	-0.06	-0.16	0.1	1					
$R \times L_W$	0.05	-0.84*	-0.95*	0.95*	-0.81*	-0.09	0.2	-0.38*	-0.33*	-0.33*	0.12	1				
DC	0.04	0.91*	1*	-0.98*	0.89*	0.15	-0.14	0.43*	0.42*	0.43*	0.15	-0.94*	1			
CCR	-0.19	0.85*	0.91*	-0.94*	0.61*	0.32*	-0.15	0.35*	-0.02	0.35*	0.29	-0.85*	0.89*	1		
V_{PC}	-0.47*	-0.2	-0.29	0.24	-0.47*	0.01	-0.13	0.06	-0.56*	-0.12	-0.16	0.2	-0.32*	-0.07	1	
LD_{PC}	-0.18	0.08	0.03	-0.06	0.08	0.2	0.16	-0.05	0.11	0	0.35*	0.05	0.03	0.04	0.02	1

* Indicates correlation

Table 5. 6 Pearson correlation matrix corresponding to $\Delta V_{Min,CC}^{85}$ for loaded trucks

	$\Delta V_{Min,CC}^{85}$	e	T_L	R	Δ	R_{PC}	L_{PC}	L_{AT}	L_C	L_{ET}	L_W	$R \times L_W$	DC	CCR	V_{PC}	LD_{PC}
$\Delta V_{Min,CC}^{85}$	1															
e	0.02	1														
T_L	0.12	0.9*	1													
R	0	-0.92*	-0.98*	1												
Δ	0.45*	0.76*	0.87*	-0.81*	1											
R_{PC}	-0.06	0.13	0.17	-0.21	-0.03	1										
L_{PC}	-0.07	-0.02	-0.17	0.16	-0.11	-0.45*	1									
L_{AT}	0.35*	0.36*	0.42*	-0.36*	0.42*	0.27	-0.34*	1								
L_C	0.68*	0.3	0.38*	-0.27	0.78*	-0.28	0.04	0.24	1							
L_{ET}	0.19	0.36*	0.42*	-0.36*	0.42*	-0.05	-0.22	0.16	0.24	1						
L_W	-0.23	0.28	0.14	-0.19	0.02	0.38*	0.11	-0.06	-0.16	0.1	1					
$R \times L_W$	-0.06	-0.84*	-0.95*	0.95*	-0.81*	-0.09	0.2	-0.38*	-0.33*	-0.33*	0.12	1				
DC	0.16	0.91*	1*	-0.98*	0.89*	0.15	-0.14	0.43*	0.42*	0.43*	0.15	-0.94*	1			
CCR	-0.14	0.85*	0.91*	-0.94*	0.61*	0.32*	-0.15	0.35*	-0.02	0.35*	0.29	-0.85*	0.89*	1		
V_{PC}	0.15	-0.06	-0.04	0.06	-0.11	0.08	-0.19	0.59*	-0.17	-0.14	0.19	0.12	-0.04	0.04	1	
LD_{PC}	-0.03	0.21	0.09	-0.12	0.06	0.35*	-0.05	-0.18	0.02	-0.03	0.49*	0.02	0.11	0.12	0.08	1

* Indicates correlation

5.3.2 Results

In modeling $\Delta V_{Min,CC}^{85}$, the independent variables were selected based on the correlation coefficients, and the linear regression models were estimated using the robust weighted least square (RWLS) method. Table 5.7 shows the operating speed correction models developed for the 85th percentile of minimum speed on the curve corresponding to the cars and loaded trucks.

Table 5. 7 Summary of correction models for the 85th percentile of minimum speed on the curve ($\Delta V_{Min,CC}^{85}$)

Vehicle	Regression models	R^2	R^2_{Adj}	RMSE (km/h)	MAD (km/h)
Car	-0.39 + 0.07L_C - 0.012L_C × D	0.937	0.931	4.06	3.48
Loaded Truck	-1.01 + 0.09L_C - 0.01L_C × G - 0.012L_C × D	0.957	0.95	1.71	1.32

For cars, the L_C is significant in explaining the variability of $\Delta V_{Min,CC}^{85}$. Similarly, for loaded trucks, the L_C is significant in explaining the variability of $\Delta V_{Min,CC}^{85}$. For both the car and loaded truck, the $\Delta V_{Min,CC}^{85}$ increases with the increasing L_C. The interaction variables in the model corresponding to the car show that the travel direction significantly influences the explanatory variable's effect on $\Delta V_{Min,CC}^{85}$. The model corresponding to the loaded truck also shows that both gradient and travel direction significantly influences the explanatory variable's effect on $\Delta V_{Min,CC}^{85}$. The explanatory variables shown in Table 5.6 are statistically significant at a 5% significance level. Further, the models were validated using the data collected at six different locations on the same highway. The Mean absolute difference (MAD) and Root mean square error (RMSE) were used to validate the models (Eqs. 4.11 & 4.12). Table 5.6 shows the RMSE and MAD statistics corresponding to the developed models. The table shows that, for cars, RMSE and MAD are 4.06 km/h and 3.48 km/h, respectively. For the loaded trucks, the correction factor could be estimated with an RMSE and MAD of 1.71 km/h and 1.32 km/h, respectively.

5.3.2.1 Analysis of interaction variables

The effect of interaction variables on the $\Delta V_{Min,CC}^{85}$ was analyzed for car and loaded trucks using the interaction plots (Figures 5.5 and 5.6). Figure 5.5 shows that the magnitude of the effect of L_C on $\Delta V_{Min,CC}^{85}$ depends on the turning direction of the curve. $\Delta V_{Min,CC}^{85}$ increases with the L_C in the case of both the left and right turning directions. But, the effect of L_C on $\Delta V_{Min,CC}^{85}$ for the cars taking the right turn is relatively higher than that of the left turn. For the loaded trucks,

Figure 5.6 (a) shows that the upward and downward gradients have a different impact on the way L_C is affecting the $\Delta V_{Min,CC}^{85}$. Both upgrade and downgrade have a positive impact on the coefficient of L_C. But, the effect of L_C on the $\Delta V_{Min,CC}^{85}$ of loaded trucks traveling on the downgrade is relatively higher than that are traveling on the upgrade. $\Delta V_{Min,CC}^{85}$ of the loaded trucks increase with the L_C irrespective of the turning direction. But, the effect of L_C is relatively higher on the $\Delta V_{Min,CC}^{85}$ of loaded trucks taking a right turn compared to that of the left turn. In the case of cars and loaded trucks, the change in $\Delta V_{Min,CC}^{85}$ with L_C is relatively lower for the left turning curves.

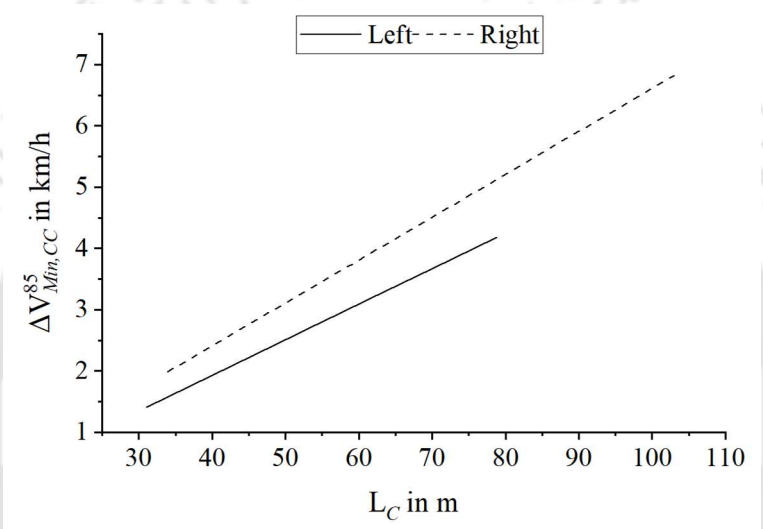

Fig. 5. 5 Interaction plot for the car showing the effect of travel direction on L_C

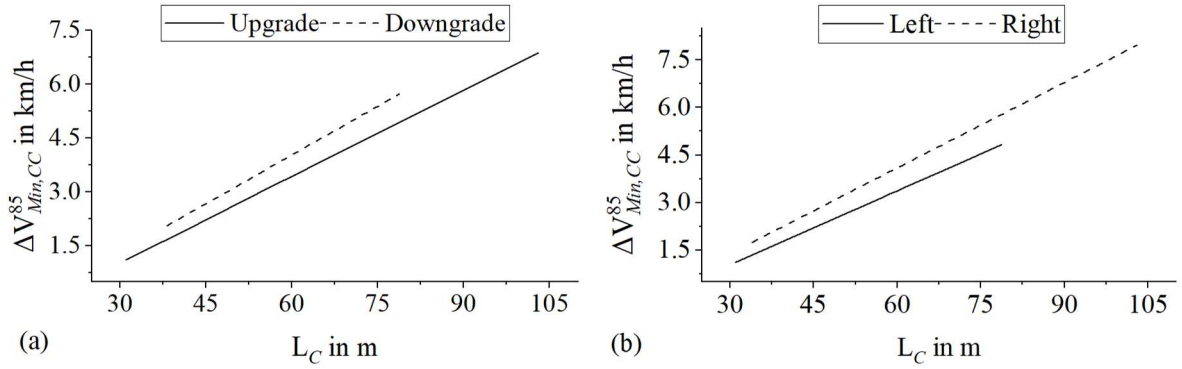

Fig. 5. 6 Interaction plots for loaded trucks showing the effect of (a) gradient on L_C; (b) travel direction on L_C

5.3.2.2 Sensitivity analysis of the independent variables

This section presents the sensitivity analysis of the independent variables that are significant in modeling $\Delta V_{Min,CC}^{85}$. The standardized coefficients of the explanatory variables in the models

corresponding to $\Delta V_{Min,CC}^{85}$ were estimated using Eq. 4.14. Table 5.8 presents the standardized coefficients of the explanatory variables of the developed models. In each model, the absolute values of the standardized coefficients were compared to have an indication of the relative importance of the variables. In the model corresponding to the car, the L_C is relatively more sensitive than the interaction variable. Similarly, in the model corresponding to the loaded truck, the L_C is relatively more sensitive than the interaction variables.

Table 5. 8 Degree of sensitivity for explanatory variables in $\Delta V_{Min,CC}^{85}$ models

Vehicle	β_1(Std β_1)	β_2(Std β_2)	β_3(Std β_3)	β_4(Std β_4)	β_5(Std β_5)	β_6(Std β_6)
Car	L_C (0.59)	L_C × D (-0.16)	-	-	-	-
Loaded truck	L_C (0.72)	L_C × G (-0.12)	L_C × D (-0.15)	-	-	-

5.5 Application of the correction factors on V_{CC}^{85}, for estimating V_{Min}^{85} and V_{Max}^{85}

In this study, data from the study of Shallam et al. (2021) were used to correct the estimated operating speeds corresponding to the center of the curve for obtaining V_{Min}^{85} and V_{Max}^{85} on the curve. Shallam et al. (2021) have estimated operating speeds for 250 horizontal curves constituting the Shillong bypass. However, considering the range of variables used for developing the correction models, V_{Min}^{85} and V_{Max}^{85} were estimated for only 191 horizontal curves. The operating speed correction models presented in the previous sections were used to estimate V_{Min}^{85} and V_{Max}^{85}. Figures 5.7 and 5.8 shows the operating speeds corresponding to the center of the curve, and the estimated V_{Min}^{85} and V_{Max}^{85}, for cars and loaded trucks, respectively.

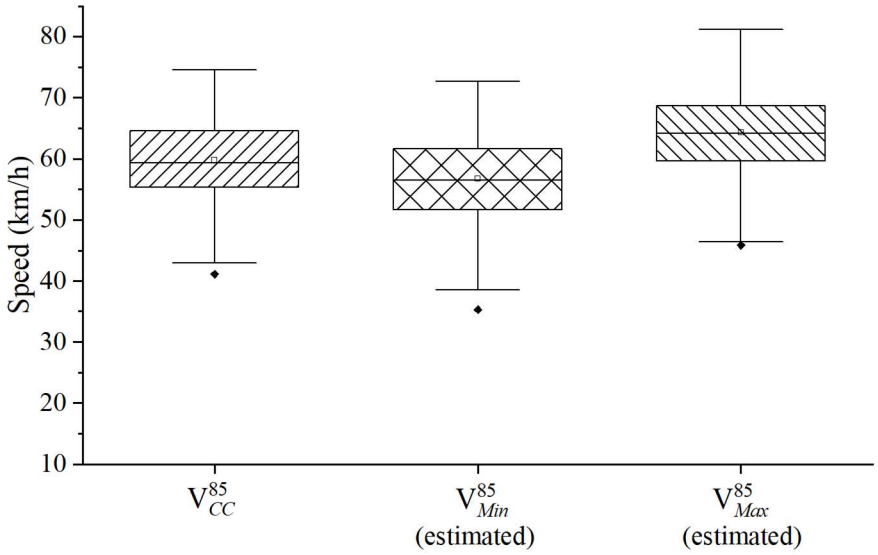

Fig. 5. 7 85th percentile speed for cars

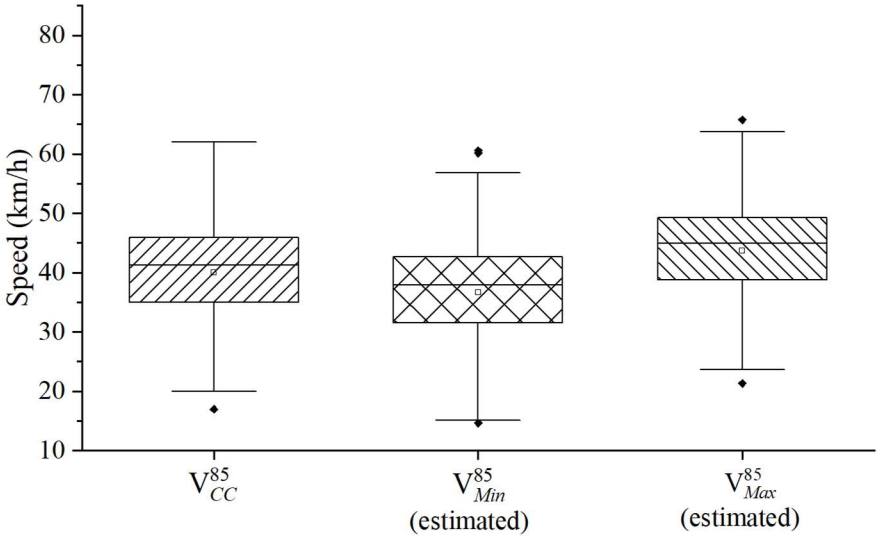

Fig. 5. 8 85th percentile speed for loaded trucks

Figures 5.7 and 5.8 show that V_{Min}^{85} corresponding to both cars and loaded trucks is lower than the V_{CC}^{85}. Whereas the V_{Max}^{85} on the curve corresponding to both car and loaded trucks are higher than the V_{CC}^{85}. To further ascertain the differences in the three-speed variables, an ANOVA test was performed for both the vehicle types with the Null hypothesis, H_o: the average V_{CC}^{85}, V_{Min}^{85}, and V_{Max}^{85} are the same. The results rejected the null hypothesis at a 5% significant level. Table 5.9 shows the ANOVA test results with the $F>F_{critical}$ and p-value <0.05 for both vehicle types. This indicates that the three-speed variables are significantly different for cars and loaded trucks.

Table 5. 9 Results of ANOVA test of the 85th percentile speeds corresponding to V_{CC}, V_{Min}, and V_{Max} for car and loaded trucks

Vehicle	F_{Cal}	*p*-value	$F_{critical}$
Car	90.33	<0.000	3.005
Loaded truck	65.2	<0.000	3.004

5.6 Summary

Considering the speed variability on the curve, this chapter developed two operating speed correction models to estimate V_{Min}^{85} and V_{Max}^{85} using V_{CC}^{85}. Length of the curve (L_C) was found to be significant in explaining the variability of the difference between V_{CC}^{85} and V_{Min}^{85}, for both car and the loaded truck. Length of the curve (L_C) and curvature change rate (CCR) were found to be significant in explaining the variability of the difference between V_{CC}^{85} and V_{Max}^{85}, for the car. For loaded trucks, the exit tangent (L_{et}) length was found to be significant in explaining the variability. The developed models were validated using the data collected at six different locations of the same study stretch. Sensitivity analyses found that the interaction variables are highly sensitive in explaining the variability of $\Delta V_{Max,CC}^{85}$. The estimated correction factors were then used and corrected the V_{CC}^{85} corresponding to 191 horizontal curves. The next chapter presents the assessment of the role of V_{Min}^{85} and V_{Max}^{85} in the evaluation of geometric design consistency.

6 Effect of speed variability on the geometric design consistency and safety

6.1 Introduction

Lamm's criteria are the most widely accepted as well as used for geometric design consistency assessment. Several studies have evaluated the consistency using the operating speed estimated from the spot speeds corresponding to the curve center and the midpoint of the tangent (Anderson et al. 1999; Hassan et al. 2000; Castro et al. 2008; Zilioniene and Vorobjovas 2011; Wang et al. 2013; Goyani et al. 2022). Further, some of the studies have explored the relationship between safety (crash data) and design consistency and found that there is a close relationship between the two (Cafiso et al. 2010; Wu et al. 2013; Montella and Imbriani 2015; Garach et al. 2016; Dhahir and Hassan 2019).

Among the Lamm's criteria, Safety Criteria I (SC I) and Safety Criteria III (SC III) are used for assessing the individual geometric elements (horizontal curves). Both these criteria use the design and operating speeds on the horizontal curve. SC I uses the absolute difference between the design and operating speeds to classify the element. This criterion classifies the element as poor when the absolute difference exceeds a specified threshold. The absolute difference is high when the operating speed is either high or low compared to the design speed.

As already mentioned, the operating speed of cars is relatively higher than the design speed at the majority of the curves. If the speed of a vehicle remains constant on the curve, the operating speed corresponding to the curve center might classify the element correctly. However, the classification may become erroneous if the speed varies on the curve. Since the speed of an individual vehicle varies, the difference between the design and operating speeds also vary depending on the speed data used for estimating the latter. From safety point of view, it can be said that a manoeuvre on the curve is unsafe when the vehicle's speed exceeds the design speed. The speed exceedance may occur at any point on the curve; hence, it is necessary to consider the maximum speed on the curve for correctly evaluating a curve. Hence, the

operating speed meant for this criterion should be the V_{Max}^{85}. Similarly, SC III uses the difference between the assumed and demanded side friction and classifies the horizontal curves. This criterion classifies the horizontal curve as poor when the demanded side friction is much higher than the assumed side friction. Similar to SC I, depending on the speed variability on the curve, the operating speed used to estimate demanded side friction of the curve plays a key role in the evaluation of SCIII.

Crash data corresponding to the study stretch (Figure 3.21) shows that the majority of crashes involve trucks/loaded trucks. Hence, this study also assesses the consistency using the operating speed of loaded trucks. It is to be noted that the presence of empty trucks is very low near all the study locations. The operating speed of loaded trucks is relatively lower than the design speed (Figure 5.8). This leads to a higher difference in the design and operating speeds; hence, SC I might classify several elements as poor. When the speed varies on the curve, and the speed is further lower at the curve center, this criterion may erroneously classify several elements as poor. Hence for trucks also, it is necessary to identify and consider the maximum speed on the curve and compare it with the design speed.

Safety Criteria II (SC II) assesses the successive geometric elements (tangent to curve). This criterion uses the absolute difference between the operating speed corresponding to successive geometric elements. SC II classifies the elements based on the magnitude of absolute difference. This criterion examines the speed harmony between the successive geometric elements. If the speed on the curve is constant, the operating speed collected at the center of the curve might capture the actual speed difference corresponding to successive elements and classifies correctly. However, considering the speed variability on the curve, the estimated operating speed should correspond to the minimum speed on the curve for the purpose of evaluating the consistency using SC II.

This chapter assesses the role of V_{Min}^{85} and V_{Max}^{85}, compared to V_{CC}^{85}, in the geometric design consistency evaluation using Lamm's safety criteria. Further, consistency analyses corresponding to V_{Min}^{85}, V_{Max}^{85}, and V_{CC}^{85} were evaluated using the crash data. The V_{CC}^{85} values corresponding to the entire alignment were estimated using the operating speed models developed by Shallam et al. (2021). Then the V_{Max}^{85} and V_{Min}^{85} were estimated using operating speed correction models presented in the previous chapter.

6.2 Assessing the role of V_{Min}^{85}, and V_{Max}^{85} in the geometric design consistency evaluation

Lamm et al. (1995) proposed three consistency measures to evaluate the geometry of a highway alignment. These consistency measures were used in the present study to assess the role of V_{Min}^{85} and V_{Max}^{85}, compared to V_{CC}^{85}, in the consistency assessment.

i. Design consistency – Evaluates the consistency of individual geometric elements in a highway alignment based on the absolute difference between the design speed (V_D) and operating speed (V_{85}). Based on the threshold of the magnitude, a geometric element is classified as good, fair, or poor.

ii. Operating speed consistency – Evaluates the consistency of successive geometric elements in a highway alignment (tangent to curve) based on the absolute difference between the operating speeds on successive elements. Based on the threshold of the magnitude, the successive pair of geometric elements (V_i^{85}, V_{i+1}^{85}) is classified as good, fair, or poor.

iii. Consistency in driving dynamics – Evaluates the consistency of horizontal curves based on the differences between the assumed side friction (f_{RA}) and demanded side friction (f_{RD}). Based on the threshold of the magnitude, a horizontal curve is classified as good, fair, or poor.

Table 6.1 shows Lamm's consistency evaluation criteria (Lamm et al. 1995). The design classes good, fair and poor in the safety criteria were assigned with the weights "1", "0", and "-1", respectively.

Table 6. 1 Quantitative range of Lamm's safety criteria

Safety Criterion	Design Class		
	Good (1)	Fair (0)	Poor (-1)
I (Design consistency)	$\lvert V_{85} - V_D \rvert \leq 10$	$10 < \lvert V_{85} - V_D \rvert \leq 20$	$\lvert V_{85} - V_D \rvert > 20$
II (Operating speed consistency)	$\lvert V_i^{85} - V_{i+1}^{85} \rvert \leq 10$	$10 < \lvert V_i^{85} - V_{i+1}^{85} \rvert \leq 20$	$\lvert V_i^{85} - V_{i+1}^{85} \rvert > 20$
III (Vehicle stability)	$f_{RA} - f_{RD} \geq +0.01$	$-0.04 \leq f_{RA} - f_{RD} < +0.01$	$f_{RA} - f_{RD} < -0.04$

In the Table, V_{85} is the operating speed; V_D is the design speed; V_i^{85} is the operating speed at the approach tangent; V_{i+1}^{85} is the operating speed on the curve; f_{RA} is the side friction corresponding to the design speed, and f_{RD} is the demanded side friction corresponding to the operating speed. f_{RA} and f_{RD} are estimated using equations 6.1 and 6.2.

Side friction assumed (f_{RA}) is: $\frac{V_D^2}{127*R} - e$ (6.1)

Side friction Demanded (f_{RD}) is: $\frac{V_{85}^2}{127*R} - e$ (6.2)

In the consistency assessment, most of the earlier studies have used V_{CC}^{85} for V_{85}, V_{i+1}^{85}, as well as for estimating f_{RD}. This study considered V_{CC}^{85} and V_{Max}^{85} in place of V_{85}, and V_{CC}^{85} and V_{Min}^{85} in place of V_{i+1}^{85} while assessing the consistency using the safety criteria I to III and carried out a comparative assessment. The present study evaluated 191 horizontal curves of the study road stretch.

6.2.1 Design consistency (Safety Criterion I)

The role of V_{Max}^{85}, compared to V_{CC}^{85}, in the design consistency evaluation (SC I) of the horizontal curves was assessed for car and loaded truck, separately. First, the design consistency of horizontal curves was evaluated for both the vehicle types by considering V_{CC}^{85} in the place of V_{85}. Then V_{Max}^{85} was considered in the place of V_{85} and evaluated the design consistency of horizontal curves. Figure 6.1 shows the percentage of horizontal curves classified as good, fair, or poor corresponding to V_{CC}^{85} and $V_{Max}^{85}$of the cars. Figure 6.2 shows the percentage of horizontal curves classified as good, fair, or poor corresponding to V_{CC}^{85} and V_{Max}^{85} of the loaded trucks. Results corresponding to the cars show that the V_{Max}^{85} based classification resulted in more number of fair or poor curves compared to that of V_{CC}^{85}. The percentage change in the classification of horizontal curves was observed to be 41.3%. Table 6.2 shows the details of the changes in the classification of curves. The table shows that the major changes in the classification occur from good to fair and fair to poor. This indicates that, capturing speed variability has a significant impact on the way the curves are classified.

Fig. 6. 1 Classification of curves based on (a) V_{CC}^{85}; (b) V_{Max}^{85}, for cars

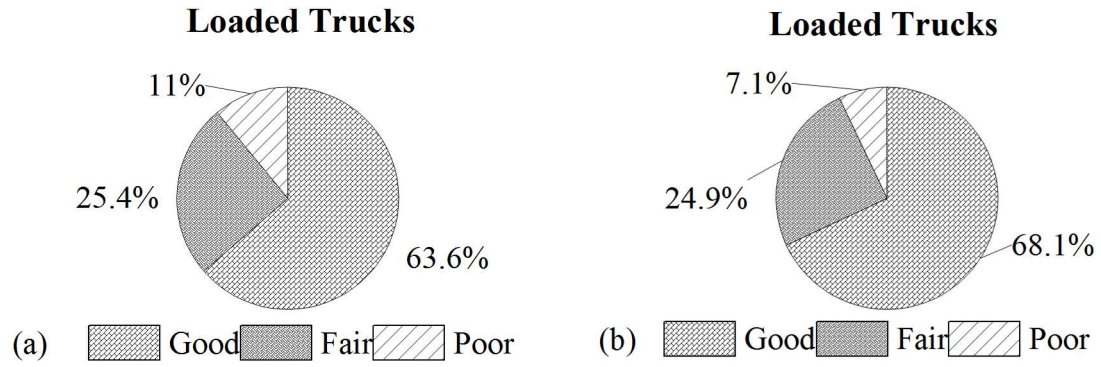

Fig. 6. 2 Classification of curves based on (a) V_{CC}^{85}; (b) V_{Max}^{85}, for loaded trucks

In contrast, results for the loaded trucks show that, the V_{Max}^{85} classified more number of horizontal curves as good compared to that of V_{CC}^{85}. The figure shows that the percentage difference in the classification are 5%, 0.5%, and 4% for good, fair and poor design classes, respectively. Application of V_{Max}^{85} affected the classification of several curves. The percentage change in the classification of individual horizontal curves is 21.2%. Table 6.2 shows the details of the changes in the classification of curves. The loaded trucks travel at lower speeds than the design speed but V_{Max}^{85} is higher than V_{CC}^{85}. Hence the application of V_{Max}^{85} reduced the difference between the design and operating speeds, leading to the above-mentioned changes in classification.

Table 6. 2 Classification change from V_{CC}^{85} to V_{Max}^{85} based SC I, for car and loaded truck

Change in classification	Percentage change, for	
	Car	Loaded truck
Good to Fair	23.1	6
Fair to Good	0	10.5
Fair to Poor	18.2	0.5
Poor to Fair	0	4.2

6.2.2 Operating speed consistency (Safety Criterion II)

In the operating speed consistency evaluation (SC II), the role of V_{Min}^{85} and V_{CC}^{85} corresponding to the car and the loaded truck was assessed separately. First, the operating speed consistency was evaluated for both vehicle types considering V_{CC}^{85} in the place of V_{i+1}. Then V_{Min}^{85} was considered in the place of V_{i+1} and evaluated the operating speed consistency. Figure 6.3 shows the percentage of successive geometric elements classified as good, fair, or poor, corresponding

to V_{CC}^{85} and V_{Min}^{85} of cars. Figure 6.4 shows the percentage of successive pairs of elements classified as good, fair, or poor corresponding to V_{CC}^{85} and V_{Min}^{85} of loaded trucks.

Fig. 6. 3 Classification of successive geometric elements based on (a) V_{CC}^{85}; (b) V_{Min}^{85}, of cars

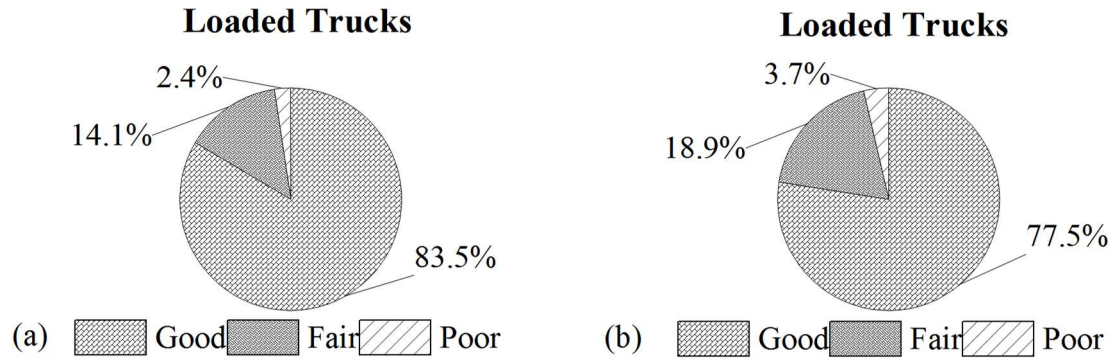

Fig. 6. 4 Classification of successive geometric elements based on (a) V_{CC}^{85}; (b) V_{Min}^{85}, of loaded trucks

Evaluation based on V_{Min}^{85} of cars classified a relatively more number of tangent-curve sections as fair and poor compared to that of V_{CC}^{85}. Figure 6.4 shows that the percentage difference for good, fair, and poor is 9.2%, 7.6%, and 1.7%, respectively. However, there is a significant change in the way the individual curves are classified. Table 6.2 shows the details of the changes in the classification of curves. The table shows that the change is significantly high from good to fair. Similarly, results for the loaded trucks show that the V_{Min}^{85} based safety criterion has classified more number of tangent-curve sections as fair and poor compared to that of V_{CC}^{85}. The percentage difference for good, fair and poor are 6%, 4.8%, and 1.3%, respectively. In this case, also, there is a significant change in the way the individual curves are classified. Table 6.2 shows the details of the changes in the classification of curves. The table shows that there is a significant change from good to fair. These changes are in the expected lines since the V_{Min}^{85} is significantly less than V_{CC}^{85}.

Table 6. 3 Classification change from V_{CC}^{85} to V_{Min}^{85} based SC II, for car and loaded truck

Change in classification	Percentage change, for	
	Car	Loaded truck
Good to Fair	10.6	11.3
Fair to Good	1.3	5.8
Fair to Poor	1.7	1.8
Poor to Fair	0	0.5

6.2.3 Vehicle Stability (Safety Criterion III)

This section presents the classification of the horizontal curves using SC III. This criterion compares the demanded side friction (f_{RD}) corresponding to the operating speed with that of the design speed. First, the vehicle stability was evaluated by considering the demanded side friction corresponding to V_{CC}^{85}. Then V_{Max}^{85} was considered in the estimation of demanded side friction and evaluated the consistency of horizontal curves. Figure 6.5 shows the percentage of horizontal curves classified as good, fair, or poor corresponding to V_{CC}^{85} and V_{Max}^{85} of cars. Figure 6.6 shows the percentage of horizontal curves classified as good, fair, or poor corresponding to V_{CC}^{85} and V_{Max}^{85} of loaded trucks.

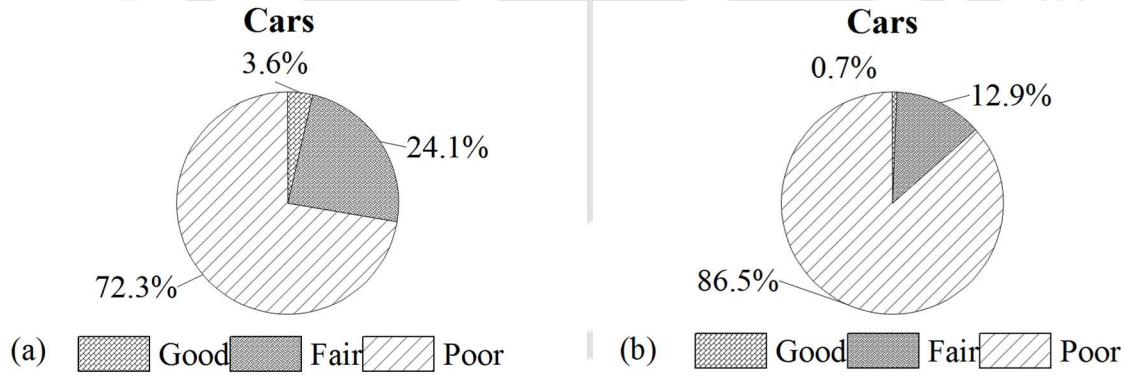

Fig. 6. 5 Classification of curves based on the friction estimated using (a) V_{CC}^{85}; (b) V_{Max}^{85}, for cars

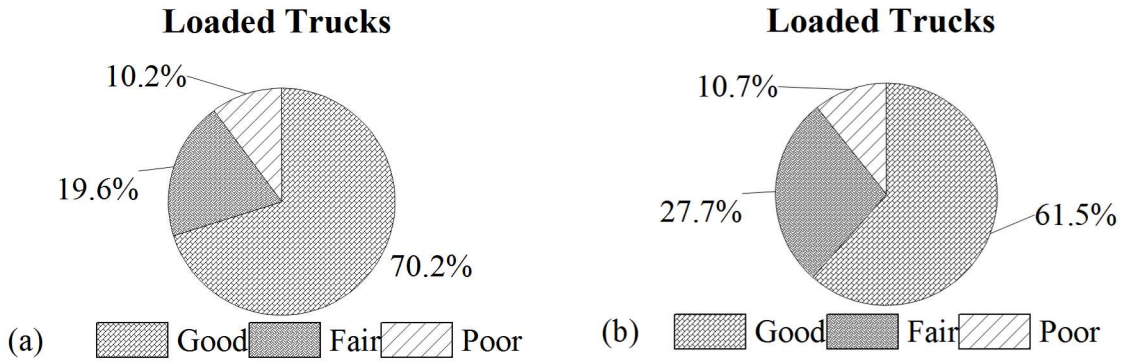

Fig. 6. 6 Classification of curves based on the friction estimated using (a) V_{CC}^{85}; (b) V_{Max}^{85}, for loaded trucks

Results corresponding to the cars show that, the V_{Max}^{85} has classified almost all the horizontal curves into fair and poor compared. The figure shows that the percentage differences in the classification are 2.9%, 11.2%, and 14.2% for good, fair and poor, respectively. However, there is a 17.5% change in the way the individual curves are classified. Table 6.4 shows that a majority of the curves classified earlier as fair are turned out to be poor. Similarly, for the loaded trucks, the V_{Max}^{85} based evaluation has classified a relatively more number of horizontal curves as fair and poor compared to V_{CC}^{85} based consistency evaluation. The figure corresponding to loaded trucks shows that the percentage differences in the classification are 8.7%, 8.1%, and 0.5% for good, fair, and poor, respectively. However, there is a change in the classification of 19.4% of the horizontal curve. Table 6.4 shows the details of changes in the classification. The table shows that the change in classification is significantly high, from good to fair. For both car and loaded truck, the V_{Max}^{85} is higher than V_{CC}^{85} thereby the demanded side friction further increases. Hence using the V_{Max}^{85} of cars and trucks for estimating the demanded side friction classifies a significant number of curves as either fair or poor.

Table 6. 4 Classification change from V_{CC}^{85} to V_{Max}^{85} based SC III, for car and loaded truck

Change in classification	Percentage change, for	
	Car	Loaded truck
Good to Fair	3	11
Good to Poor	0	1
Fair to Good	0	1.6
Fair to Poor	14.2	2.6
Poor to Good	0	1.8
Poor to Fair	0	1.3

6.2.4 Overall safety module

The consistency assessment based on safety criteria I to III from the previous sub-sections indicated that the geometric elements (curve/ tangent to curve) exhibit different design safety levels with respect to the individual safety criteria. This is because each safety criterion represents a separate safety aspect in the geometric design (Lamm et al. 2007). For a more concise description of the safety evaluation process, Eberhard (1997) developed a simple approach to combine the three safety criteria called the overall safety module. The overall safety module is defined as the average of the defined weights for all three safety criteria. Table 6.5 shows the classification criteria for the overall safety module.

Table 6. 5 Classification criteria for overall safety module

Design level SC I, SC II, SC III	Weighting factor	Average value of the three safety criteria
Good	+1.0	$x \geq 0.5$
Fair	0.0	$-0.5 < x < +0.5$
Poor	-1.0	$x \leq -0.5$

In the table, x is the average value of the three safety criteria and is computed using Eq. 6.3.

$$x = \frac{(SC\ I + SC\ II + SCIII)}{3} \tag{6.3}$$

For instance, if a particular horizontal curve is classified according to SC I, SC II, and SC III as good (weighting factor = 1), fair (weighting factor = 0), and fair (weighting factor = 0). Then the overall safety module is computed as an average of the three weighting factors as $x = \frac{1+0+0}{3}$, i.e., $x = 0.33$. According to Table 6.2, x is in the range of $-0.5 < x < +0.5$; thus, the overall safety module classified the particular horizontal curve as a fair design. Figure 6.7 shows the percentage of horizontal curves classified as good, fair or poor corresponding to V_{CC}^{85} and, V_{Max}^{85} and V_{Min}^{85} of cars, based on the overall safety module. Figure 6.8 shows the percentage of horizontal curves classified as good, fair, or poor corresponding to V_{CC}^{85} and, V_{Max}^{85} and V_{Min}^{85} of loaded trucks, based on the overall safety module.

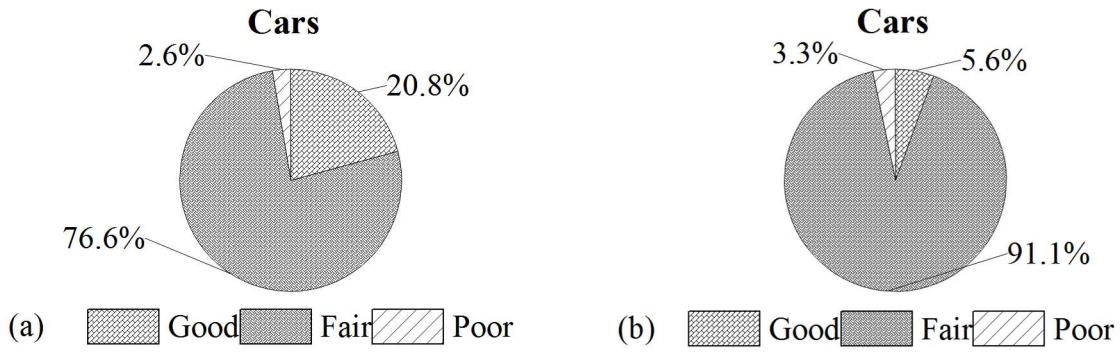

Fig. 6. 7 Classification of curves based on overall safety module using (a) V_{CC}^{85}; (b) V_{Max}^{85} and V_{Min}^{85}, for cars

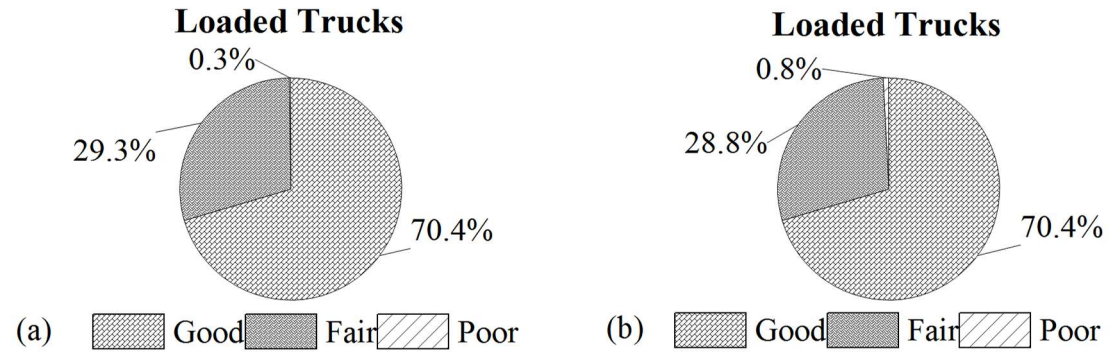

Fig. 6. 8 Classification of curves based on overall safety module using (a) V_{CC}^{85}; (b) V_{Max}^{85} and V_{Min}^{85}, for loaded trucks

Results show that the overall safety module using V_{Max}^{85} and V_{Min}^{85} of cars classified most of the horizontal curves as fair and poor. Further, the comparative assessment shows that the classification of around 18.2% of the horizontal curves has changed after using V_{Max}^{85} and V_{Min}^{85}. Table 6.6 shows the detailed percentage classification differences from the V_{CC}^{85} to V_{Max}^{85} based SC III. From the table, the classification of horizontal curves was changed from good to fair, fair to poor and poor to fair design classes. For the loaded trucks, the classification of the overall safety module based on V_{Max}^{85} and V_{Min}^{85}, and V_{CC}^{85} is almost the same. Also, the classification of 21.5% of the horizontal curves has changed after using V_{Max}^{85} and V_{Min}^{85}. Table 6.6 shows the details of the changes in classification of individual curves. The table shows that the change in classification is significantly high, from good to fair.

Table 6. 6 Classification change from V_{CC}^{85} to V_{Max}^{85} and V_{Min}^{85} based overall safety module, for car and loaded truck

Change in classification	Percentage change, for	
	Car	Loaded truck
Good to Fair	15.2	10.5
Fair to Good	0	10
Fair to Poor	1.7	1
Poor to Fair	1.0	0

To understand the effectiveness of V_{Max}^{85} and V_{Min}^{85} in the safety criteria, it is necessary to compare the safety criteria with the crash data. Classification of endangerment levels proposed by Schneider (1999) was used to evaluate each geometric element based on the crash data. The following section presents the level of endangerment based on the crash data.

6.3 Level of endangerment

The effectiveness of V_{Max}^{85} and V_{Min}^{85} in the safety criteria/safety module was assessed by comparing the results corresponding to the safety criteria with the actual crash data. The endangerment level based on the actual crash data proposed by Schneider (1999) was used in the present study. A particular geometric element is classified as low, medium, and high endangerment based on the crash frequency corresponding to each geometric element. Table 6.7 presents the classification of endangerment levels proposed by Schneider (1999).

Table 6. 7 Endangerment level classification (Schneider 1999)

Endangerment	Weighting factor	Crash frequency
Low	+1.0	Not more than 1
Medium	0.0	Not more than 2
High	-1.0	More than 2

To perform the vehicle-specific analysis, the crash data corresponding to cars and trucks are distinguished based on the crash reports. The crash data corresponding to eight years, from December 2013 to March 2021, shows that 19% of crashes involved car and 74% of crashes involved trucks. Table 6.8 shows the percentage frequency of horizontal curves based on the number of crashes at each location, for cars and trucks, respectively.

Table 6. 8 Percentage frequency of the horizontal curves based on the number of crashes for cars and trucks

Vehicle class		Number of crashes				
		0	1	2	3	>3
Percentage no. of curves	Car	87.79	10.56	1.32	0.33	0
	Trucks	64.66	23.04	7.33	2.62	2.36

Table 6.9 shows the percentage frequency of horizontal curves corresponding to different endangerment levels for cars and trucks, respectively.

Table 6. 9 Percentage frequency of the horizontal curves based on the endangerment level for cars and trucks

Vehicle class		Endangerment level		
		Low	Medium	High
Percentage no. of curves	Car	98.35	1.32	0.33
	Trucks	87.7	7.33	4.98

Tables 6.8 and 6.9 show that the number of horizontal curves having more than one crash is relatively very low for cars. Thus, the analysis of geometric design consistency with safety was performed using the crash data corresponding to trucks. The analysis of geometric design consistency with safety (endangerment) for the trucks is presented in the following section.

6.4 The level of agreement between geometric design consistency and safety

A relationship between the safety criteria and the endangerment level was established through the level of agreement proposed by Schneider (1999). Table 6.10 shows the levels of agreement between the safety criteria and endangerment. For instance, when a safety criterion classifies a particular geometric element (horizontal curve) as good design (+1), a full level of agreement is reached if the endangerment level is low (+1). A partial agreement is defined if the safety criteria classify a geometric element as fair design (0) and its endangerment is low (+1). A disagreement arises when a geometric element is defined by the safety criteria and endangerment as either good-high or poor-low.

Table 6. 10 Level of agreement between safety criteria and endangerment levels

			Endangerment		
			Low	**Medium**	**High**
Safety	**Design class**	**Factor**	+1	0	-1
criteria	**Good**	+1	Full agreement (2)	Partial agreement (1)	Disagreement (0)
	Fair	0	Partial agreement (1)	Full agreement (2)	Partial agreement (1)
	poor	-1	Disagreement (0)	Partial agreement (1)	Full agreement (2)

The levels of agreement for trucks, based on V_{CC}^{85} and, V_{Max}^{85} and V_{Min}^{85}, were analyzed separately and compared. With respect to V_{CC}^{85}, the percentages of level of agreement corresponding to safety criteria I, II, and III with the crash data are 71.3%, 83.5%, and 76.57%, respectively. Whereas, when using V_{Max}^{85} and V_{Min}^{85}, the percentages of level of agreement corresponding to safety criteria I, II, and III with the crash data are 79.3%, 84.6%, and 78.01%, respectively. Further, the evaluation based on individual safety criteria indicated different design safety levels for each horizontal curve. This is as expected since each safety criterion represents a separate safety aspect of geometric design. Thus, to have a fast and comprehensive overview of the horizontal curves, a safety module that combines the safety criteria (Eberhard et al. 1997), was used for further analyses. Tables 6.11 and 6.12 show number of curves with various level of agreement corresponding to the overall safety module and endangerment based on V_{CC}^{85} and, V_{Max}^{85} and V_{Min}^{85}, respectively.

Table 6. 11 Level of agreement based on V_{CC}^{85}, for loaded truck

			Endangerment		
			Low	Medium	High
	Design class	Factor	1	0	-1
Safety module	Good	1	233	21	15
	Fair	0	101	7	4
	Poor	-1	1	0	0

Table 6. 12 Level of agreement based on V_{Max}^{85} and V_{Min}^{85}, for loaded truck

			Endangerment		
			Low	Medium	High
	Design class	Factor	1	0	-1
Safety module	Good	1	253	12	4
	Fair	0	81	15	14
	Poor	-1	1	1	1

The overall level of agreement between the overall safety module and endangerment level corresponding to V_{CC}^{85} and, V_{Max}^{85} and V_{Min}^{85} are 79.3% and 84.4%, respectively. Tables 6.10 and 6.11 show that the consistency assessment corresponding to V_{CC}^{85} has classified 21 (75%)

medium endangered and 15 (78.95 %) high endangered horizontal curves as good. Whereas the consistency assessment corresponding to V_{Max}^{85} and V_{Min}^{85} has classified 12 (42.8 %) medium endangered and only 4 (21.05 %) high endangered horizontal curves as good. Besides, the comparative assessment of each location showed that around 21.5% of the horizontal curves have a different level of agreement. Thus, this study highlights the necessity of considering V_{Max}^{85} and V_{Min}^{85} for geometric design consistency assessment. Considering V_{Max}^{85} and V_{Min}^{85} in the consistency evaluation, helps the designers, planners, and researchers in an effective identification of poor geometric elements.

6.5 Crash frequency modeling

This section presents the crash frequency modeling with an aim to establish the usefulness of speed variability analysis in the safety assessment. Crashes involving trucks were considered for the safety assessment. The crash frequency models were developed considering various operating speed variables corresponding to the three safety criteria. The independent variables also include the geometric variables corresponding to curve, approach tangent, and departing tangent. Poisson regression and negative binomial regression models are the two most popular approaches used to model crash data (Anderson et al. 2000; Cafiso et al. 2010; Ona et al. 2014; Nalo et al. 2020). The major requirement for modeling Poisson regression is that the mean of the crash count should be equal to its variance. When the variance of the crash count is larger than the mean, the data is said to be over-dispersed or under-dispersed if the variance of the crash count is less than the mean. Negative binomial regression is used to model the over-dispersed data.

The data corresponding to 191 horizontal curves was used for crash frequency modeling. Table 6.13 presents the statistical summary of crash data, the geometric features corresponding to the horizontal curves, and the truck's operating speed variables. The features shown in the table are corresponding to both the travel directions.

Table 6. 13 Descriptive statistics of the geometric and operating speed variables of the study locations

Parameter	Minimum	Maximum	Mean	Standard deviation
No. of crashes	0	13	0.61	1.23
Length of the curve (m)	29.765	113.407	54.85	20.73
Length of the approach tangent (m)	1	322.28	64.5	64.4
Length of the exit tangent (m)	1	262.9	59.77	55.93
Super elevation (%)	2.5	10	6.7	2.42
Deflection angle (degrees)	23.98	120.613	60.11	27.77
Degree of curvature (degrees)	8.73	21.84	17.17	4.98
Grade (%)	-6	6	0	4.53
$\lvert \mathbf{V}_{CC}^{85} - V_D \rvert$	0.1	33	9.6	7
$\lvert \mathbf{V}_{i}^{85} - \mathbf{V}_{CC}^{85} \rvert$	0.0	48.7	5.6	5.6
$f_{RA} - \mathbf{f}_{RD}^{CC}$	-0.4	0.9	0	0.1
$\lvert \mathbf{V}_{Max}^{85} - V_D \rvert$	0	28.7	8	6.2
$\lvert \mathbf{V}_{i}^{85} - \mathbf{V}_{Min}^{85} \rvert$	0	45.5	6.4	6
$f_{RA} - \mathbf{f}_{RD}^{Max}$	-0.4	0.8	0	0.1
$\mathbf{V}_{AT}^{85}$	19	70.3	39.6	8.84

The mean and variance of eight-year crash data on the study curves are found to be 0.61 and 1.52, respectively. The statistics show that the data is over-dispersed. Thus, in modeling crash frequency, negative binomial regression was preferred over Poisson regression.

In the Poisson regression model, the probability of intersection i having y_i accidents per year (where y_i is a non-negative integer) is given by

$$P(y_i) = \frac{e^{-\lambda_i}\lambda_i^{y_i}}{y_i!}, \; i = 1,2,3, \ldots, n \tag{6.4}$$

Where, $P(y_i)$ is the probability of intersection i having y_i accidents per year and λ_i is the Poisson parameter for intersection i, which is equal to intersection i's expected number of accidents per year, E[y_i]. Poisson regression models are estimated by specifying the Poisson parameter λ_i (the expected number of events per unit time period), as a function of explanatory variables. The most common relationship between explanatory variables and Poisson parameter is the log-linear model,

$$\lambda_i = e^{\beta x_i} \text{ or equivalently } \ln(\lambda_i) = \beta x_i \tag{6.5}$$

The negative binomial regression model is derived by rewriting Eq. 6.5 as

$$\lambda_i = e^{(\beta X_i + \varepsilon_i)} \tag{6.6}$$

$$\ln(\lambda_i) = \beta_o + \beta_1 X_{i1} + \beta_2 X_{i2} + \beta_3 X_{i3} + \ldots\ldots + \beta_k X_{ik} + \varepsilon_i \tag{6.7}$$

Where β is the vector of estimated parameters and ε_i is the Gamma-distributed disturbance term with mean one and variance α. In the present study, the expected number of crashes per period is given as

$$E[y_i] = \lambda_i = e^{\beta X_i} \tag{6.8}$$

Where, X_i are the explanatory variables. In this section, first, the crash frequency models were developed with the operating speed differences corresponding to the three safety criteria that were based on V_{CC}^{85} and, V_{Max}^{85} and V_{Min}^{85}. Then the crash frequency models were developed with the operating speed differences corresponding to the three safety criteria that were based on V_{Max}^{85} and V_{Min}^{85} and geometric variables.

6.5.1 Crash frequency modeling with the operating speed differences

The level of agreement between the safety criteria and crash data presented in previous sections shows the significance of V_{Max}^{85} and V_{Min}^{85} in geometric design consistency evaluation. To further ascertain the significance of V_{Max}^{85} and V_{Min}^{85}, crash frequency models, reflecting the three safety criteria were developed. Corresponding to safety criterion 1, two different models were estimated. The first model was developed as a function of the absolute difference between V_D and operating speed V_{CC}^{85}. The second model was developed as a function of the difference between V_D and V_{Max}^{85}.

Corresponding to safety criterion II, two different models were developed where the first model was developed as a function of the absolute difference between operating speed on the approach tangent (V_i^{85}) and V_{CC}^{85}. The second model was developed as a function of the absolute difference between operating speed on the approach tangent (V_i^{85}) and V_{Min}^{85}. Corresponding to safety criterion III, two different models were developed. The first model was developed as a function of the difference between assumed side friction (f_{RA}) based on V_D and the demanded side friction (f_{RD}^{CC}) based on V_{CC}^{85}. The second model was developed as a function of the difference between assumed side friction (f_{RA}) based on V_D, and the demanded

side friction (f_{RD}^{Max}) based on V_{Max}^{85}. Table 6.14 presents the negative binomial models corresponding to the three safety criteria.

Table 6. 14 Summary of negative binomial models corresponding to the three safety criteria

Models based on V_{CC}^{85}				
Model		Coefficient	*p*-value	AIC
1	Intercept	-0.49	0.0016	812.8
	$\lvert V_{CC}^{85} - V_D \rvert$	-0.001	0.938	
2	Intercept	-0.45	0.0005	812.56
	$\lvert V_i^{85} - V_{CC}^{85} \rvert$	-0.0087	0.607	
3	Intercept	-0.46	<0.000	811.39
	$f_{RA} - f_{RD}^{CC}$	-1.49	0.258	
Models based on V_{Min}^{85} and V_{Max}^{85}				
		Coefficient	*p*-value	AIC
1	Intercept	-0.72	<0.000	809.83
	$\lvert V_{Max}^{85} - V_D \rvert$	0.0255	0.07	
2	Intercept	-0.77	<0.000	806.53
	$\lvert V_i^{85} - V_{Min}^{85} \rvert$	0.037	0.006	
3	Intercept	-0.48	<0.000	798.61
	$f_{RA} - f_{RD}^{Max}$	-4.9	0.0003	

The models corresponding to V_{CC}^{85} indicate that the coefficients are not statistically significant. Further, the direction corresponding to the model coefficient is not as expected. Whereas the models corresponding to V_{Max}^{85} and V_{Min}^{85} indicate that the coefficients are statistically significant, and the direction of the model coefficient is logical in explaining the crash data. Moreover, the Akaike Information Criteria (AIC) value also signifies that the models based on V_{Min}^{85}, and V_{Max}^{85} are preferable to the V_{CC}^{85}-based models. Thus, the results obtained strongly recommend to consider V_{Max}^{85} and V_{Min}^{85} on the horizontal curves while assessing the geometric design consistency. Considering the V_{Max}^{85} and V_{Min}^{85} in the consistency evaluation aids the highway and safety engineers in effectively identifying unsafe elements of a highway alignment.

6.5.2 Crash frequency modeling with the operating speed differences and geometric variables

Three crash frequency models were developed as a function of operating speed differences corresponding to safety criteria and geometric variables. The first model was developed as a

function of the difference between V_D and V_{Max}^{85} (SC-I), and geometric variables. The second model was developed as a function of the absolute difference between operating speed on the approach tangent (V_i^{85}) and operating speed on the curve (V_{Min}^{85}) (SC-II), and geometric variables. The third model was developed as a function of the difference between assumed side friction (f_{RA}) based on V_D, and the demanded side friction (f_{RD}^{Max}) based on V_{Max}^{85} (SC-III), and geometric variables. Table 6.15 presents the crash frequency models corresponding to the three safety criteria, and geometric variables developed using negative binomial regression.

Table 6. 15 Summary of negative binomial models corresponding to the three safety criteria and geometric variables

Model	Parameter	Coefficient	P-value	AIC
1	Intercept	-1.095	<0.000	799.4
	$\lvert V_{Max}^{85} - V_D \rvert$	0.0255	0.07	
	Δ	0.007	<0.000	
2	Intercept	-1.075	<0.000	797.9
	$\lvert V_i^{85} - V_{Min}^{85} \rvert$	0.032	0.02	
	Δ	0.0065	0.0012	
3	Intercept	-1.54	<0.000	780.95
	$f_{RA} - f_{RD}^{Max}$	-5.06	<0.000	
	L_C	0.018	<0.000	

In the model-1, along with the speed difference between design speed and V_{Max}^{85} (SC-I), deflection angle (Δ) is significant. In model-2 also, along with the operating speed difference between V_i^{85} and V_{Max}^{85} (SC-II), deflection angle (Δ) is significant. In the model-3, along with the difference between assumed side friction (f_{RA}) based on V_D, and the demanded side friction (f_{RD}^{Max}) based on V_{Max}^{85} (SC-III), length of the curve (L_C) is significant. The direction of the model coefficients is logical in explaining the crash data. Among the three safety criteria, the speed variable corresponding to SC II is relatively better in predicting the crash frequency.

6.6 Summary

This chapter assessed the role of speed variability in the evaluation of geometric design consistency of horizontal curves. Speed variability was considered in terms of V_{Max}^{85} and V_{Min}^{85}. The three safety criteria developed by Lamm et al. (1995) were used for evaluating the consistency. A total of 151 and 191 horizontal curves from the study road section were evaluated to assess the role of speed variability in the geometric design consistency for cars and loaded trucks, respectively. The consistency evaluation for cars and loaded trucks

corresponding to V_{Max}^{85} and V_{Min}^{85} were compared with that of V_{CC}^{85}. For cars, the analysis has shown a significant change in the classification of horizontal curves, i.e., from good to fair and fair to poor design classes. Similarly, the analysis of horizontal curves corresponding to loaded trucks has shown a significant change in the classification, i.e., from good to fair, fair to good, fair to poor and poor to fair design classes. Moreover, the classification of curves corresponding to the car was significantly different among the three safety criteria. In terms of the level of agreement, V_{Max}^{85} and V_{Min}^{85}- based consistency evaluation has shown a better match of the endangerment compared to that of V_{CC}^{85}.

To further ascertain the relevance of V_{Max}^{85} and V_{Min}^{85} in the evaluation of geometric design consistency, crash frequency models were developed as a function of operating speed (or differences in them) corresponding to various safety criteria. The developed models clearly highlighted the importance of V_{Max}^{85} and V_{Min}^{85} in the safety assessment. Further, three crash frequency models were developed with the operating speed differences corresponding to the three safety criteria and geometric variables. Deflection angle (Δ) and length of the curve (L_C) were found to be significant in explaining the crash frequency.

7 Conclusion

7.1 Overview

The thesis presents various aspects of geometric design consistency and safety assessment of the horizontal curves of a two-lane undivided rural highway passing through mountainous terrain. The speed data collection plays a major role in the assessment of geometric design consistency and safety. Thus, the first aspect focused in this research was the collection of naturalistic vehicle trajectories on the horizontal curves located in a mountainous region. Second, the analysis of speed variability on the horizontal curves through continuous acceleration and speed profiles for the geometric design consistency assessment. Third, the development of correction models for V_{CC}^{85} and estimate V_{Max}^{85} and V_{Min}^{85} on the curve. Fourth, assessing the role of V_{Max}^{85} and V_{Min}^{85} in the geometric design consistency evaluation and safety. The following sections present the major findings, contributions of the research, and scope for further studies.

7.2 Findings of the research

This section presents the major findings of the present study corresponding to the above-mentioned aspects of the geometric design consistency and safety assessment.

7.2.1 Naturalistic vehicle trajectory extraction

For a highway alignment passing through mountainous terrain, a multiple-homography-based coordinate transformation technique is necessary to collect naturalistic vehicle trajectory data using a videography-based image processing. The proposed technique was developed based on Direct Linear Transform Technique (DLT) and was evaluated using the observed speed profiles.

The comparative analysis showed that the speed profiles estimated using the multiple-homography approach are more accurate (RMSE of 0.44 km/h) compared to that of a single homography approach, where the RMSE varied between 1.5 to 3.7 km/h. These findings highlight the necessity of using multiple homography technique in the videography-based naturalistic trajectory data collection for the highway alignment passing through mountainous terrain.

7.2.2 Analysis of acceleration profiles

The analysis of acceleration profiles corresponding to cars and loaded trucks on the horizontal curves was performed through continuous acceleration and speed profiles. In the analysis of acceleration profiles, it was found that a majority of drivers of both vehicle types tend to adopt two different driving patterns. One of the patterns was that the vehicle enters the curve in deceleration mode and departs in acceleration mode. The other pattern was that the vehicle enters the curve in acceleration mode and departs the curve in deceleration mode.

Further, the deceleration and acceleration length measured from the point of curvature found that cars and loaded trucks decelerated up to 70% and 40% of the curve length. Similarly, it was found that cars and loaded trucks accelerated up to 50% and 30% of the curve length, respectively. The driving patterns indicated that the corresponding locations of minimum and maximum speed on the curve are not fixed. Moreover, the acceleration behaviour on the curve corresponding to the car and loaded trucks was statistically different.

7.2.3 Analysis and modeling of speed variability

The operating speed profiles revealed that the speed on the curve is not constant. The assessment of minimum and maximum speed locations on the curve found that in the majority of cases, the corresponding minimum and maximum speed locations occur at either the 1st or 3rd segment of the curve. Further, the statistical analysis corresponding to the speed variables V_{Max}^{85}, V_{Min}^{85}, and V_{CC}^{85} found that

a. The V_{Min}^{85} was statistically less than V_{Max}^{85}
b. The V_{Min}^{85} and V_{CC}^{85} are statistically different
c. The V_{Max}^{85} and V_{CC}^{85} are statistically different

Further, considering the V_{Max} and V_{Min}, the maximum speed difference on the curve was modeled to understand the speed variability on the curve. The analysis found that CCR and V_{PC} are significant in modeling the $Max\Delta_{85}V$ for cars. The maximum speed difference on the curve increases with the decreasing CCR and V_{PC}. Whereas L_C and CCR were found to be significant in modeling $Max\Delta_{85}V$ of loaded trucks. Here, the maximum speed difference on the curve increases with the increasing curve length but decreases with the increasing CCR. Moreover, gradient and travel direction were found to have a differential impact on the way the other determinants are influencing the speed variability.

7.2.4 Development of operating speed correction models

Given the speed variability on the curve, consistency evaluation based on the operating speed corresponding to the curve centre would lead to erroneous results. For a realistic evaluation, it is necessary to estimate V_{Max}^{85} and V_{Min}^{85}, which can be used for assessing the design and operating speed consistencies. However, identifying the point at which the minimum and maximum speeds occur on the curve is not possible without having continuous speed profile data. At the same time, collecting naturalistic vehicle trajectories using videography approach on the horizontal curves in mountainous terrain is not possible in all the scenarios. In this scenario, this study estimated the correction factors (ΔV_{MaxCC}^{85} and ΔV_{MinCC}^{85}) for the operating speed corresponding to the centre of the curve. The estimated correction factors were then used to estimate V_{Max}^{85} and V_{Min}^{85} on the curve.

7.2.5 Role of V_{Max}^{85} and V_{Min}^{85} in the assessment of geometric design consistency and safety

The geometric design consistency was assessed using V_{CC}^{85} and, V_{Max}^{85} and V_{Min}^{85} corresponding to the car and loaded trucks, and the results were compared. The comparison of individual curve classification corresponding to V_{CC}^{85} and, V_{Max}^{85} and V_{Min}^{85} reveals significant changes across the criteria.

The assessment of overall safety module corresponding to V_{Max}^{85} and V_{Min}^{85} of car has shown that most of the horizontal curves were classified as fair and poor. For the loaded trucks, the assessment of overall safety module based on V_{CC}^{85} and, V_{Max}^{85} and V_{Min}^{85} was almost the same. The effect of change in classification, due to V_{Max}^{85} and V_{Min}^{85}, on the consistency evaluation was assessed through level of agreement. The level of agreement between safety criteria and the crashes corresponding to trucks showed that considering V_{Max}^{85} and V_{Min}^{85} in geometric design consistency improves the identification of poorer sections compared to that of V_{CC}^{85}.

The crash frequency models corresponding to the three safety criteria revealed that speed differences based on V_{Max}^{85} and V_{Min}^{85} have a significant impact on crash frequencies. Other than the speed variables, Deflection angle (Δ) and Curve length (L_C) play a significant role in predicting the crash frequency. The magnitude and direction of the coefficients are significant and logical in explaining the crash data. Thus, the results presented in the study strongly recommend to consider V_{Max}^{85} and V_{Min}^{85} on the horizontal curves while assessing the geometric design consistency.

7.3 Contributions of the research

The major contributions of the study include:

1. The study proposed a multiple homography-based coordinate transformation technique for collecting naturalistic vehicle trajectory data on the two-lane undivided rural highways passing through mountainous terrain.
2. Considering the speed variability on the curve, this study signifies the estimation of V_{Max}^{85} and V_{Min}^{85} for geometric design consistency and safety evaluation of the horizontal curves in two-lane rural highways passing through mountainous terrain.

7.4 Limitations and Future scope

The limitations and future scope of the study are as follows.

1. The scope of the analysis presented in this research is limited to daylight and dry weather conditions.
2. The analysis of driver behavior presented in this study corresponds to free-flowing vehicles. However, for the two-lane undivided highways, the presence of vehicles in the opposite direction might affect the driver's behavior. Further studies may consider the presence and absence of vehicles in the opposite stream.
3. In assessing safety criterion II, this study did not consider the individual speed difference between successive geometric elements since the collected trajectory data was limited to horizontal curves.
4. The role of tangents and transition curves in the speed variability on the horizontal curves located in mountainous terrain can be studied.
5. In crash frequency modelling, zero-inflated regression models for both Poisson and negative binomial models that handle large zero densities in the dataset can be developed.

References

AASHTO. (1994). *A Policy on Geometric Design of Highways and Streets*. American Association of State Highway and Transportation Officials (AASHTO), Washington, DC, U.S.

AASHTO. (2001). *A Policy on Geometric Design of Highways and Streets*. American Association of State Highway and Transportation Officials (AASHTO), Washington, DC, U.S.

AASHTO. (2004). *A Policy on Geometric Design of Highways and Streets*. American Association of State Highway and Transportation Officials (AASHTO), Washington, DC, U.S.

AASHTO. (2011). *A Policy on Geometric Design of Highways and Streets*. American Association of State Highway and Transportation Officials (AASHTO), Washington, DC, U.S.

AASHTO. (2018). *A Policy on Geometric Design of Highways and Streets*. American Association of State Highway and Transportation Officials (AASHTO), Washington, DC, U.S.

Ahmed, I. (2013). Road infrastructure and road safety. *Transport and Communications Bulletin for Asia and the Pacific*, *83*, 19-25.

Alexander, G. J. (1986). *Driver expectancy in highway design and traffic operations*. US Department of Transportation, Federal Highway Administration, Office of Traffic Operations.

Al-Masaeid, H. R., Hamed, M., Aboul-Ela, M., & Ghannam, A. G. (1995). Consistency of horizontal alignment for different vehicle classes. *Transportation Research Record*, (1500).

Andjus, V., & Maletin, M. (1998). Speeds of cars on horizontal curves. *Transportation Research Record*, *1612*(1), 42-47.

Anderson, I. B., Bauer, K. M., Harwood, D. W., & Fitzpatrick, K. (1999). Relationship to safety

of geometric design consistency measures for rural two-lane highways. *Transportation research record*, *1658*(1), 43-51.

Amrutsamanvar, R. B., Muthurajan, B. R., & Vanajakshi, L. D. (2021). Extraction and analysis of microscopic traffic data in disordered heterogeneous traffic conditions. *Transportation letters*, *13*(1), 1-20.

Akoglu, H. (2018). User's guide to correlation coefficients. *Turkish journal of emergency medicine*, *18*(3), 91-93.

BRS (Basic Road Statistics). 2018. *Basic Road Statistics in India 2019.* New Delhi, India: MORTH.

Bella, F. (2007). Parameters for evaluation of speed differential: contribution using driving simulator. *Transportation research record*, *2023*(1), 37-43.

Bella, F. (2008). Driving simulator for speed research on two-lane rural roads. *Accident Analysis & Prevention*, *40*(3), 1078-1087.

Bella, F. (2014). Driver performance approaching and departing curves: driving simulator study. *Traffic injury prevention*, *15*(3), 310-318.

Bärgman, J. (2016). *Methods for analysis of naturalistic driving data in driver behavior research*. Chalmers Tekniska Hogskola (Sweden).

Barmpounakis, E. N., Vlahogianni, E. I., Golias, J. C., & Babinec, A. (2019). How accurate are small drones for measuring microscopic traffic parameters?. *Transportation letters*, *11*(6), 332-340.

Cafiso, S., Di Graziano, A., La Cava, G., Lamm, R., & Heger, R. (2004). In-field data collection for driving behavior analysis using the DIVAS instrumented car. In *14th International Congress of the Italian Society of Highway Infrastructure, Florence, Italy*.

Cafiso, S., Di Graziano, A., Di Silvestro, G., La Cava, G., & Persaud, B. (2010). Development of comprehensive accident models for two-lane rural highways using exposure, geometry, consistency and context variables. *Accident Analysis & Prevention*, *42*(4), 1072-1079.

Castro, M., Sánchez, J. A., Vaquero, C. M., Iglesias, L., & Rodríguez-Solano, R. (2008). Automated GIS-based system for speed estimation and highway safety evaluation. *Journal of Computing in Civil Engineering*, *22*(5), 325-331.

Castro, M., Sánchez, J. F., Sánchez, J. A., & Iglesias, L. (2011). Operating speed and speed differential for highway design consistency. *Journal of transportation engineering*, *137*(11), 837-840.

Calvi, A., & Bella, F. (2014). Modeling speed differential parameters in day and night environments using driving simulator. *Procedia Engineering*, *84*, 648-661.

Choudhari, T., & Maji, A. (2019). Effect of horizontal curve geometry on the maximum speed reduction: a driving simulator-based study. *Transportation in developing economies*, *5*(2), 1-8.

Camacho-Torregrosa, F. J., Pérez-Zuriaga, A. M., Campoy-Ungría, J. M., & García-García, A. (2013). New geometric design consistency model based on operating speed profiles for road safety evaluation. *Accident Analysis & Prevention*, *61*, 33-42.

Chen, L., Armstrong, C. W., & Raftopoulos, D. D. (1994). An investigation on the accuracy of three-dimensional space reconstruction using the direct linear transformation technique. *Journal of biomechanics*, *27*(4), 493-500.

Cohen, J., P. Cohen, S. G. West, and L. S. Aiken. 2003. *Applied multiple regression/correlation analysis for the behavioral sciences.* Mahwah, NJ: Lawrence Erlbaum Associates.

Chatterjee, S., & Mächler, M. (1997). Robust regression: A weighted least squares approach. *Communications in Statistics-Theory and Methods*, *26*(6), 1381-1394.

Chatterjee, S., & Mitra, S. (2019). Safety assessment of two-lane highway using a combined proactive and reactive approach: Case study from Indian national highways. *Transportation research record*, *2673*(7), 709-721.

Chaudhari, P. M., Goyani, J., Arkatkar, S., Joshi, G., & Easa, S. M. (2022). Design consistency evaluation of two-lane rural highways in hilly terrains. *Transportation research procedia*, *62*, 75-82.

Dubrofsky, E. (2009). Homography estimation. *Diplomová práce. Vancouver: Univerzita Britské Kolumbie*, *5*.

Donnell, E. T., Ni, Y., Adolini, M., & Elefteriadou, L. (2001). Speed prediction models for trucks on two-lane rural highways. *Transportation Research Record*, *1751*(1), 44-55.

Donnell, E., Wood, J., Himes, S., & Torbic, D. (2016). Use of side friction in horizontal curve

design: A margin of safety assessment. *Transportation Research Record*, *2588*(1), 61-70.

Dhahir, B., & Hassan, Y. (2018). Studying driving behavior on horizontal curves using naturalistic driving study data. *Transportation research record*, *2672*(17), 83-95.

Dhahir, B., & Hassan, Y. (2019a). Modeling speed and comfort threshold on horizontal curves of rural two-lane highways using naturalistic driving data. *Journal of Transportation Engineering, Part A: Systems*, *145*(6), 04019025.

Dhahir, B., & Hassan, Y. (2019b). Using horizontal curve speed reduction extracted from the naturalistic driving study to predict curve collision frequency. *Accident Analysis & Prevention*, *123*, 190-199.

de Oña, J., Garach, L., Calvo, F., & García-Muñoz, T. (2014). Relationship between predicted speed reduction on horizontal curves and safety on two-lane rural roads in Spain. *Journal of transportation engineering*, *140*(3), 04013015.

Eberhard, O. (1997). *Development of an Operating Speed Background for Roadway Sections with Grades≥ 6 Percent, as well as Analysis and Evaluation of Selected Road Sections, Based on Three Safety Criteria* (Doctoral dissertation, Master Thesis, Institute for Highway and Railroad Engineering, University of Karlsruhe (TH), Germany).

Fung, G. S. K., Yung, N. H. C., & Pang, G. K. (2003). Camera calibration from road lane markings. *Optical Engineering*, *42*(10), 2967-2977.

Furedy, J. J., Heslegrave, R. J., and Scher, H. (1992). "T-wave amplitude utility revisited: some physiological and psychophysiological considerations." *Biological Psychology*, 33(2–3), 241–248.

Fitzpatrick, K., Krammes, R. A., & Fambro, D. B. (1997). Design speed, operating speed and posted speed relationships. *Institute of Transportation Engineers. ITE Journal*, *67*(2), 52.

Farah, H., Van Beinum, A., & Daamen, W. (2017). Empirical speed behavior on horizontal ramp curves in interchanges in the Netherlands. *Transportation Research Record*, *2618*(1), 38-47.

Fitzpatrick, K., Elefteriadou, L., Harwood, D. W., Collins, J. M., McFadden, J., Anderson, I. B., ... & Passetti, K. (2000a). *Speed prediction for two-lane rural highways* (No. FHWA-RD-99-171). United States. Federal Highway Administration.

Fitzpatrick, K., Wooldridge, M. D., Tsimhoni, O., Collins, J. M., Green, P., Bauer, K. M., ... & Poggioli, B. (2000b). *Alternative design consistency rating methods for two-lane rural highways* (No. FHWA-RD-99-172).

Fitzpatrick, K., Parham, A. H., & Brewer, M. A. (2002). *Treatments for crashes on rural two-lane highways in Texas* (No. FHWA/TX-02/4048-2).

Fitch, G. M., & Hanowski, R. J. (2012). Using naturalistic driving research to design, test and evaluate driver assistance systems. *Handbook of intelligent vehicles*, 559-580.

Greer, M. (2012). *Electricity marginal cost pricing: applications in eliciting demand responses*. Elsevier.

Gibreel, G. M., Easa, S. M., Hassan, Y., & El-Dimeery, I. A. (1999). State of the art of highway geometric design consistency. *Journal of transportation engineering*, *125*(4), 305-313.

Goyani, J., Chaudhari, P., Arkatkar, S., Joshi, G., & Easa, S. M. (2022). Operating speed prediction models by vehicle type on two-lane rural highways in Indian hilly terrains. *Journal of transportation engineering, Part A: Systems*, *148*(3), 04022001.

García, A., Llopis-Castelló, D., Camacho-Torregrosa, F. J., & Pérez-Zuriaga, A. M. (2013). New consistency index based on inertial operating speed. *Transportation research record*, *2391*(1), 105-112.

Garach, L., Calvo, F., Pasadas, M., & de Ona, J. (2014). Proposal of a new global model of consistency: Application in two-lane rural highways in Spain. *Journal of Transportation Engineering*, *140*(8), 04014030.

Guzman, J. (1996). *Comparison of day and night vehicular speeds on horizontal curves on rural two-lane highways* (Doctoral dissertation, Texas A&M University).

Ghosh, P. (2018). *Numerical, symbolic and statistical computing for chemical engineers using MATLAB*. PHI Learning Pvt. Ltd.

Heger, R. (1995). "Driving Behavior and Driver Mental Workload As Criteria of Highway Geometric Design Quality." *International Symposium on Highway Geometric Design Practices*, Boston, 1918–1933.

Hirsh, M. (1987). Probabilistic approach to consistency of highway alignment. *J. Transp. Eng*, *113*(3), 268-276.

Hassan, Y., Gibreel, G., & Easa, S. M. (2000). Evaluation of highway consistency and safety: practical application. *Journal of transportation engineering*, *126*(3), 193-201.

Hassan, Y., Sayed, T., & Tabernero, V. (2001). Establishing practical approach for design consistency evaluation. *Journal of transportation Engineering*, *127*(4), 295-302.

He, X., & Yung, N. H. C. (2007). New method for overcoming ill-conditioning in vanishing-point-based camera calibration. *Optical Engineering*, *46*(3), 037202.

Llopis-Castelló, D., González-Hernández, B., Pérez-Zuriaga, A. M., & García, A. (2018). Speed prediction models for trucks on horizontal curves of two-lane rural roads. *Transportation research record*, *2672*(17), 72-82.

Jacob, A., & Anjaneyulu, M. V. L. R. (2013). Operating speed of different classes of vehicles at horizontal curves on two-lane rural highways. *Journal of Transportation Engineering*, *139*(3), 287-294.

Jacob, A., Dhanya, R., & Anjaneyulu, M. V. L. R. (2013). Geometric design consistency of multiple horizontal curves on two-lane rural highways. *Procedia-social and behavioral sciences*, *104*, 1068-1077.

Joshi, A. K., Joshi, C., Singh, M., & Singh, V. (2014). Road traffic accidents in hilly regions of northern India: What has to be done?. *World journal of emergency medicine*, *5*(2), 112.

Krammes, R. A., Brackett, R. Q., Shafer, M. A., Ottesen, J. L., Anderson, I. B., Fink, K. L., ... & Messer, C. J. (1995). *Horizontal alignment design consistency for rural two-lane highways* (No. FHWA-RD-94-034). United States. Federal Highway Administration.

Koenker, R., & Bassett Jr, G. (1978). Regression quantiles. *Econometrica: journal of the Econometric Society*, 33-50.

Lamm, R., Hayward, J. C., & Cargin, J. G. (1986). Comparison of different procedures for evaluating speed consistency. *Transportation Research Record*, *1100*, l0-20.

Lamm, R., & Choueiri, E. M. (1987). Recommendations for evaluating horizontal design consistency based on investigations in the state of New York. *Transportation Research Record*, *1122*(68), e78.

Lamm, R., Choueiri, E. M., Hayward, J. C., and Paluri, A. (1988). Possible design procedure to promote design consistency in highway geometric design on two-lane rural

roads. *Transportation Research Record*, *1195*, 111.

Lamm, R., Choueiri, E. M., & Mailaender, T. H. E. O. D. O. R. (1990). Comparison of operating speeds on dry and wet pavements of two-lane rural highways. *Transportation research record*, *1280*(8), 199-207.

Lamm, R., Choueiri, E. M., & Mailaender, T. (1991). Side friction demand versus side friction assumed for curve design on two-lane rural highways. *Transportation Research Record*, *1303*, 11-21.

Lamm, R., Guenther, A. K., & Choueiri, E. M. (1995). Safety module for highway geometric design. *Transportation Research Record*, *1512*(9), 7-15.

Lamm, R., Wolhuter, K. M., Beck, A., & Rusher, T. (2001). Introduction of a new approach to geometric design and road safety. *SATC 2001*.

Lamm, R., Beck, A., Ruscher, T., Mailaender, T., Cafiso, S., and Lacava, G. (2007). *How to make Two-Lane Rural Roads Safer*. WIT, Southampton, U.K.

Leisch, J. E., & Leisch, J. P. (1977). New concepts in design-speed application. *Transportation Research Record*, *631*, 4-14.

Leisch, J. E. (1977). Dynamics of highway design for safety. *Transportation*, *6*(1), 71-83.

Li, C., Wei, Y., Chappell, R., & He, X. (2011). Bent line quantile regression with application to an allometric study of land mammals' speed and mass. *Biometrics*, *67*(1), 242-249.

Messer, C. J. (1980). *Methodology for evaluating geometric design consistency* (No. 757).

McLean, J. R. (1974). Driver behaviour on curves-a review. In *Australian Road Research Board (ARRB) Conference, 7th, 1974, Adelaide* (Vol. 7, No. 5).

Morrall, J. F., & Talarico, R. J. (1994). Side friction demanded and margins of safety on horizontal curves. *Transportation Research Record*, *1435*, 145.

McFadden, J., & Elefteriadou, L. (2000). Evaluating horizontal alignment design consistency of two-lane rural highways: Development of new procedure. *Transportation Research Record*, *1737*(1), 9-17.

Misaghi, P., & Hassan, Y. (2005). Modeling operating speed and speed differential on two-lane rural roads. *Journal of Transportation Engineering*, *131*(6), 408-418.

MORTH (Ministry of Road Transport and Highways). 2016. *Road accidents in India 2016.* New Delhi, India: MORTH.

MORTH (Ministry of Road Transport and Highways). 2017. *Road accidents in India 2017.* New Delhi, India: MORTH.

MORTH (Ministry of Road Transport and Highways). 2018. *Road accidents in India 2018.* New Delhi, India: MORTH.

MORTH (Ministry of Road Transport and Highways). 2019. *Road accidents in India 2019.* New Delhi, India: MORTH.

MORTH (Ministry of Road Transport and Highways). 2020. *Road accidents in India 2020.* New Delhi, India: MORTH.

MORTH (Ministry of Road Transport and Highways). 2021. *Road accidents in India 2021.* New Delhi, India: MORTH.

Malaghan, V., Pawar, D. S., & Dia, H. (2020). Modeling operating speed using continuous speed profiles on two-lane rural highways in India. *Journal of transportation engineering, Part A: Systems*, *146*(11), 04020124.

Malaghan, V., Pawar, D. S., & Dia, H. (2021). Exploring maximum and minimum operating speed positions on road geometric elements using continuous speed data. *Journal of transportation engineering, Part A: Systems*, *147*(8), 04021039.

Malaghan, V., Pawar, D. S., & Dia, H. (2022a). Speed prediction models for heavy passenger vehicles on rural highways based on an instrumented vehicle study. *Transportation letters*, *14*(1), 39-48.

Malaghan, V., & Pawar, D. S. (2022b). A short-term naturalistic driving study on predicting comfort thresholds for horizontal curves on two-lane rural highways. *Journal of transportation engineering, Part A: Systems*, *148*(8), 04022045.

Montella, A., Pariota, L., Galante, F., Imbriani, L. L., & Mauriello, F. (2014b). Prediction of drivers' speed behavior on rural motorways based on an instrumented vehicle study. *Transportation Research Record*, *2434*(1), 52-62.

Montella, A., Galante, F., Imbriani, L. L., Mauriello, F., & Pernetti, M. (2014a). Simulator evaluation of drivers' behaviour on horizontal curves of two-lane rural

highways. *Advances in Transportation Studies: An International Journal*, *34*, 91-104.

Montella, A., & Imbriani, L. L. (2015). Safety performance functions incorporating design consistency variables. *Accident Analysis & Prevention*, *74*, 133-144.

Munigety, C. R., Vicraman, V., & Mathew, T. V. (2014). Semiautomated tool for extraction of microlevel traffic data from videographic survey. *Transportation Research Record*, *2443*(1), 88-95.

Maji, A., Sil, G., & Tyagi, A. (2018). 85th and 98th percentile speed prediction models of car, light, and heavy commercial vehicles for four-lane divided rural highways. *Journal of Transportation Engineering, Part A: Systems*, *144*(5), 04018009.

Nalo, T., Chatterjee, S., & Mitra, S. (2020). Operating speed and accidents at horizontal curves: insights from two-lane rural highway in mixed traffic operation. *International Journal for Traffic & Transport Engineering*, *10*(4).

Ni, D. (2015). *Traffic flow theory: Characteristics, experimental methods, and numerical techniques*. Butterworth-Heinemann.

Poe, C. M., & Mason Jr, J. M. (2000). Analyzing influence of geometric design on operating speeds along low-speed urban streets: mixed-model approach. *Transportation Research Record*, *1737*(1), 18-25.

Polus, A., & Mattar-Habib, C. (2004). New consistency model for rural highways and its relationship to safety. *Journal of transportation engineering*, *130*(3), 286-293.

Polus, A., Fitzpatrick, K., & Fambro, D. B. (2000). Predicting operating speeds on tangent sections of two-lane rural highways. *Transportation Research Record*, *1737*(1), 50-57.

Passetti, K. A., & Fambro, D. B. (1999). Operating speeds on curves with and without spiral transitions. *Transportation research record*, *1658*(1), 9-16.

Pérez-Zuriaga, A. M., Garcia Garcia, A., Camacho-Torregrosa, F. J., & D'Attoma, P. (2010). Modeling operating speed and deceleration on two-lane rural roads with global positioning system data. *Transportation Research Record*, *2171*, 11-20.

Pérez-Zuriaga, A. M., Garcia, A., & Camacho Torregrosa, F. J. (2011). *Study of tangent-to-curve transition on two-lane rural roads with continuous speed profiles* (No. 11-2548).

Pérez-Zuriaga, A. M., Camacho-Torregrosa, F. J., & García, A. (2013). Tangent-to-curve

transition on two-lane rural roads based on continuous speed profiles. *Journal of transportation engineering*, *139*(11), 1048-1057.

Park, Y. J., Park, C. H., & Chon, K. S. (2003). Development of potential measures to evaluate the safety of curves in rural highways. *KSCE Journal of Civil Engineering*, *7*(3), 233-242.

Qu, X., Wang, S., & Zhang, J. (2015). On the fundamental diagram for freeway traffic: A novel calibration approach for single-regime models. *Transportation Research Part B: Methodological*, *73*, 91-102.

Richl, L., & Sayed, T. (2005). Effect of speed prediction models and perceived radius on design consistency. *Canadian Journal of Civil Engineering*, *32*(2), 388-399.

Rosey, F., & Auberlet, J. M. (2012). Trajectory variability: Road geometry difficulty indicator. *Safety science*, *50*(9), 1818-1828.

Sil, G., Nama, S., Maji, A., & Maurya, A. K. (2020). Modeling 85th percentile speed using spatially evaluated free-flow vehicles for consistency-based geometric design. *Journal of Transportation Engineering, Part A: Systems*, *146*(2), 04019060.

Shallam, R. D. K., Venthuruthiyil, S. P., Chunchu, M., & Siddagangaiah, A. K. (2019). Empirical analysis of operating speed performance on undivided hilly roads. *Journal of Transportation Engineering, Part A: Systems*, *145*(8), 04019034.

Shallam, R. D. K., Venthuruthiyil, S. P., Chunchu, M., & Siddagangaiah, A. K. (2021). Operating speed modeling for the rural highways passing through hilly terrain. *Journal of transportation engineering, Part A: Systems*, *147*(5), 04021015.

Sun, Y., Xu, H., Wu, J., Zheng, J., & Dietrich, K. M. (2018). 3-D data processing to extract vehicle trajectories from roadside LiDAR data. *Transportation research record*, *2672*(45), 14-22.

Schoepflin, T. N., & Dailey, D. J. (2003). Dynamic camera calibration of roadside traffic management cameras for vehicle speed estimation. *IEEE Transactions on Intelligent Transportation Systems*, *4*(2), 90-98.

Spacek, P. (2005). Track behavior in curve areas: attempt at typology. *Journal of transportation engineering*, *131*(9), 669-676.

Siegel, A. F. (2016). *Practical business statistics*. Academic Press.

Taylor, J. I., and Thompson, H. T. (1977). *Identification of hazardous location by kernel density*. (No. FHWA-RD-77-83) Federal Highway Administration, Washington, DC.

Schneider, B. (1999). *Development of a Superior Safety Module for the Evaluation of the Danger of Two-Lane Rural Roads in Tune with the Actual Accident Situation* (Doctoral dissertation, Master Thesis, Institute for Highway and Railroad Engineering, University of Karlsruhe (TH), Germany).

Tsai, R. (1987). A versatile camera calibration technique for high-accuracy 3D machine vision metrology using off-the-shelf TV cameras and lenses. *IEEE Journal on Robotics and Automation*, *3*(4), 323-344.

Venthuruthiyil, S.P., & Chunchu, M. (2020b). SAVETRAX: A semi-automated image processing based vehicle trajectory extractor, in: *99th Annual Meeting of Transportation Research Board,* Washinton, D.C., United States.

Venthuruthiyil, S.P., & Chunchu, M. (2020a). Image-based naturalistic driving data compilation for the critical assessment of operational efficiency and safety of vehicles. *Working Paper.*

Venthuruthiyil, S. P., & Chunchu, M. (2018). Trajectory reconstruction using locally weighted regression: A new methodology to identify the optimum window size and polynomial order. *Transportmetrica A: Transport Science,* 14(10), 881-900.

Venthuruthiyil, S. P., & Chunchu, M. (2020c). Vehicle path reconstruction using Recursively Ensembled Low-pass filter (RELP) and adaptive tri-cubic kernel smoother. *Transportation Research Part C: Emerging Technologies,* 120, 102847.

Venthuruthiyil, S. P., (2021). *Rajectory-based proactive safety assessment of road traffic*. PhD. Thesis, Indian Institute of Technology Gwahati, Guwahati, Assam, India.

Wang, L. L., & Tsai, W. H. (1991). Camera calibration by vanishing lines for 3-D computer vision. *IEEE Transactions on Pattern Analysis and Machine Intelligence*, *13*(4), 370-376.

Wu, J., Xu, H., Zheng, Y., Zhang, Y., Lv, B., & Tian, Z. (2019). Automatic vehicle classification using roadside LiDAR data. *Transportation Research Record*, *2673*(6), 153-164.

Wu, K. F., Donnell, E. T., Himes, S. C., & Sasidharan, L. (2013). Exploring the association between traffic safety and geometric design consistency based on vehicle speed

metrics. *Journal of transportation engineering*, *139*(7), 738-748.

Wang, Y., Xu, G., & Bai, H. (2013). Operating speed based alignment consistency evaluation using driving simulator: case studies from Taigan freeway in Jiangxi, China. *Promet-Traffic&Transportation*, *25*(1), 23-31.

World Health Organisation https://www.who.int/news-room/fact-sheets/detail/road-traffic-injuries, 20th June 2022.

Wooldridge, M., Bauer, K., Green, P., & Fitzpatrick, K. (1999). Comparison of driver visual demand in test track, simulator, and on-road environments. Prepared for Transportation Research Board, 79 th Annual Meeting, Washington DC.

Wooldridge, M. D., Fitzpatrick, K., Koppa, R., & Bauer, K. (2000). Effects of horizontal curvature on driver visual demand. *Transportation Research Record*, *1737*(1), 71-77.

Wan, Y., Huang, Y., & Buckles, B. (2014). Camera calibration and vehicle tracking: Highway traffic video analytics. *Transportation research part C: Emerging technologies*, *44*, 202-213.

Xu, J., Luo, X., & Shao, Y. M. (2018). Vehicle trajectory at curved sections of two-lane mountain roads: a field study under natural driving conditions. *European Transport Research Review*, *10*(1), 1-16.

Xu, J., Lin, W., Wang, X., & Shao, Y. M. (2017). Acceleration and deceleration calibration of operating speed prediction models for two-lane mountain highways. *Journal of Transportation Engineering, Part A: Systems*, *143*(7), 04017024.

Xiao, Z. (2009). Quantile cointegrating regression. *Journal of econometrics*, *150*(2), 248-260.

Žilionienė, D., & Vorobjovas, V. (2011). Correspondence of Horizontal and Vertical Alignment with Safe Driving Conditions on Low-Volume Roads. *Transportation research record*, *2203*(1), 49-56.

List of Publications

Journals

- **A. V. A. Bharat Kumar**, Suvin P. V., Mallikarjuna C. (2022). Vehicle trajectory data extraction from the horizontal curves of mountainous roads. *Transportation Letters: The International Journal of Transportation Research*.

- Shallam R.D.K., **A. V A. Bharat Kumar**, Mallikarjuna C., Anjan Kumar S. (2022). Safety and Consistency Assessment of a Two-Lane Rural Highway Passing Through Mountainous Terrain. *Journal of Transportation Engineering, Part A: Systems*. (DOI: 10.1061/JTEPBS.0000761)

- **A. V. A. Bharat Kumar**, Mallikarjuna C. (2023). Determinants of speed variability on the horizontal curves of two-lane undivided rural highways passing through mountainous terrain. *International Journal of Injury Control and Safety Promotion.* (***Under review***).

- **A.V. A. Bharat Kumar**, Mallikarjuna C., Shallam R.D.K. (2023). Analysis and modeling of deceleration and acceleration lengths on the horizontal curves of two-lane undivided rural highways passing through mountainous terrain. (***To be submitted***).

- **A. V. A. Bharat Kumar**, Shallam R.D.K., Mallikarjuna C. (2023). Assessing the Role of Minimum and Maximum Speed on the Horizontal Curves of Two-lane Undivided Rural Highways Passing Through Mountainous Terrain in Design Consistency and Safety Evaluation (***To be submitted***).

Conferences

- **A.V. A. Bharat Kumar**, K.Srinivas Rao., Tanpuii Darlong., Mallikarjuna C. (2022). Empirical analysis and modeling of deceleration length on the horizontal curves of two-lane undivided rural highways passing through mountainous terrain. In the 26th International conference of Hongkong Society for Transportation Studies, 12-13 December 2022 (***accepted for publication in proceedings***).

- **A.V. A. Bharat Kumar**, Tanpuii Darlong., Mallikarjuna C. (2022). Analysis and Modelling of Acceleration Behavior on the Horizontal curves of Two-lane Undivided Rural Highways Passing Through Mountainous Terrain. In the 14th International Conference on Transportation Planning and Implementation Methodologies for Developing Countries (TPMDC), 19-21 December 2022 (***accepted for publication in TiDE Journal***).